Development and Validation of a Computational Fluid Dynamics Hydrodynamic Model of the Stewart 34 for Velocity Prediction Program Applications

Jean-Baptiste Roger Guillaume SOUPPEZ
9997513

Supervisor:
Dr. Stuart E. NORRIS

Master of Engineering Studies in Yacht Engineering
MechEng 775 – Yacht Engineering Project

Department of Mechanical Engineering
The University of Auckland
November 2014

Abstract

The prediction of the hydrodynamic behaviour of sailing yachts is a key component of modern yacht design, particularly to assess the theoretical performance of a design through a velocity prediction program. The increasing computational power now offers an alternative to towing tank testing: computational fluid dynamics. The work conducted on the development and validation of a computational fluid dynamics hydrodynamic model of the Stewart 34 sailing yacht for velocity prediction program applications is presented in this report.

An empirical resistance model has initially been developed based on the Delft Systematic Yacht Hull Series. The method has been described and its limitations highlighted, the main ones being the resistance prediction in semi-displacement mode and the side force prediction at high leeway angle. The method is however reliable for common designs in displacement mode and is particularly efficient since only a few design inputs are required.

In a second time, the use of the Rankine source panel code FS-Flow led to a computational fluid dynamics hydrodynamic model of the Stewart 34, validated against an experimental benchmark, as done for the empirical resistance calculations. Instabilities in the panel code at high Froude numbers resulted in a loss of accuracy. Furthermore, the panel code did not prove suitable at high leeway angles. FS-Flow appears to have some limitations when handling the hydrodynamic model of sailing yachts; its intended use primarily being the comparison of ship designs.

A total of three velocity prediction programs have been developed. An empirical 4 degrees of freedom one enabled to ascertain the test matrix for the Stewart 34. A second 4 degrees of freedom one was realised with WinDesign to provide a reference and comparison with the final 6 degrees of one done using FS-Equilibrium. This final velocity prediction program gathers the experimental hydrodynamic and aerodynamic models and was validated against available upwind full scale data to ensure its reliability.

A complete performance prediction for the Stewart 34 was therefore achieved based on experimental data, mostly focussing on the hydrodynamic model ascertained using both empirical and computational fluid dynamics methods, thus meeting the objectives set for this project. Finally, areas of further improvement and future work have been recommended.

Acknowledgements

The author would like to thank the following individuals for their much appreciated contribution to this project.

- Dr. Stuart Norris, supervisor of the project, for his invaluable help and support throughout the duration of the project.
- David Le Pelley, owner of *Pride*, for his help and information inherent to the Stewart 34.
- Dr. Heikki Hansen, and the FutureShip company, for providing the CFD and VPP software essential to the project, and his much appreciated advice regarding the velocity prediction program.
- George Backhus, author of "*Stewart 34 Yachting: the first 50 years*", for providing a copy of his book and the original plans of the Stewart 34.
- Marco Boscarino and Lan Yu, for sharing their experimental aerodynamic data, used for the realisation of the VPP.

Table of Contents

List of Figures

List of Tables

List of Symbols

$1+k$	Form factor
Af	Frontal area
$Alat$	Lateral area
$Amax$	Maximum section area
Ap	Projected area
AR	Aspect ratio
AR_e	Effective aspect ratio
AR_g	Geometric aspect ratio
Aw	Waterplane area
b	Span
BAD	Boom above deck
$\overline{BM}$	Metacentric radius
BOA	Beam overall
Bwl	Waterline beam
$\bar{c}$	Mean chord length
Ca	Roughness coefficient
C_{Di}	Induced drag coefficient
C_{Dp}	Parasitic drag coefficient
C_{Dw}	Windage drag coefficient
CE	Centre of effort
Cf	ITTC 57 Frictional coefficient
C_L	Lift coefficient
CLR	Centre of lateral resistance
Cm	Midship area coefficient
Cp	Prismatic coefficient
C_{PP}	Propeller drag coefficient
Cr	Root chord length
Ct	Total resistance coefficient
Ct	Tip chord length
Cv	Viscous coefficient
Cw	Wave coefficient
f	Froude's friction coefficient
f	Flat
E	Mainsail foot
EMH	Mast height
FA	Freeboard
Fh	Side force
Fn	Froude number
FPP	Forward perpendicular
g	Acceleration due to gravity
$\overline{GG'}$	Centre of gravity correction
$\overline{GM}$	Metacentric height
$\overline{Gz}$	Righting lever
HA	Heeling arm
HM	Heeling moment
I	Fore triangle height
I_t	Second moment of area of a tank
I_{xx}	Second moment of area of the waterplane
J	Fore triangle base
KSF	Keel side force
LCB	Longitudinal centre of buoyancy aft of amidships
LCB_{fpp}	Longitudinal centre of buoyancy from the forward perpendicular
LCF	Longitudinal centre of flotation aft of amidships
LCF_{fpp}	Longitudinal centre of flotation from the forward perpendicular
LOA	Length over all
LP	Luff perpendicular
L_{pp}	Length between perpendiculars
Lwl	Waterline length
MD	Mast diameter
p	Power
P	Mainsail luff
SAC	Sectional area coefficient
Sc	Upright canoe body wetted surface area
$Sc\varphi$	Heeled canoe body wetted surface area
SF	Side force
SL	Spinnaker luff
SSF	Sail side force
r	Reef
Ra	Roughness resistance
Rf	Frictional resistance
Ri	Induced resistance
Rn	Reynolds number
Rp	Propeller resistance
Rr	Residuary resistance
Rt	Total resistance
$Rt\varphi$	Heeled total resistance
Rv	Viscous resistance
$Rv\varphi$	Heeled viscous resistance
Rw	Wave resistance
$Rw\varphi$	Heeled wave resistance
T	Overall draft
t/c	Thickness/chord ratio
Tc	Canoe body draft
Te	Effective draft
Tr	Taper ratio
V	Velocity
Va	Apparent wind speed
VCB	Vertical centre of buoyancy
VCG	Vertical centre of gravity
Vt	True wind speed
Zcb_{app}	Vertical centre of buoyancy of an appendage

List of Greek Symbols

α	Rudder angle of attack
β	Yaw angle
βa	Apparent wind angle
βt	True wind angle
Δ	Displacement
Δx	Mesh grid spacing
ΔRr	Delta in residuary resistance
$\Delta Rr\varphi$	Delta in heeled residuary resistance
∇app	Appendages displaced volume
∇c	Canoe body displaced volume
θ	Pitch angle
λ	Leeway angle
μ	Viscosity
ρ	Density
φ	Heel angle

List of Acronyms

AWA	Apparent Wind Angle
AWS	Apparent Wind Speed
CDF	Computational Fluid Dynamics
DSYHS	Delft Systematic Yacht Hull Series
FSE	Free Surface Effect
GCI	Grid Convergence Index
IGES	Initial Graphics Exchange Specification
ITTC	International Towing Tank Conference
NURBS	Non-Uniform Radial B-Splines
ORC	Offshore Racing Congress
RANSE	Reynolds Averaged Navier-Stokes Equations
Sysser	Systematic Serie
TFWT	Twister Flow Wind Tunnel
TWA	True Wind Angle
TWS	True Wind Speed
VCG	Vertical Centre of Gravity
VMG	Velocity Made Good
VPP	Velocity Prediction Program
YRU	Yacht Research Unit

Chapter 1: Introduction

1.1 Project Outline

The ability to predict the velocity and behaviour of a boat enables to refine the design in a first place, and then to optimise the performances on the water. This is the crucial role played by Velocity Prediction Programs (VPP) in modern yacht design; hence the need for a reliable hydrodynamic model.

Previously, the evaluation of the hydrodynamic resistance and side force was done using either empirical calculations, or towing tank tests. The Delft Systematic Yacht Hull Series (DSYHS) offers a good starting point for common hull forms; however, this empirical method does not suit every boat, and the accuracy is questionable. A much more accurate option is towing tank testing; unfortunately this process is time consuming, very expensive, and requires the appropriate facilities, which are not available in New Zealand.

With the evolution of technology rose a new method that would fill the gap between the inaccurate and inexpensive empirical methods, and the more reliable but expensive and time consuming towing tank testing: Computational Fluid Dynamics (CFD). In theory, CFD enables to achieve a reliable hydrodynamic model, faster and at a lesser cost than towing tank testing. A panel code approach has been adopted in this instance for its lesser solving time compared to a Reynolds-Averaged Navier-Stokes solver.

The project has been developed with a particular emphasis on the validation of the methods proposed. As a result, towing tank data have been used as a benchmark to validate the DSYHS calculations as well as the panel code, in order to have confidence in the accuracy of the final hydrodynamic model. This is mainly motivated by the absence of publications and information related to the use of the panel code FS-Flow.

This project will provide an insight into the use and reliability of CFD-based hydrodynamic resistance and side force for VPP applications, focussing on a given boat: the Stewart 34.

The vessel has been chosen as it is used as a test boat by the Yacht Research Unit (YRU) and so experimental sail data is available [99, 12]. However, the absence of hydrodynamic model for the boat prevents the creation of an accurate VPP, hence the primary objective of this project, which is a continuation of the work undertaken by Sammour [79].

First of all, the DSYHS and the CFD analysis will be validated against the experimental data of the Sysser 62, elected as a benchmark thanks to its resemblance with the Stewart 34. An empirical and a CFD hydrodynamic model will then be developed for the Stewart 34. Finally, the experimental sail data will be used to realise a 6 degrees of freedom VPP.

The project being focused on the Stewart 34, the vessel will be presented in the following section, essentially based on the publication by George Backhus on the history of the Stewart 34 Class [2].

1.2 Stewart 34

Designed by Robert Stewart in 1959, the Stewart 34 is undeniably a major part of New Zealand maritime history. The 34 feet vessel seduced by both its speed on the water and the large accommodation volume, making it a competitive racer as well as a comfortable family cruiser. The design slightly evolved over the years, the most significant evolution being the change from wood to fibreglass. Nonetheless, accurately calculated ballast weights enable both types of boats to race together, leading to one of the largest one-design fleet in New Zealand [2].

Digitalised copies of the original sailplan and linesplan, conserved at the *New Zealand Maritime Museum* in Auckland, are respectively presented in Figure 1 and Figure 2.

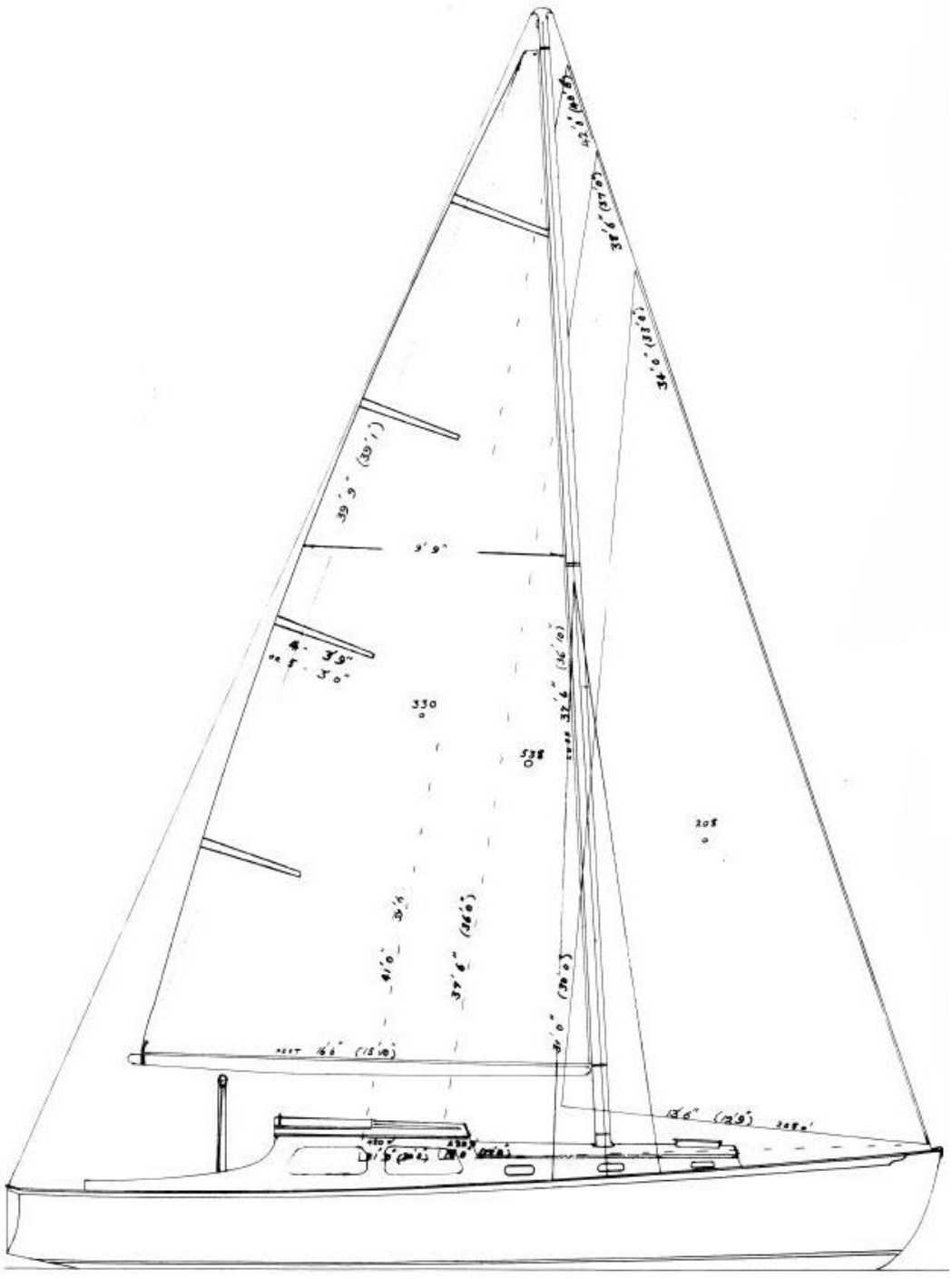

Figure 1: *Stewart 34 sailplan [85].*

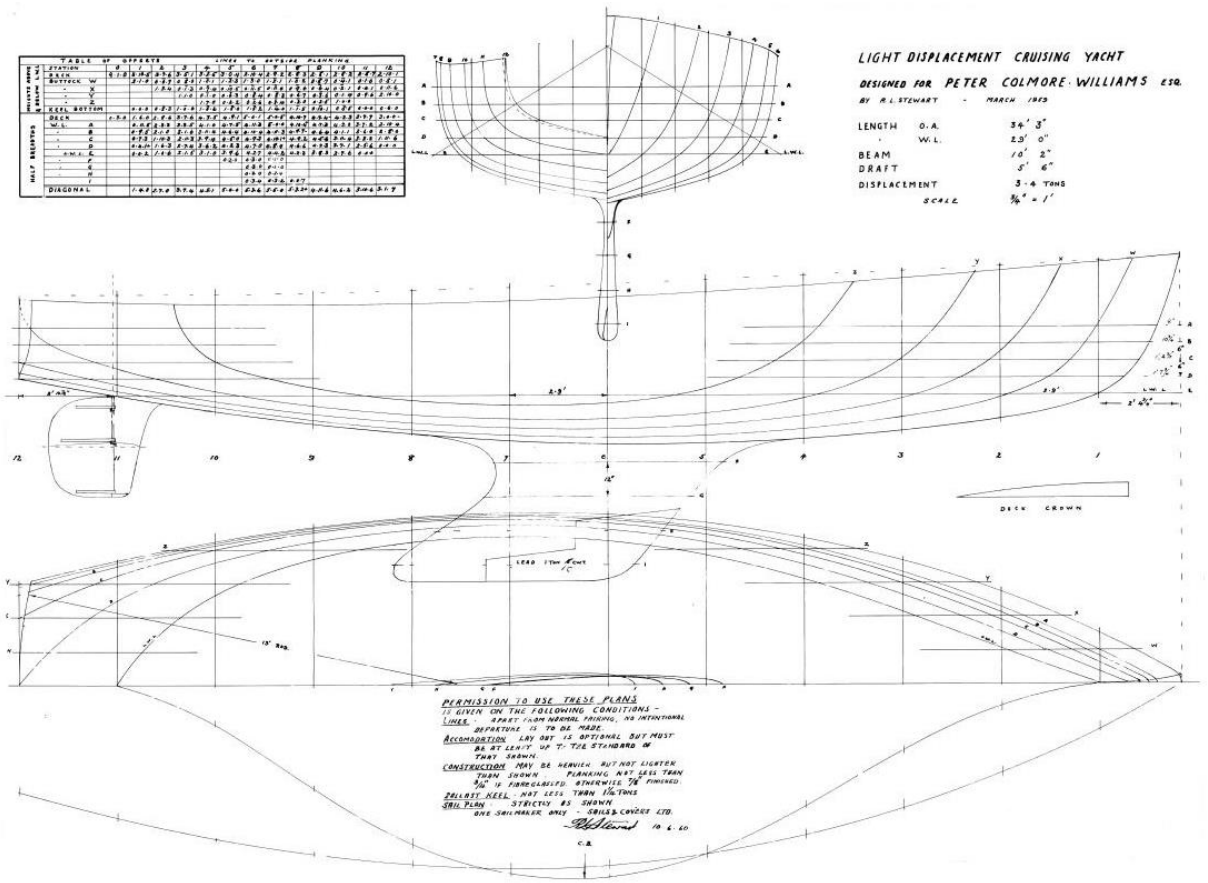

Figure 2: *Stewart 34 linesplan [84].*

The project will be based on a particular vessel, *Pride*, weighed at 5100 kg. The hydrostatics of the vessel for this particular displacement are listed in Table 1 and will be the basis of the empirical resistance model presented in Chapter 3.

Stewart 34 Hydrostatics	
Length over all - LOA (m)	10.44
Waterline length - Lwl (m)	9.45
Beam over all - BOA (m)	3.10
Waterline beam - Bwl (m)	2.71
Canoe body draft - Tc (m)	0.53
Total draft - T (m)	1.67
Total displacement - Δ (t)	5.10
Canoe body volume - ∇c (m^3)	4.67
Wetted surface area - Sc (m^2)	19.20
Waterplane area - Aw (m^2)	17.37
LCB from FPP - LCB_{fpp} (m)	4.89
LCF from FPP - LCF_{fpp} (m)	5.18
Prismatic coefficient - Cp	0.54
Midship coefficient - Cm	0.65

Table 1: *Hydrostatics of the Stewart 34 Pride.*

Furthermore, it is to be noted that the vessel considered does not feature the skeg-rudder illustrated on the linesplan (Figure 2) but the Gray Dixon rudder: a later design improvement of the Stewart 34 [2], shown in Figure 3. As a result, the hydrodynamic model will be developed for this rudder configuration.

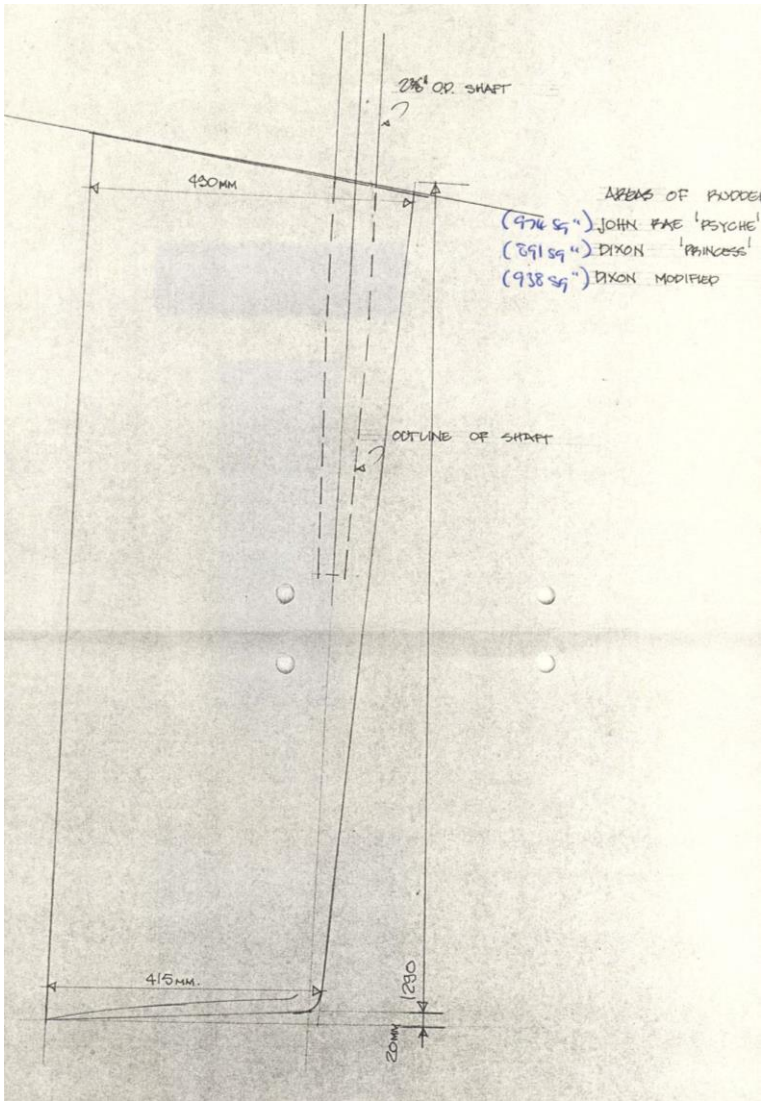

Figure 3: *Gray Dixon Rudder [2].*

Having introduced the Stewart 34, the background and previous work will be presented in order to set the context and motivations behind the topic tackled in this project.

Chapter 2: Previous work

For the past few years, the Yacht Research Unit (YRU) has undertaken experimental work on the sails of the Stewart 34, at both model and full scale. Aerodynamic coefficients have been ascertained for upwind [99] and downwind [12] sails, with particular emphasis on depowering, clearly demonstrating the intended use for VPP purposes.

This calls for a full hydrodynamic model of the yacht in order to obtain the resistance and side force to balance the aerodynamic drive and side force, and therefore predict the performances of the Stewart 34.

The most notable work in this area was performed in 2012 by Sammour [79] that developed a CFD hydrodynamic model based on the panel code FS-Flow, leading to an upwind VPP of the Stewart 34. However, some limitations and areas of further improvement have been identified, and are detailed hereafter:

1. The use of the Delft Systematic Yacht Hull Series (DSYHS) as an empirical resistance model was not thoroughly defined, and its application and limitations were not clearly established. The method will therefore be described and validated against an experimental benchmark in order to identify possible limitations before being applied to the Stewart 34. All aspects of the DSYHS have been gathered and presented by Keuning and Sonnenber [56] in 1998. However, updates parts of the methods have been published in more recent years, mainly regarding the appendages [53] and bare hull [54] calculations.

2. The hydrodynamic model did not consider the rudder, which is a non-negligible component both in terms of resistance and side force generated. This also raises the issue of the keel wake modelling with a panel code. The original plans of the Gray Dixon rudder have been obtained [2] and checked against to measurements realised on the boat, thus enabling to model and include the rudder as part of the CFD simulations and resulting hydrodynamic model of the Stewart 34.

3. No validation of the panel code was conducted. The analysis is performed with FS-Flow [24], a panel code that is not widely used, and for which no publication is available (with the exception of the user manual [26]). The panel code was developed for the purpose of comparing ship designs, and very little is known about its potential ability to model sailing yachts. A careful validation against experimental results is therefore required to ensure the reliability of the hydrodynamic model of the Stewart 34. The project will also aim at providing details regarding the general use of the panel code to facilitate future use.

4. The range of parameters previously considered for the CFD simulations appears quite extensive and not relevant to the sailing behaviour of the yacht. On the one hand, the range of leeway tested (from -2° to 10°) extends beyond the sailing range of leeway angles, resulting in unnecessary computations. On the other hand, the heel angles have been tested up to 20° only when the VPP ascertains heel angles greater than 30°. There is therefore a large source of uncertainty introduced, and an extended range of heel angles should be tested for. To remedy this issue, and empirical VPP will be developed at an early stage of the project to establish the relevant test matrix.

5. The stability of the Stewart 34 was assessed thanks to an inclining experiment [79]. However, the rise in centre of gravity due to the presence of the inclining weights on deck during the experiment was not accounted for. As a result, the centre of gravity and inherent stability curve ascertained are not representative of the actual boat. The stability calculations will therefore be performed from the raw data of the experiment in order to establish the location of the vertical centre of gravity of the Stewart 34, and then used to develop the righting lever curve.

6. Due to the absence of data for downwind sails, only the upwind VPP has been assessed by Yu [99]. The experimental aerodynamic model of the Stewart 34 for downwind sails has recently been developed [12] based on model scale testing performed at the Twisted Flow Wind Tunnel. Aerodynamic data including depowering is therefore available. Furthermore, despite the experimental CFD hydrodynamic model of the Stewart 34 previously developed, the VPP appears to be based on the empirical resistance modules of the VPP [99]. Inputting the actual CFD data generated will be tackled in this instance, leading to a complete experimental velocity prediction for the Stewart 34.

Particular attention will be paid to improve those various aspects in order to provide a thoroughly defined empirical model based on the DSYHS as well as a validated CFD model. The refined stability of the vessel and the latest downwind wind tunnel data will then be used to ascertain an accurate 6 degrees of freedom VPP of the Stewart 34.

Chapter 3: DSYHS Empirical Hydrodynamic Model

The Delft Systematic Yacht Hull Series (DSYHS) gathers over 70 hulls towing tank tested, the results for the first 62 of them being available online [18]. From the results, regression formulae have been developed to predict the resistance of a given vessel based on its principal dimensions and design ratios. This empirical method is only valid provided the design fits within the range of parameters considered by the DSYHS; but the idea that the resistance can be estimate based on design parameters only, as opposed to a defined hull shape, enables to consider the resistance at a very early stage of the design, prior to drawing the actual hull shape. Despite the debatable accuracy of the method, the DSYHS stands nowadays as a perfectly valid resistance prediction method, even if a refined resistance prediction based on either towing tank testing or CFD would be advised for the final design, especially when speed is a critical factor.

The resistance model and inherent calculations will be presented for the hull and appendages, in upright and heeled and yawed cases. The validity of the DSHYS prediction will be assessed against a vessel with known towing tank results before being applied to the Stewart 34.

3.1 Resistance Models

The resistance of yachts can be broken down according to two resistance models: the original Froude model presented by William Froude in 1872 [21, 22] and the more recent model adopted at the 1978 International Towing Tank Conference (ITTC) [41, 42].

3.1.1 Froude Model

The resistance model proposed by William Froude strips down the resistance into two main components: frictional resistance Rf and residuary resistance Rr [21, 42]. Froude considers the frictional resistance to be equal to the resistance of a flat plate having the same wetted area as the boat, the other components of resistance being comprised in the residuary resistance; mathematically the total resistance Rt is therefore given by:

$$Rt = Rf + Rr \qquad \textbf{Equation 1}$$

After testing a wide range of flat plates, Froude derived a formula to estimate the frictional resistance [4, 42] based on the wetted area Sc and the velocity V:

$$Rf = f \times Sc \times V^{1.825} \qquad \textbf{Equation 2}$$

Where f is the friction coefficient, defined as:

$$f = \frac{1}{1000} \times \left(\left(0.1392 + \frac{0.258}{2.68 + Lwl} \right) \times \rho_{water} \right) \qquad \textbf{Equation 3}$$

Froude's resistance model is still valid nowadays; in fact, it is the resistance model adopted by the DSYHS for reasons explained in Section 3.1.4. However, the expression for the friction coefficient has been refined over the years.

3.1.2 Friction Coefficient

The introduction of the Reynolds number Rn in 1883 [76] led to new definitions of the friction coefficient [4] eventually leading to the ITTC 1957 formula [32]:

$$Cf = \frac{0.075}{(\log_{10} Rn - 2)^2}$$ ***Equation 4***

From this new friction coefficient, the ITTC developed an alternative resistance model.

3.1.3 ITTC 78 Model

The main difference in the ITTC 78 resistance model is the introduction of a form factor $1 + k$ which multiplied by the frictional resistance gives the 3 dimensional viscous resistance Rv [41]:

$$Rv = (1 + k) \times Rf$$ ***Equation 5***

Where Rf is based on the ITTC 57 friction coefficient:

$$Rf = \frac{1}{2} \times \rho \times Sc \times V^2 \times Cf$$ ***Equation 6***

The form factor represents the effect of the hull shape on the friction resistance, hence its definition of a 3D viscous resistance as opposed to the 2D flat plates considered by Froude.

The remaining components of the resistance are gathered in the wave resistance Rw, giving the ITTC resistance model as:

$$Rt = Rv + Rw$$ ***Equation 7***

The value of the form factor for a given boat is ascertained using the Prohaska method.

3.1.4 Prohaska Method

The Prohaska method [72] enables to assess the value of the form factor based on towing tank testing. Prohaska makes similar assumptions as the ITTC 78 (stated in equations 5 and 7), which in terms of coefficients gives:

$$Cv = (1 + k) \times Cf$$ ***Equation 8***

$$Ct = Cv + Cw$$ ***Equation 9***

According to Baba [1] at low speeds, the wave coefficient Cw can be calculated by:

$$Cw = a \times Fn^4$$ ***Equation 10***

Combining equations 8, 9 and 10:

$$Ct = a \times Fn^4 + (1 + k) \times Cf$$ ***Equation 11***

Dividing by Cf:

$$\frac{Ct}{Cf} = a \times \frac{Fn^4}{Cf} + (1 + k)$$ ***Equation 12***

Therefore giving the equation of a straight line of the form:

$$y = m \times x + c$$ **Equation 13**

Where:

$$y = \frac{Ct}{Cf} \qquad m = a \qquad x = \frac{Fn^4}{Cf} \qquad c = 1 + k$$

Plotting Fn^4/Cf against Ct/Cf, the y-intercept of the best fit line will give the form factor $1 + k$. This is known as a Prohaska Plot, only valid for slow speeds where the wave resistance is negligible and the viscous drag is the dominant component of the resistance. As a result, values of Fn^4/Cf greater than 4 should not be considered [4].

The Prohaska method requires experimental data to establish the form factor. The absence of numerical method to calculate $1 + k$, coupled with the will to offer an alternative method to towing tank testing led the DSYHS not to consider the form factor [59] effectively basing their resistance breakdown on Froude's model.

The DSYHS calculation process and inherent hydrodynamic model is thoroughly presented and detailed in Appendix A, and will be used for the purpose of the validation of the method.

3.2 Validation

In order to validate the DSYHS method, the resistance prediction will be compared to actual towing tank data for a known vessel from the DSYHS database [18]. For the validation to be more relevant, a suitable hull must be selected among the 62 available.

3.2.1 Delft Representative Hull Form

The selected DSYHS hull must cover an appropriate range of Froude numbers and a wide range of experimental results. In addition, a hull similar to the Steward 34 in terms of design parameters must be chosen. Finally, the hull shape must resemble the Stewart 34, with similar design features.

Initially, series with limited experimental data have been eliminated. A statistical analysis of the difference in design parameters has been conducted on the remaining series. Finally, the representative hull has been chosen among the best statistical matches based on the design resemblance with the Stewart 34, illustrated in Figure 4.

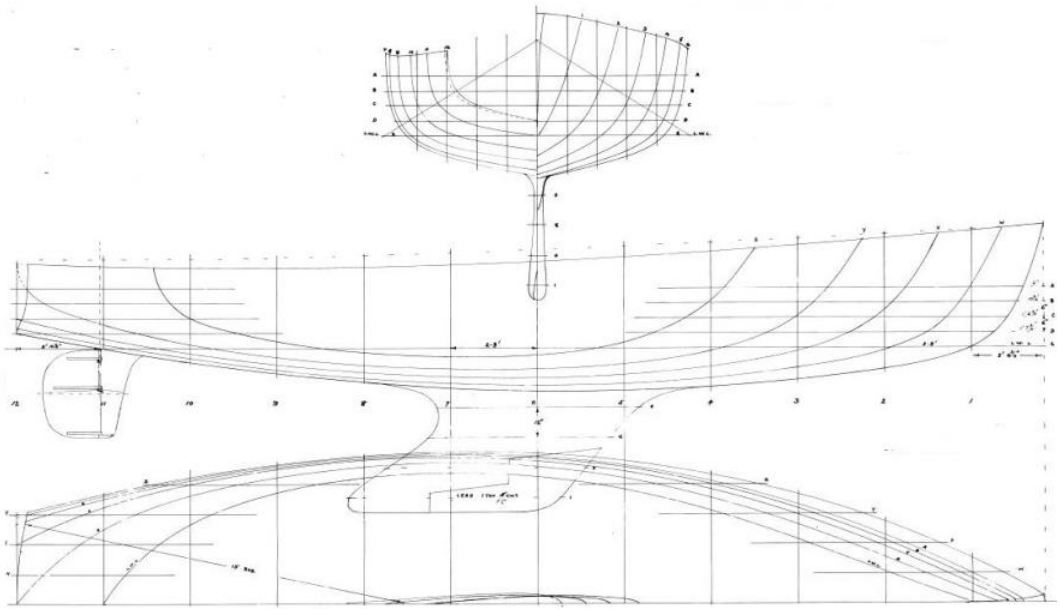

Figure 4: *Original linesplan of the Stewart 34, drawn by Robert Stewart in 1959 [84].*

The Sysser 62, shown in Figure 5, has been elected as the most appropriate representative hull form. Its 6% relative difference in design parameters does not make it the statistically closest, but it is the most suitable in terms of hull resemblance.

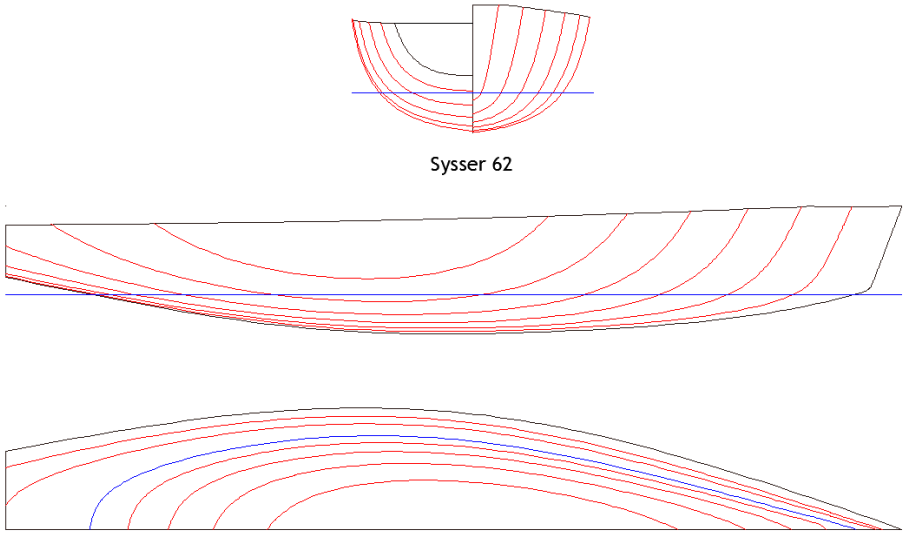

Figure 5: *Sysser 62 linesplan [18].*

Despite being the closest in terms of design ratios, the Sysser 3 presented in Figure 6 unfortunately has nothing in common with the Stewart 34: long stem overhang, high stern one, small and narrow transom and tumblehome (inward slope of the topsides due to the maximum beam occurring below the sheer line). Those design features make it inappropriate for a relevant comparison.

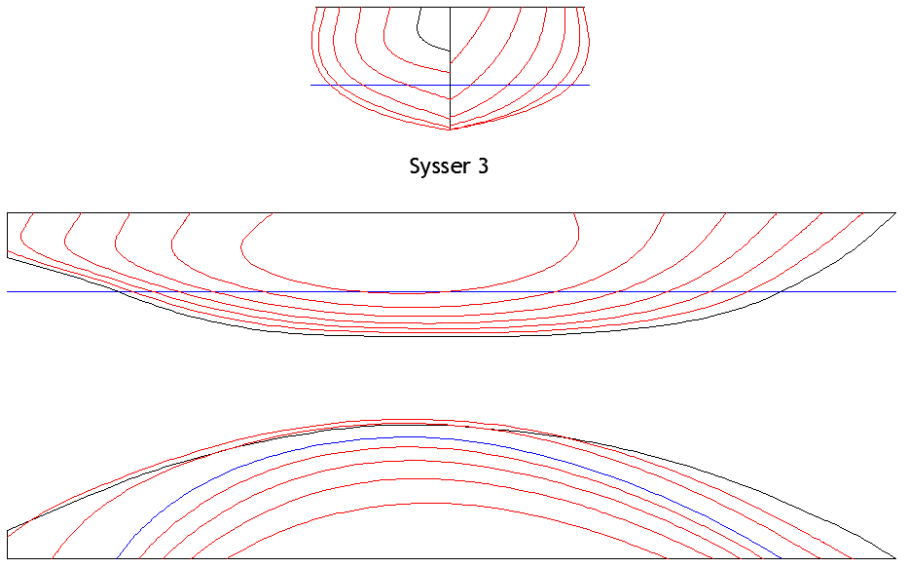

Figure 6: *Sysser 3 linesplan [18].*

Having selected a representative hull resembling the Stewart 34, the DSYHS will be applied to the Sysser 62 and the results will be compared to the available towing tank experimental data.

3.2.2 Method Validation

The resistance model proposed by the DSYHS will be validated for the Sysser 62 in upright and heeled and yawed conditions to identify the accuracy and restrictions of the method. All experimental data presented have been retrieved from the DSYHS online database [18].

3.2.2.1 Upright

The total hull resistance presented in Figure 7 exhibits very similar results up to a Froude number of 0.50, where the calculation method starts to overestimate the resistance.

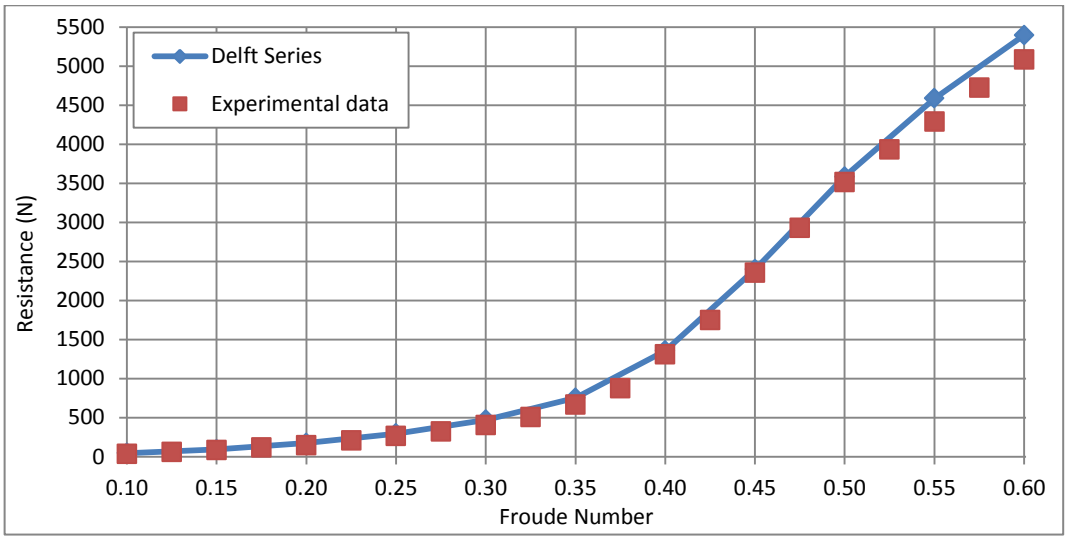

Figure 7: *Upright total hull resistance, Sysser 62.*

Conversely, applying the method to the Sysser 3 previously introduced reveals a perfect fit even at high Froude numbers. The Sysser 62 is one of the latest DSYHS, and is therefore representative of more modern designs, whereas the Sysser 3 is typical of the early hull forms tested by Delft: the calculation method therefore does not seem to be appropriate for more recent designs at high Froude numbers.

A possible explanation is the tendency for recent boats to reach semi-displacement mode (boat starting to climb over its own bow wave) much earlier and more efficiently, resulting in large differences past a Froude number of 0.40 (where the waterline length is equal to the wave length). Dividing the resistance by the displacement of the boat enables to observe this behaviour for the Sysser 3 and Sysser 62, the former experiencing a severe increase in resistance from a Froude Number of 0.40. On the other hand, the Sysser 62 is less affected by the resistance increase, and the lower experimental resistance at higher Froude numbers would suggests that the boat reached semi-displacement mode.

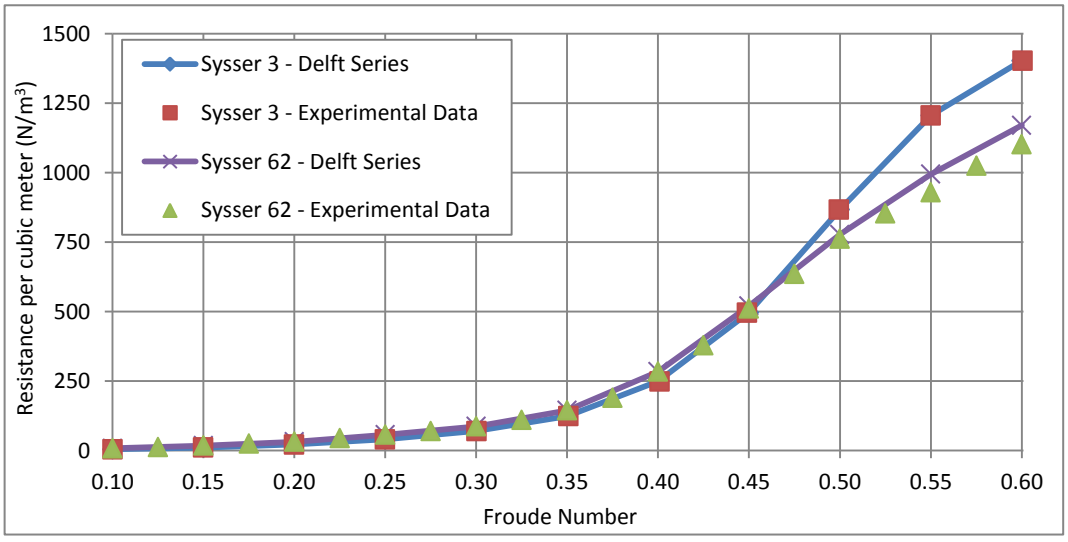

Figure 8: *Total upright resistance of the Sysser 3 and Sysser 62.*

Figure 8 clearly demonstrates the decrease in resistance achieved by reaching semi-displacement mode for the Sysser 62; note that the resistance has been expressed in Newton per cubic meter of displacement to achieve a more relevant comparison of the two very different designs.

The Froude number at which a boat reaches semi-displacement mode is dependent on the hull shape, and therefore cannot be reliably factored in by the calculation method. This can be observed on the wave patterns of a typical modern and older yacht towing tank tested at Southampton Solent University [6] and presented in Appendix B.

Semi-displacement mode is where the main limitation of the regression method employed by the DSYHS lies: the hull shape will impact on the sailing mode, and every vessel will exhibit a different behaviour. The regression coefficients result in an averaging of the resistance once the boat reaches semi-displacement mode. For vessels able to get into semi-displacement mode at a low Froude numbers (such as the Sysser 62) this will result in an over-predicted resistance. Examples of both under and over predicted resistance published by Delft University [54] are presented in Appendix C.

3.2.2.2 Heeled and yawed

The total resistance and side force have been tested for Froude numbers from 0.30 to 0.45, at 10°, 20° and 30° of heel and 3.1° and 6.1° of leeway. This limited range of parameters therefore impacts on the ability to validate the calculation method proposed by the DSYHS. Comparisons of the results are presented in Figure 9 for 10° of heel. For further details and results at 20° and 30° of heel, see Appendix D. The total resistance and side force are respectively presented on the left hand side and right hand side.

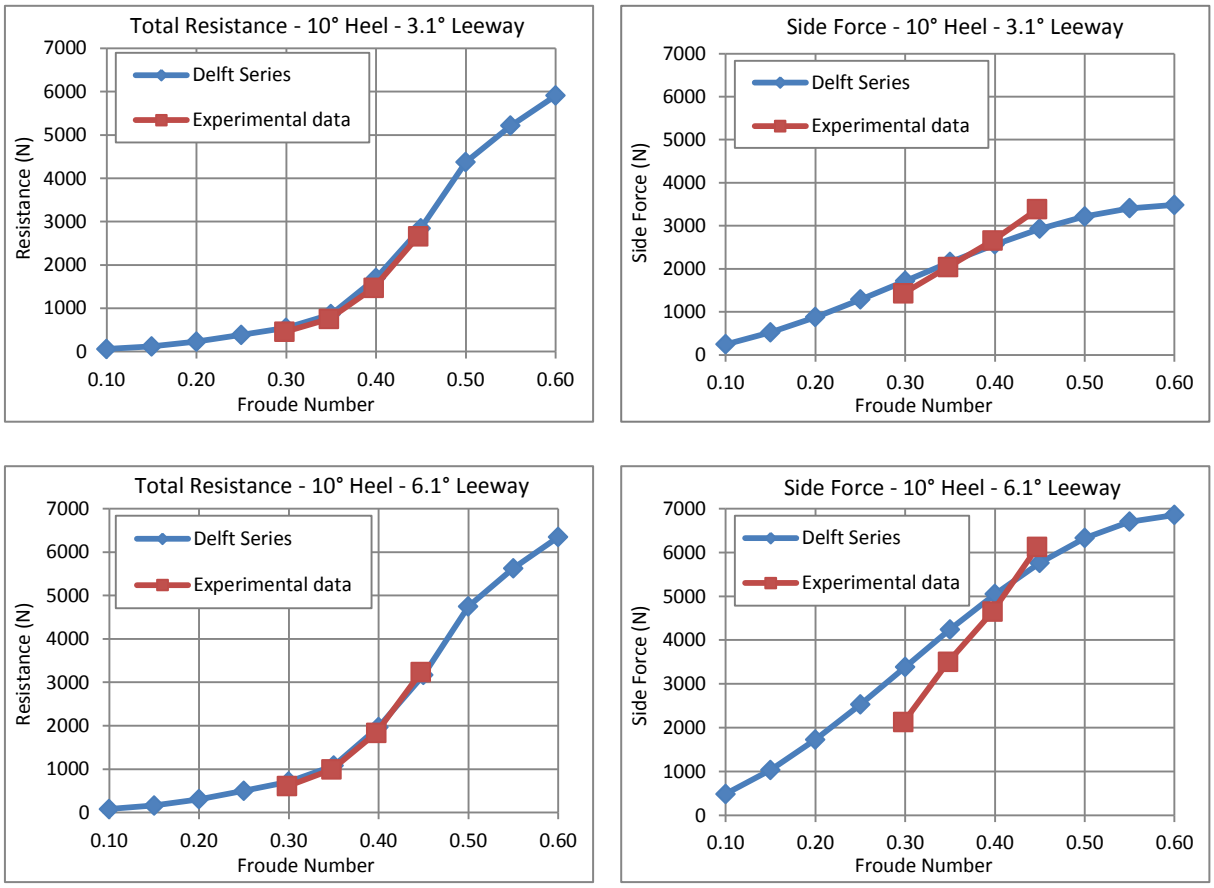

Figure 9: *DSYHS and experimental data [18] comparison at 10° of heel.*

Over the range of parameters considered, the resistance prediction remains accurate. However, the side force prediction does not always yield satisfactory results. It only appears to be relatively accurate at small leeway angle (less than 3°) and below a Froude number of 0.4.

The prediction of the side force is a vital component of a VPP, and more accurate results than established by the DSYHS will be required. If the extended keel method (see Appendix A.4) proved to be reliable for the resistance prediction, it is however not suitable for the side force assessment at high leeway angle. It is to be noted that the benchmark used for validation is the result of experimental towing tank testing, and therefore comprises a certain level of uncertainties.

3.2.3 Uncertainties

The uncertainties related to the towing tank testing of Delft models have not been quantified in any of the DSYHS publications, and the description of the experimental setup [51] provides insufficient data for a quantitative analysis. As a result, a qualitative analysis of potential uncertainties will be discussed. The uncertainty analysis of towing tank results is defined in the ITTC procedures and guidelines [46] and divided in four sections: hull geometry, speed, resistance, and temperature/density/viscosity.

3.2.3.1 Hull Geometry

The hull form geometry is not considered as such due to the difficulty to assess the difference between the model and its design. The two parameters taken into account are the waterline length and wetted surface area of the model. Under the ITTC model manufacturing regulation [45], a tolerance of ±1mm is allowed in all direction.

The waterline length can therefore vary by ±2mm; for the 2078mm model of the Sysser 62, and uncertainty of ±0.096% is introduced.

The wetted surface area will be affected by a ±2mm change in waterline length and beam, and a ±1mm change in draft. Assuming a constant block coefficient and wetted area coefficient, the uncertainty regarding the model volume can be assessed, leading to the wetted surface area:

$$WSA = 2.696 \times \sqrt{\nabla c \times L_{pp}} \qquad \textbf{Equation 14}$$

For the Sysser 62, the wetted surface area uncertainty is ±0.76%.

Model manufacturing accuracy also has repercussions on the hydrostatics of the ballasted model that will not be tested on its actual design waterline.

3.2.3.2 Speed

Due to the absence of data on measurement and data acquisition technique, the uncertainty inherent to the model speed cannot be quantified. The resistance being proportional to the speed squared, the accuracy is of crucial importance to the results.

3.2.3.3 Resistance

Calibration, data acquisition and reduction are unquantifiable due to the lack of information made available in the Delft publications. This area generally gathers most of the uncertainty [90], and can partially be illustrated for the Sysser 62. Both the bare hull and appended upright resistance results are available [18]. Subtracting the former from the later will reveal the resistance due to the appendages, which is presented in Figure 10.

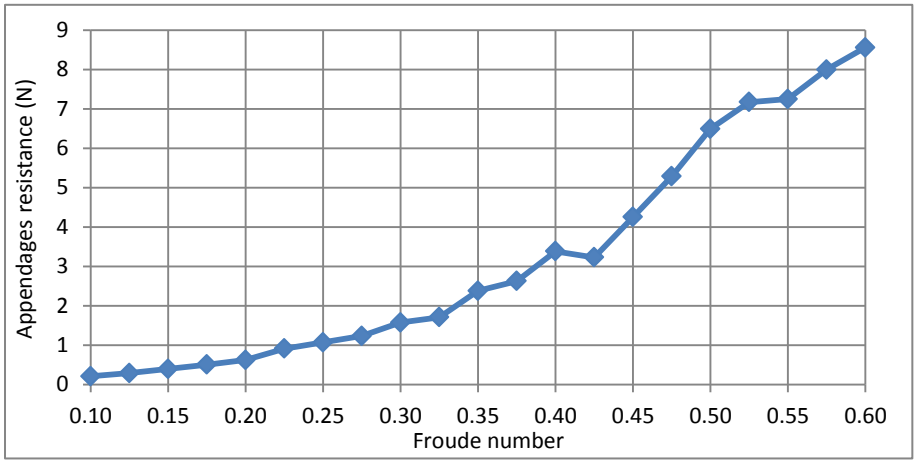

Figure 10: *Experimental appendages resistance of the Sysser 62 [18].*

Noise in the data is clearly visible in this instance, and highlights uncertainties in the experimental towing tank tests of the Sysser 62. Furthermore, Figure 10 illustrated that the appendages resistance cannot simply be added on to the bare hull one as suggested by the calculation method.

3.2.3.4 Temperature/density/viscosity

For the recorded water temperature, the ITTC provides a corresponding value for the density and viscosity of the water [47], the accuracy of the tank thermometer is therefore an additional source of inaccuracy. Whether the temperature is recorded for each run or averaged is unknown. For the upright resistance curve, 21 runs have been realised. Assuming 20 minutes in between each runs (so that the tank can settle down), 7 hours are required to complete the experiment. The temperature of the room and therefore the tank is likely to vary over such a period of time.

3.2.3.5 Conclusions

A wide range of uncertainties will impact the accuracy of the results. Although not all quantifiable in this instance, uncertainties revealing a certain level of inaccuracy have been illustrated. The experimental data considered for the validation of the DSYHS and the panel code is therefore subject to a certain degree of leeway that must be taken into account when comparing the resistance model with the experimental values.

3.2.4 Conclusions

The DSYSH calculation method applied to the Sysser 62 has been compared with the actual towing tank testing data, for which the uncertainties have been qualitatively assessed. The resistance prediction in upright condition appears to be validated for Froude numbers up 0.50, at which point the method cannot cope with the yacht entering semi-displacement mode. This is however not a major issue as many yachts are very unlikely to reach such a high Froude number in normal sailing conditions.

On the other hand, the side force prediction model appears to significantly lack accuracy past 3° of yaw. If sufficient keel area has been provided by the designer, the yacht should not have to sail at a yaw angle much higher than 3°; nevertheless, a more reliable side force prediction will be required. Conclusions inherent to the heeled and yawed case should however be treated with care due to the very limited amount of experimental data available.

There are clear limitations to the DSYHS, which justifies the need for a more advanced method such as CFD to achieve an accurate VPP. In order to have an initial estimate of the resistance of the Stewart 34 before undertaking the CFD analysis, the DSYHS resistance calculation method will be applied to the Stewart 34.

3.3 Application to the Stewart 34

Having validated the resistance calculation method for a yacht very similar to the Stewart 34, it can now be applied, after ensuring that the vessel meets the appropriate range of parameters.

3.3.1 DSYHS Range of Parameters

For the DSYHS to apply, the considered vessel must fit within the range of parameters covered, as presented in Table 2.

Parameter		Range			Stewart 34	Comply?
Length-Beam Ratio	Lwl/Bwl	2.73	to	5	3.49	Yes
Beam-Draft Ratio	Bwl/Tc	2.46	to	19.38	5.02	Yes
Length-Displacement Ratio	$Lwl/\nabla c^{1/3}$	4.34	to	8.5	5.65	Yes
Longitudinal Centre of Buoyancy	LCB_{fpp}	0.00%	to	-8.20%	-1.69%	Yes
Longitudinal Centre of Flotation	LCB_{fpp}	-1.80%	to	-9.50%	-4.80%	Yes
Prismatic Coefficient	Cp	0.52	to	0.60	0.54	Yes
Midship Area Coefficient	Cm	0.65	to	0.78	0.65	Yes
Loading Factor	$Aw/\nabla c^{2/3}$	3.78	to	12.67	6.21	Yes

Table 2: *DSYHS range of parameters [58].*

The Stewart 34 meets all requirements stated by the DSYHS [58], the method can therefore be applied to obtain a preliminary estimate of the resistance and side force.

3.3.2 Application of the DSYHS to the Stewart 34

The principal dimensions of the Stewart 34 ascertained based on the original linesplan [84] have been input in the DSYHS spreadsheet created, giving the upright resistance breakdown presented in Figure 11. Further details on the hydrodynamics of the Stewart 34 are presented in Appendix H.

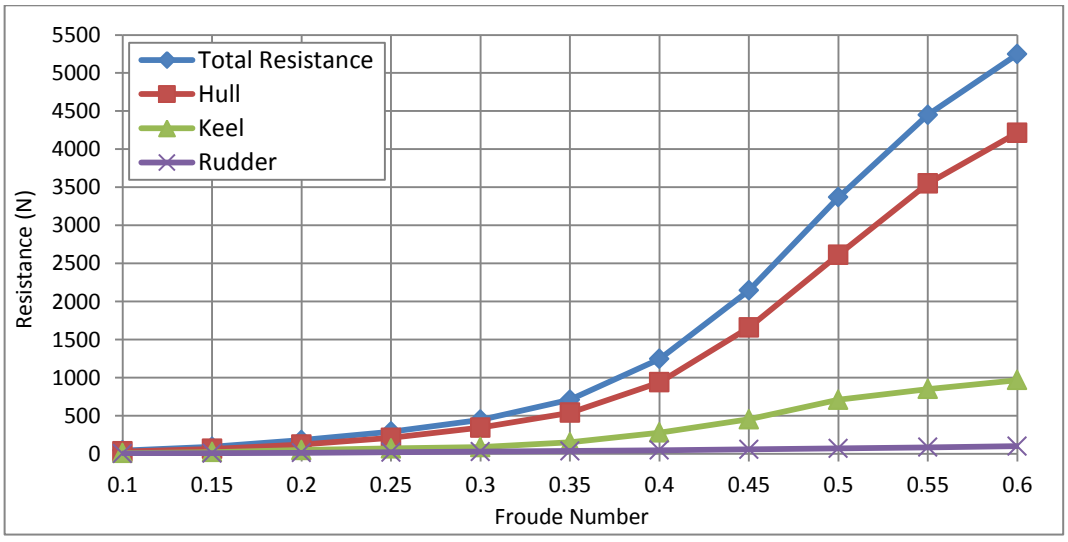

Figure 11: *Stewart 34 upright resistance components.*

Based on the validated DSYHS, the resistance model of the Stewart 34 can be ascertain for a wide range or Froude numbers in heeled and yawed conditions. There are however some restrictions to this resistance model.

3.3.3 Additional considerations

Further resistance components, not part of the DSYHS, needs to be considered. They are namely: propeller drag, roughness, windage, and added resistance due to waves.

3.3.3.1 Propeller drag

The DSYHS does not consider the drag generated by the shaft and propeller, as those are not replicated on the tested models. The propeller resistance Rp is given by:

$$Rp = 1/2 \times \rho \times Af \times V^2 \times C_{PP} \qquad \textbf{Equation 15}$$

Where Af is the frontal area of the propeller (established from measurements realised on the vessel) and C_{PP} is the propeller drag coefficient, which is dependent on the type of propeller (fixed, free to rotate, or folding). The Stewart 34 having a folding propeller, a value of 0.06 would be considered by Larsson and Eliasson [54]. However, more recent experiments [66] suggest that 0.09 is more appropriate, and will therefore be used for the calculation procedure.

3.3.3.2 Roughness

The hull of a towing tank model is manufactured to a very high finish, however real yachts suffer from hull roughness that can be caused by weeds growing on the hull, the presence of seacocks and impellers, irregularity in the surface, and natural wear and tear. The shipping industry uses a roughness coefficient Ca of 0.0004 [62], a value that has then been adopted and is now widely used in the small craft industry as well. The roughness resistance Ra can therefore be calculated:

$$Ra = 1/2 \times \rho \times Sc \times V^2 \times Ca \qquad \textbf{Equation 16}$$

Note that roughness also applies to appendages, in which case the wetted surface of the appendages is to be used.

3.3.3.3 Windage

The windage represents the air drag of the vessel, and will be accounted for as part of the experimental aerodynamic model.

3.3.3.4 Added Resistance due to Waves

For the purpose of the empirical resistance model, the added resistance due to waves will not be considered. Despite the simplified model proposed by the DSYHS [56], the added resistance due to waves remains very difficult to establish, especially given the virtually infinite environmental conditions the boat could be exposed to; hence the method is impractical for VPP use. Moreover, there is no experimental data available to validate the DSYHS approximation and ensure its reliability.

3.3.3.5 Conclusions

In addition to the DSYHS resistance prediction, the propeller drag and roughness have been added to complete the resistance model and improve the accuracy. However, due to its impracticality and the impossibility to validate the method, the added resistance due to waves has been neglected. The final empirical resistance breakdown for the Stewart 34 is presented in Figure 12 for the upright case.

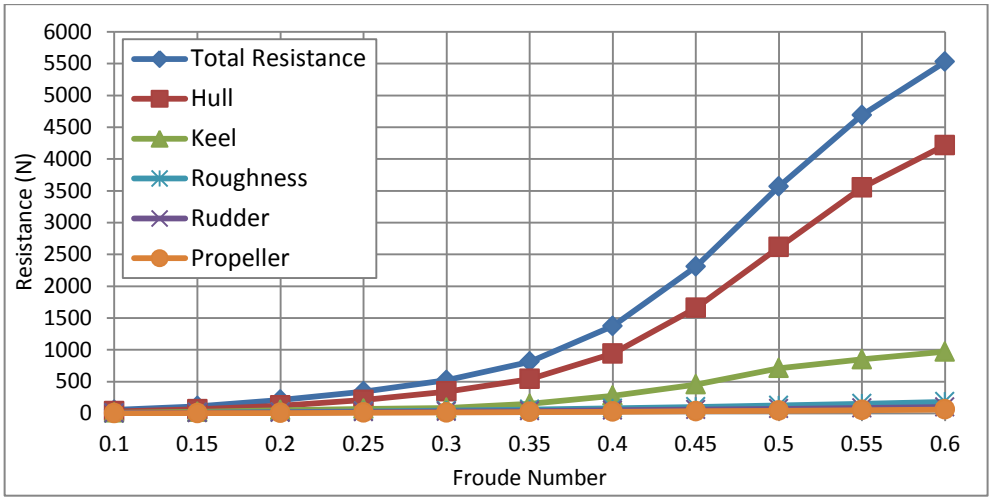

Figure 12: *Stewart 34 final upright resistance components.*

The DSYHS prediction in sailing condition is presented in Appendix H. It is to be noted that the DSYHS is a work in constant progress: the up to date method has been used, however, some changes can be expected in the future.

3.4 DSYHS: Present and Future Work

The work undertaken by the University of Delft since the 1970s is in constant evolution. New models are tested every year, trying to reflect the evolution of yacht design, thus leading to a wider range of parameters covered. The beam/draft ratio Bwl/Tc and slenderness ratio $Lwl/\nabla c^{1/3}$ are the two parameters for which the range has been considerably increased. Improvements in composite materials and design now lead to much lighter boats, where stability is a key factor (comfort for cruising, power for racing, and required compliance with class rules), leading to higher beam/draft and slenderness ratios than 30 years ago.

Another crucial step in the refinement of the DSYHS took place in early 2013, when the full database was made available to the public [18], leading to some independent analysis on the subject. The combination of the towing tank testing results and model geometry is an opportunity for various CFD analysis, such as the building of a CFD database of the Delft models [38], or validation of a CFD code against a benchmark, which is the approach taken in this project.

The most recent work inherent to the DSYSH was published in August 2014 by Remmlinger [74], with a statistical approach to the method, aiming to develop a refined and optimised regression method. The influence of various parameters on the resistance has been assessed and a transition zone between Froude numbers of 0.35 and 0.45 has been identified, highlighting the change in influence of the parameters on the resistance at higher Froude numbers, eventually concluding on the need for different sets of coefficients and possibly equations to cope with the two distinct sailing regimes, namely displacement and semi-displacement. This is where to current work undertaken by the University of Delft is focused [54].

One of the main limitations to the evolution of the DSYHS appears to be the will to provide a consistent method throughout the time and large range of model tested. For instance, if a Reynolds length of 70% of the waterline was suitable for the original models, the University of Delft now recognises that 90% would be a more suitable value [57]; however for the sake of consistency with the original method, all models remain subjected to the 70% Reynolds length.

Nevertheless, the recent open access to the DSYHS database coupled with the increasing use of CFD will provide some new insights into the accuracy and reliability of the current regression method, as well as opportunities to improve empirical resistance predictions.

3.5 Conclusions

The resistance model proposed by the DSYHS has been validated against a towing tank tested vessel resembling the Stewart 34. Despite its accuracy, the method revealed some limitations:

- Only a vessel in displacement mode can be considered: the method did not prove to be valid in the semi-displacement mode region, starting at a Froude number of 0.50 for the Sysser 62.
- If the resistance prediction is valid for high leeway angles, the same is not true for the side force that is only valid for small angles of leeway up to 3°.
- The range of Froude numbers is restricted to a maximum of 0.60 [56].
- The range of heel angles considered by the DSYHS is limited to 30° [56].
- For the method to apply, the considered vessel must fit in the range of parameters covered.

The validation of the DSYHS has been undertaken for the Sysser 62, a DSYHS vessel, chosen for its resemblance with the Stewart 34 and the availability of the towing tank results and geometry. A more relevant validation could be achieved if based on a yacht that is not part of the DSYHS. However, no towing tank data and model geometry could be found; this constitutes an area where future work could be performed. Furthermore, it is interesting to note that the DSYHS calculation method does not fully match one of the DSHYS it is based on.

The Stewart 34 meeting all the DSYHS requirement in terms of design parameters, an initial and relatively accurate resistance model can be developed for any conditions up to a Froude number of 0.50, a heel angle of 30° and a yaw angle of 3°, which would provide just about enough information for a preliminary VPP, but not for a complete and accurate one.

In order to refine the resistance prediction and consequently the VPP, a more advanced method must be used to maximise the accuracy: this is the role played by Computational Fluid Dynamics.

Chapter 4: CFD Analysis and Validation

In recent years, towing tank testing has been replaced by CFD, as illustrated by the change in use of those two design tools in the America's Cup from 1995 to 2010, presented in Figure 13.

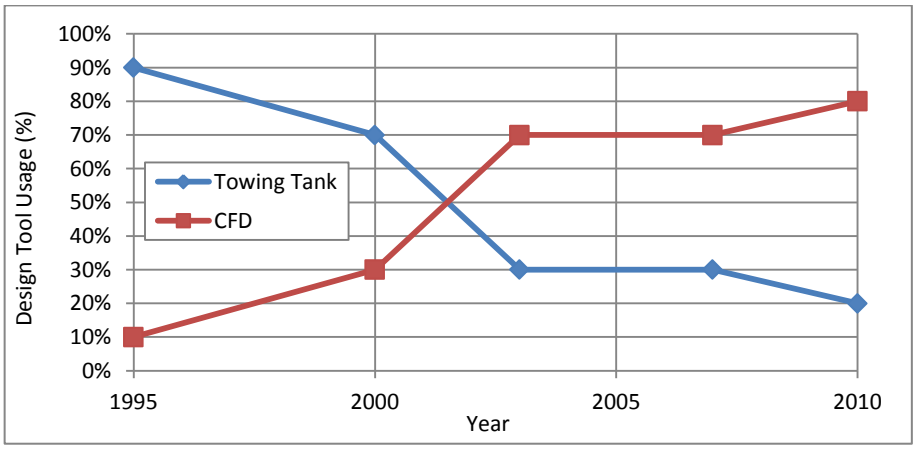

Figure 13: *Design tool usage in the America's Cup from 1995 to 2010. Data edited from [91].*

Progress made in both fluid dynamics and computational power have made CFD a very attractive tool, which is much cheaper and less time consuming than towing tank testing (providing sufficient computational resources are available). In addition, towing tank facilities are not always available: there are none in New Zealand for instance; hence the interest in CFD for the resistance prediction of yachts and the resulting VPP applications.

Computational fluid dynamics will be introduced, and the choice of the proposed method will be discussed. The absence of documentation relative to FS-Flow will lead to a detailed setup of the software aiming at providing a useful reference for future use. The software will then be validated against the experimental results of the Sysser 62 [18]. Finally, the hydrodynamic model of the Stewart 34 will be ascertained and compared with the DSYHS, focussing on the relevant range of parameters required for the velocity prediction program.

4.1 Rankine Source Panel Code

Computational fluid dynamics problems can be tackled in one of two ways: RANSE (Reynolds-Averaged Navier-Stokes Equations) or Rankine source panel code, based on potential flow theory. The later method has been chosen for its much shorter computation time. Advantages and disadvantages of the method will be introduced and the panel code selected will then be presented.

4.1.1 Fast Solving

A panel code only models the free surface and not the entire flow domain, resulting in much less equations to be solved, hence the much faster solving time. A large range of simulations are to be performed: preliminary tests to evaluate the software and its various configurations (countless runs), mesh refinement and convergence study (144 runs), validation against the known experimental results for the Sysser 62 (63 runs), and finally simulation of the Stewart 34 over a complete range of sailing conditions for VPP purposes (216 runs). The fast solving of the panel code is therefore desirable: each run can be performed in a matter of minutes, when several hours would be required for a RANSE solver.

As a result, the panel code can be used on a conventional laptop or desktop, whereas a cluster would be required if a RANSE analysis was conducted, introducing a dependency on the availability of computational resources. In this instance, all tests have been performed with 4 CPU (central processing units) at 1.73 GHz and 6.00 Go of RAM (random-access memory).

Solving time is the major advantage of panel code that led to its use over RANSE. Panel code however has some disadvantages that will influence the accuracy of the simulations.

4.1.2 Disadvantages of Panel Code

4.1.2.1 Inviscid Flow

One of the assumptions of potential flow is the inviscid nature of the flow, i.e. the flow has no viscosity. In the case of a sailing yacht, the viscous drag component is therefore not solved for, but empirically added using the ITTC 1975 friction coefficient [32] and the dynamic wetted surface area, taking into account the wave pattern and free surface deformation generated. This constitutes a rough approximation compared to RANSE where the boundary layer can accurately be modelled, and thus the viscous resistance obtained.

4.1.2.2 Wake Issue

With a panel code, the wake needs to be modelled. In the case of a sailing yacht, the wake of the keel is a critical component that has a large influence on the flow experienced by the rudder. The wake must therefore be defined. In FS-Flow, the panel code used, the wake is automatically generated. There is however only minimal control over it, and the tip vortex and inherent roll up are not modelled.

4.1.2.3 Kutta Condition

In order to calculate the lift, the Kutta condition (flow leaving the trailing edge tangentially [63]) has to be enforced. This condition makes it difficult to define a yacht hull as a lifting body: the side force generated by the asymmetry of the waterplane as the yacht heels is therefore neglected. While the Kutta condition is valid for foils, it is insensitive to separation and stall, and its use at high leeway angle is debatable.

The main disadvantages of panel codes have been presented; the precise panel code employed for the hydrodynamic model of the Sysser 62 and the Stewart 34 will now be presented.

4.1.3 FS-Flow

Part of the FutureShip software suite developed by Germanischer-Lloyds [26], FS-Flow [24] has been used for this project. Although presented as a general purpose code, FS-Flow has been developed with a clear emphasis on ship design, and more precisely optimisation of ships forebody. Indeed, the user manual [26] clearly states that:

"*The integral resistance values are primarily indicative. However, it is commonly agreed […] that the design ranking is still correct*".

The panel code therefore appears to have been primarily developed to compare and select ship designs; this is the first factor that justifies the need for a validation of the panel code. The second one is the absence on literature relative the use or results generated by FS-Flow.

The use and features of FS-Flow will first be presented in Section 4.2. To ascertain the reliability of the code for sailing yachts, it will then be validated against the experimental towing tank data of the Sysser 62, presented in Section 4.3.

4.2 FS-Flow: Setup and Use

In the absence of guidance on the use of the software, some general comments and description of the panel code and its setup are described in this section

4.2.1 Converting Geometry

The model of the Sysser 62 is made available by Delft University [18] as a Maxsurf file (.msd), however, an IGES file (.igs) is required to be input into FS-Flow. Maxsurf [9] itself is not able to convert the file into an IGES. The Maxsurf model therefore needs to be exported as 3D NURBS, then opened in Hydrolink [7] where the model can be saved as a 3D IGES. Unfortunately, Maxsurf and FS-Flow do not share the same reference coordinate system. Being a yacht design software, Maxsurf presents a starboard view of the boat and therefore uses a right handed coordinate system, whereas FS-Flow operates in a left handed coordinate system. The model therefore needs to be transformed into a left handed coordinate system before being input in FS-Flow. This has been realised using Rhinoceros [77].

4.2.2 Importing Geometry

When importing the model into FS-Flow, only one half is modelled. Importing two separate halves did not prove to be a suitable solution. The geometry must therefore be duplicated within FS-Flow; this has been achieved using the code presented in Figure 14.

```
Name GEOMETRYNAME
Type poly
columns 2
Surfaces Port,Starboard

Port <<eod_Port
Type igs
file FILENAME.igs
index 0
Orientation Exch
Scale 1,1,1
eod_Port

Starboard <<eod_Starboard
Type igs
file FILENAME.igs
index 0
Orientation Exch, ReverseU
Scale 1,-1,1
Transform R:1,0,0,-180
eod_Starboard
```

Figure 14: *Code for importing the model geometry into FS Flow.*

The keel and rudder have been imported in a similar fashion, but can alternatively be modelled using the NACA profile generator part of FS-Flow.

4.2.3 Meshing

FS-Flow features an automatic mesh generator; a range of mesh types are available depending on the nature of the geometry modelled, as presented hereafter.

4.2.3.1 Hull Mesh

Specifically designed for hulls, the hull mesh generates ranking source panels on the selected surface. The definition of the intersection with the free surface results in only the underwater part of the hull being modelled (thus ascertaining the wetted area used for the empirical viscous drag calculation). The hull mesh is remapped after each iteration to take into account the changes in the free surface.

4.2.3.2 Free Surface and Transom Mesh

The free surface mesh enables to model the surface of the water. It needs to start upstream, end downstream, and extend wider than the model; the intersections with the hull also need to be properly defined. The free surface is divided into 3 areas: a port and starboard side, and a transom mesh. The different mesh areas (hull mesh (1), port (2), starboard (3) and transom (4)) are presented in Figure 15, while the hull and free surface intersections definitions are to be found in Table 3.

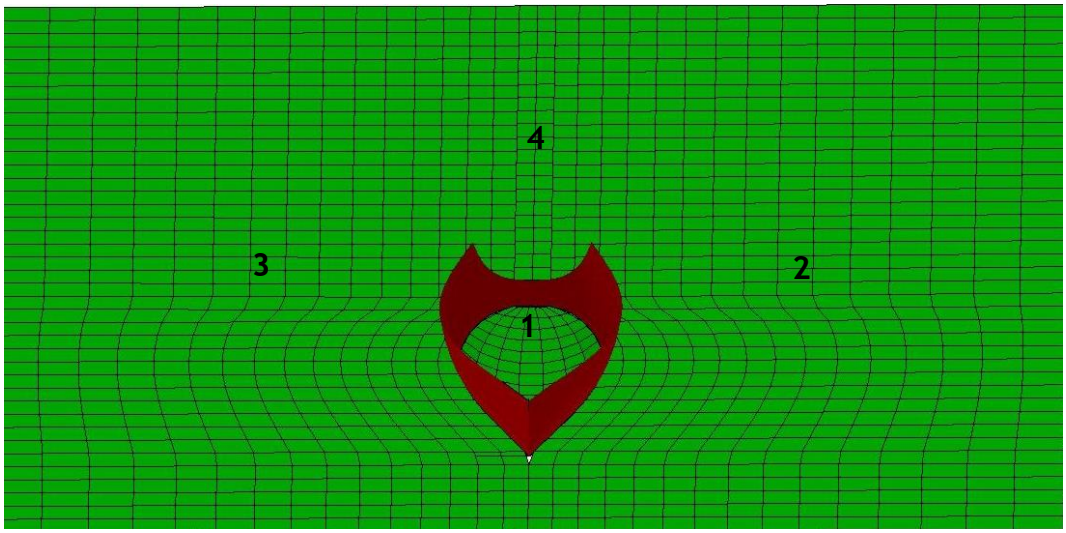

Figure 15: *Sysser 62 meshing (exaggerated for clarity) realised in FS-Flow.*

Mesh	Intersection type	Intersection code
Port	Intersection4	2:Hull
Starboard	Intersection2	4:Hull
Transom	Intersection1	3:Hull

Table 3: *Free surface intersections.*

4.2.3.3 Lift Mesh

Elements generating lift (such as the keel and rudder), are meshed using a lift mesh, that also feature an automatic wake generation, as shown for the keel wake in green in Figure 16.

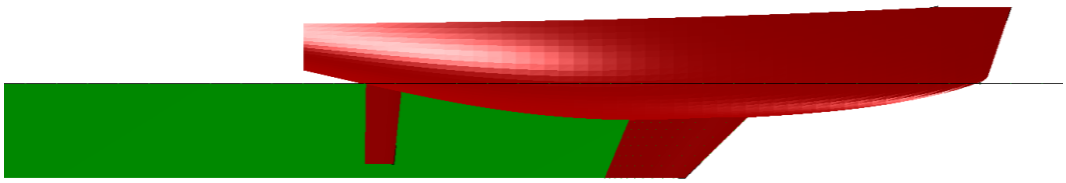

Figure 16: *Illustration of the keel wake for the Sysser 62.*

Once the geometries are meshed, various parameters need to be set up before solving.

4.2.4 Set up

The setup of the major control categories are presented in this section.

4.2.4.1 Viscous Drag

For the computation of the viscous drag, a range of correlation lines are proposed: the ITTC 1957 has been selected as it the most used and the one recommended by the ITTC [43]. The Reynolds length can also be selected. In the case of the Sysser 62, 0.7 has been chosen to match the DSYHS assumption [56] and provide a more relevant comparison. However, for the Stewart 34, 0.9 has been used as it is more representative of modern designs [56].

4.2.4.2 Body

The weight of the yacht and position of the centre of gravity are to be specified, as well the location of the centre of effort. The experimental aerodynamic model of the Stewart 34 [99] has been used to assess the position of the centre of effort. The average value for upwind has been used, despite the changes inherent to the trim of the sails, heel angle and apparent wind angle.

4.2.4.3 Flow

The flow speed and direction can be adjusted in order to achieve the desired Froude numbers and leeway angles. In addition, the model has been set to be free to heave and trim, replicating the conditions of towing tank testing.

4.2.4.4 Fluid

Fluid density and viscosity have been specified: fresh water for the Sysser 62 since it has been tested in a fresh water towing tank, and sea water for the Stewart 34 to replicate its sailing environment.

4.2.4.5 Convergence

The main convergence criterion concerns the wave height, and has been set to 0.0001. At the highest Froude numbers, when convergence was not achieved, dropping the convergence criterion to 0.0005 proved to have a positive impact.

4.2.4.5 Relax

Relaxation factors for multiple parameters can be specified. A value of 0.7 has been used up to a Froude number of 0.35; past this point, the relaxation factor was dropped to 0.2 in order to reduce the instabilities of the code and achieve convergence at higher Froude number.

Finally, the simulations can be performed; a number of iteration will be carried out until convergence is achieved.

4.2.5 Results

A typical result window is show in Figure 17; the wave height is plotted on the top half, while the iteration diagram is displayed on the bottom half.

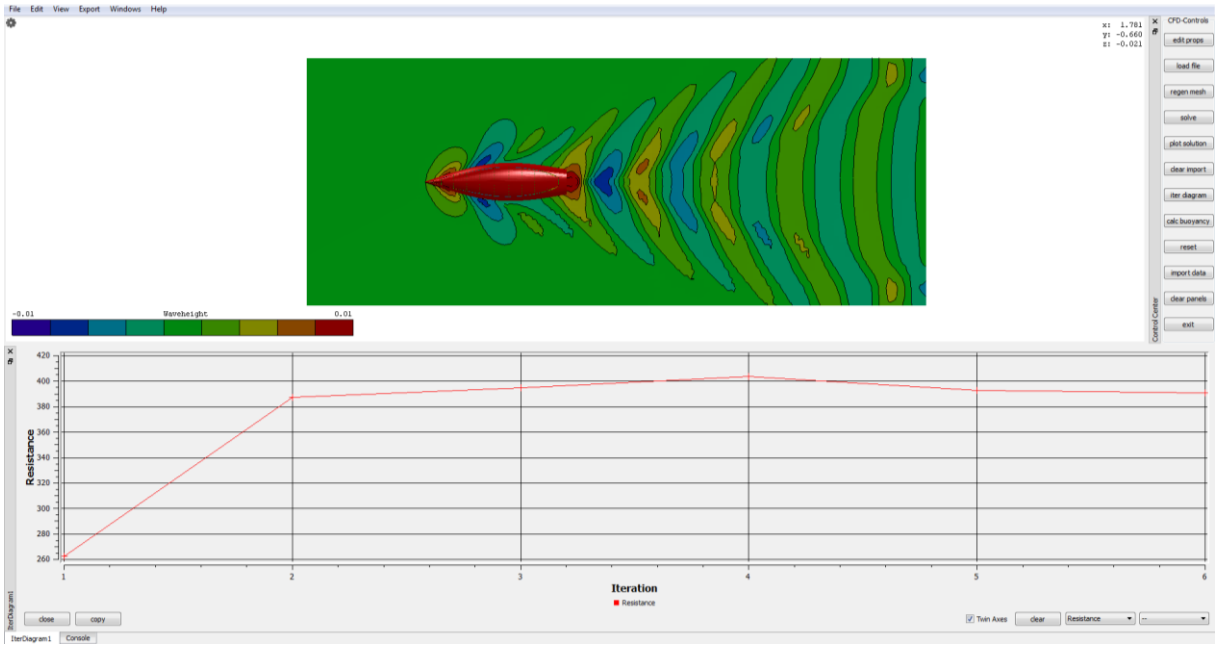

Figure 17: *Typical FS-Flow simulation.*

The setup of the software has been introduced, further aspects such as the domain size and mesh density will be ascertained as part of the validation before generating results for the Sysser 62 and Stewart 34.

4.3 Verification and Validation: Sysser 62

The relatively little use of FS-Flow and the absence of inherent publications make the validation an important part of the analysis.

The aim is to compare the results achieved using the panel code with the experimental data of Sysser 62 to ascertain the level of accuracy of the CFD analysis. Considering the incapacity of the DSYHS to precisely calculate the resistance at high Froude numbers due to the change of sailing regime, this would have represented an area of particular interest. However, the panel code developed instabilities past a Froude number of 0.35, and no convergence was possible past 0.50.

A convergence study will be undertaken to establish the optimum mesh density to minimize computation time while maximising the accuracy. The impact of the dimensions of the free surface and its influence of the accuracy of the results is also to be studied.

4.3.1 Domain Size

Domain sizes are generally defined in term of the length L of the yacht. For a fixed mesh density (Δx=0.05), the upright resistance of the Sysser 62 has been assessed for 4 domain sizes: 7L long by 3L wide, 5L long by 2L wide, 4L long by 1.5L wide and 3L long by 1L wide. The domain size proved to have no impact on the resistance prediction; the difference (Δ) in resistance between the CFD calculation and experimental results is presented in Figure 18. All results are within the repeatability accuracy of the panel code. The only noticeable difference is the shorter solving time for smaller domains. Indeed, the mesh density being constant, a smaller domain results in less elements, and therefore less equations to solve.

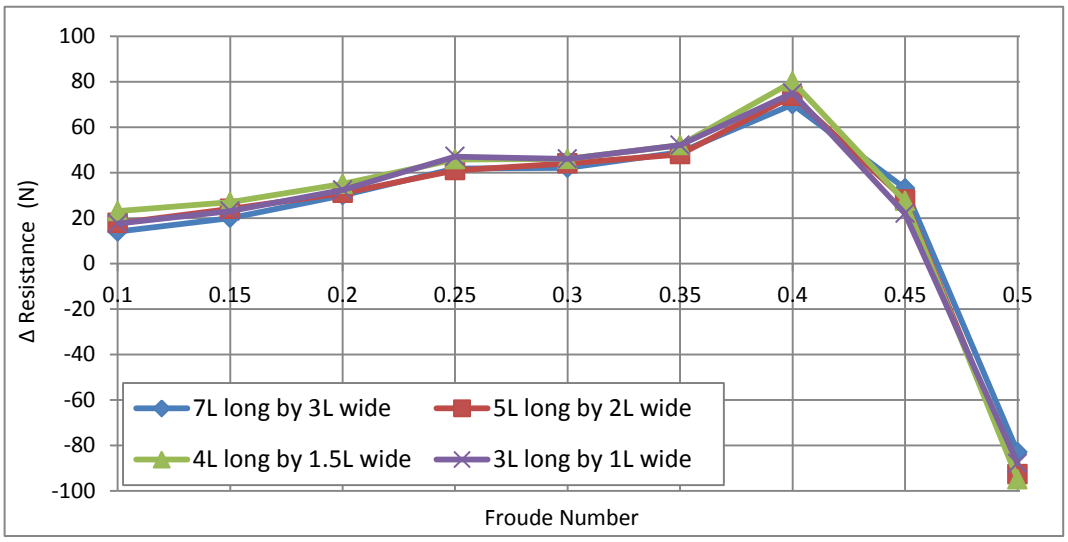

Figure 18: *Impact of the domain size on the resistance (Δx=0.05).*

Despite the temptation to go for the smallest domain size since the results are identical for a lesser solving time, the domain size retained is 5L long (1L upstream, 3L downstream) by 2 L wide. On the one hand, the solving time is still only of the order of a few minutes. On the other hand, it enables to visually check the free surface deformation and wave pattern, ensuring it matches the Kelvin wave pattern for instance.

4.3.2 Kelvin Wave Pattern

The waves generated by a vessel obeys the Kelvin wave pattern, with two characteristic angles: 19.47° and 54.4°, both appear to be correct on the free surface deformation generated by FS-Flow, as depicted in Figure 19.

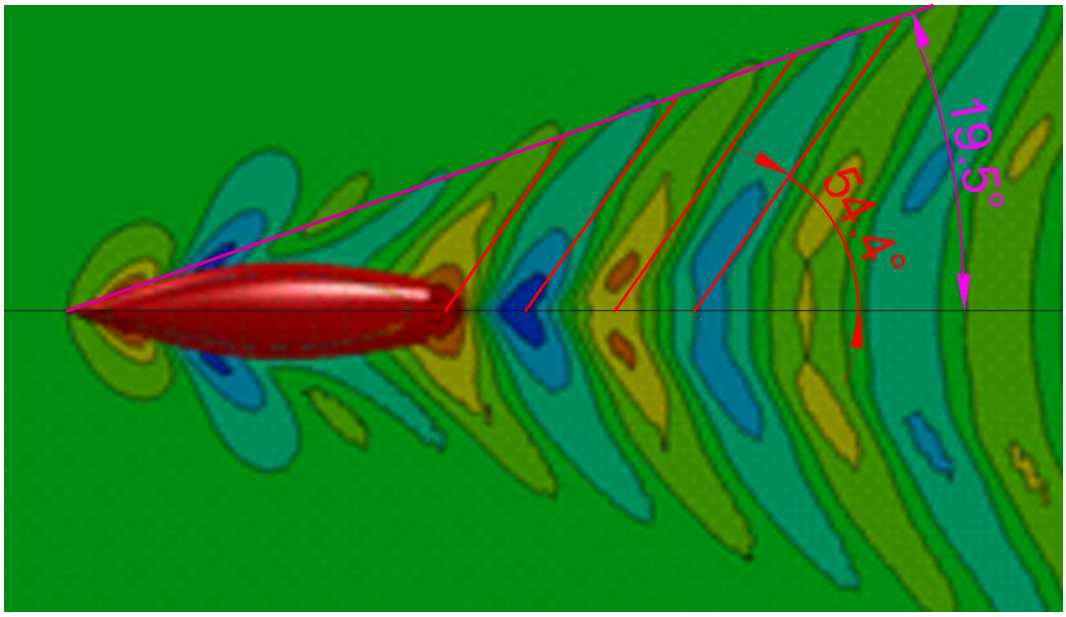

Figure 19: *Kelvin wave pattern check.*

4.3.3 Mesh Density

For the established domain size (5L by 2L), a mesh refinement study has been conducted for Δx having the value of: 0.20, 0.10, 0.05, 0.025. Note that the panel code did not prove to be able to handle a mesh finer than Δx = 0.025, crashing at the first iteration.

As expected, the finer the mesh the lesser the resistance difference between the experimental data and the CFD results, as illustrated in Figure 20.

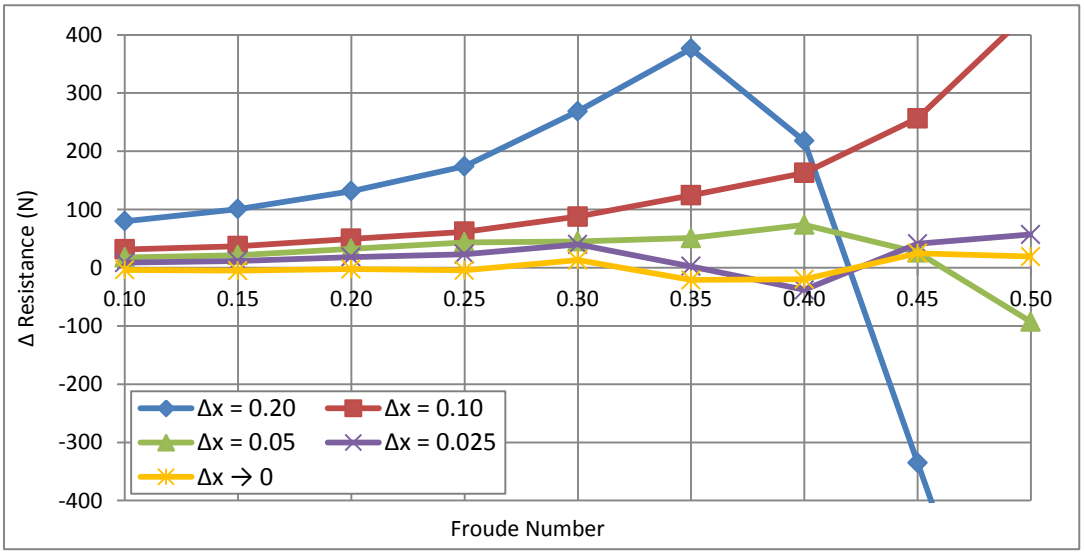

Figure 20: *Impact of the mesh density on the resistance.*

It is to be noted that the orange line represents the solution to which the panel code tends as the mesh gets infinitely fine, as highlighted in the convergence study.

4.3.4 Convergence Study

A convergence study has been conducted in accordance with the ITTC guidelines [46]: considering at least 3 solutions (4 are presented in this instance), with Δx as the only varying parameter.

As the mesh is refined, the solution appears to vary linearly with Δx (thus demonstration the first order nature of the panel code) and tends towards a specific value. A typical example is shown for a Froude number of 0.25 in Figure 21.

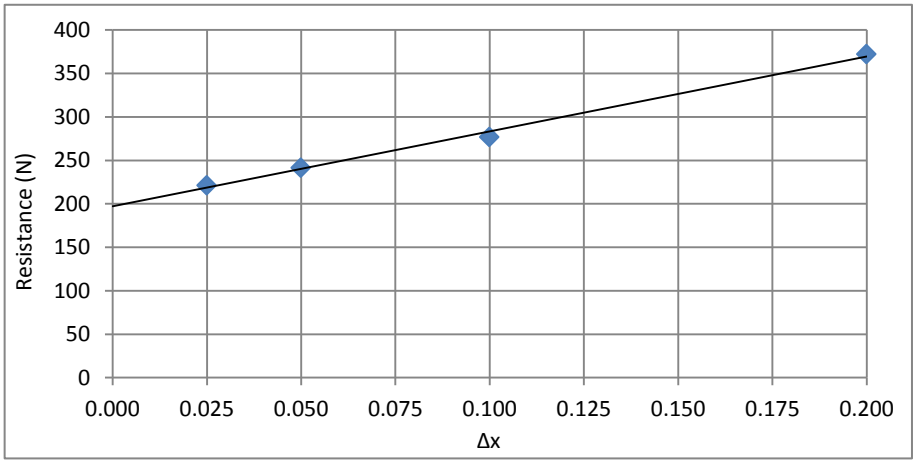

Figure 21: *Convergence study at Fn = 0.25.*

This is however only valid up to a Froude number of 0.35. At higher Froude numbers, the panel code does not provide a consistent convergence as the mesh is refined. Figure 22 exhibits such behaviour at a Froude number of 0.45, which demonstrates the instability of the panel code and inherent issues regarding the results at high Froude numbers.

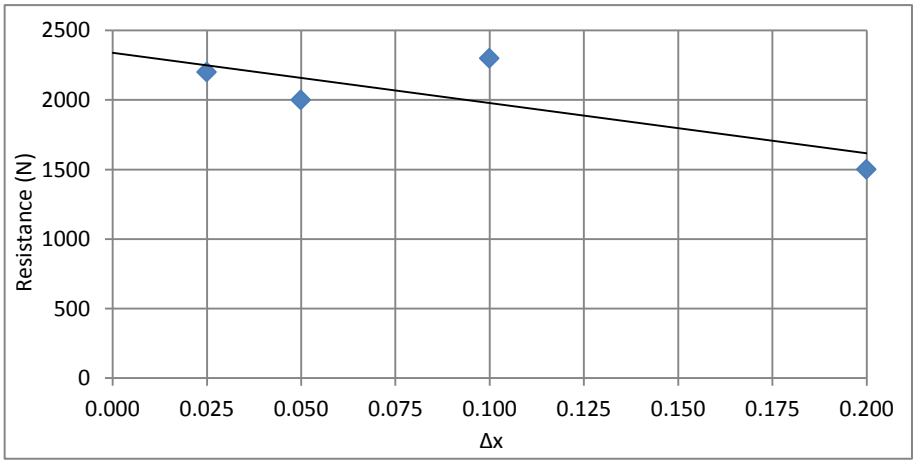

Figure 22: *Convergence study at Fn = 0.45.*

The use of a finer mesh will therefore be closer to the solution the panel code tends to; the drawback being the increased solving time.

4.3.5 Error Estimation

The discretization error and grid convergence index (GCI) have been assessed respectively based on Richardson extrapolation and the Roache and Celik error estimation, both detailed in [15].

First of all, the grid size h is ascertained for 3 different meshes based on the number of elements N and the area A (since the free surface mesh is 2 dimensional) [15]:

$$h = \left[\frac{A}{N}\right]^{1/2} \quad \textbf{Equation 17}$$

Where $h_1 < h_2 < h_3$. The grid refinement factor r can then be established, aiming at values higher than 1.3 [15]:

$$r_{21} = \frac{h_2}{h_1} \quad \textbf{Equation 18}$$

For $r_{21} \neq r_{32}$, the apparent order p is given by [15]:

$$p = \frac{1}{\ln(r_{21})}\left|ln\left|\frac{\varepsilon_{32}}{\varepsilon_{21}} + \ln\frac{r_{21}^p - s}{r_{32}^p - s}\right|\right| \quad \textbf{Equation 19}$$

Where:

$$\varepsilon_{21} = f_2 - f_1 \quad \textbf{Equation 20}$$

And:

$$s = 1 \cdot sign\left(\frac{\varepsilon_{32}}{\varepsilon_{21}}\right) \quad \textbf{Equation 21}$$

From the solutions f ascertained for different grid sizes, the extrapolated solution f_{ext} is [15]:

$$f_{ext}^{21} = \frac{r_{21}^p f_1 - f_2}{r_{21}^p - 1} \quad \textbf{Equation 22}$$

Furthermore, the approximate relative error e_a can be found [15]:

$$e_a^{21} = \left|\frac{f_1 - f_2}{f_1}\right| \quad \textbf{Equation 23}$$

As well as the extrapolated relative error e_{ext} [15]:

$$e_{ext}^{21} = \left|\frac{f_{extrap}^{21} - f_1}{f_{ext}^{21}}\right| \quad \textbf{Equation 24}$$

Finally, the grid convergence index GCI can be ascertained [15]:

$$GCI^{21} = \frac{Fs|e_a^{21}|}{r_{21}^p - 1} \quad \textbf{Equation 25}$$

Where the safety factor Fs has been taken as 1.25 since 3 grid sizes have been considered.

The results for the upright resistance at Froude numbers of 0.10, 0.30 and 0.50 are presented in Table 4, once again highlighting instabilities in the code at higher Froude numbers, resulting in a large error and GCI.

Richardson Extrapolation and Roache and Celik Error Estimation			
Fn	0.10	0.30	0.50
r_{21}	1.42	1.42	1.42
r_{32}	1.49	1.49	1.49
ε_{32}	3.74	42.69	534.32
ε_{21}	1.05	10.06	279.71
p	3.21	3.49	1.73
F^{12}_{ext}	35	359	3479
e^{21}_{a}	3.0%	2.8%	8.9%
e^{21}_{ext}	1.4%	1.1%	9.5%
GCI^{21}	1.8%	1.4%	13.1%

Table 4: *Richardson extrapolation and error estimation at various Froude numbers.*

4.3.6 Solving time

Much faster solving time was achieved by slowly increasing the boat speed and restarting from the previous solution. In fact, for the highest Froude numbers where the code is unstable, convergence was only possible by starting at a lower Froude number and slowly increasing the speed.

The solving time of the panel code is very quick: for the finest mesh at the highest Froude number, less than 10 minutes per run was required. The solving time appears to vary quasi-linearly with the boat speed, as depicted in Figure 23. This is due to the greater number of iterations required as the boat speed is increased.

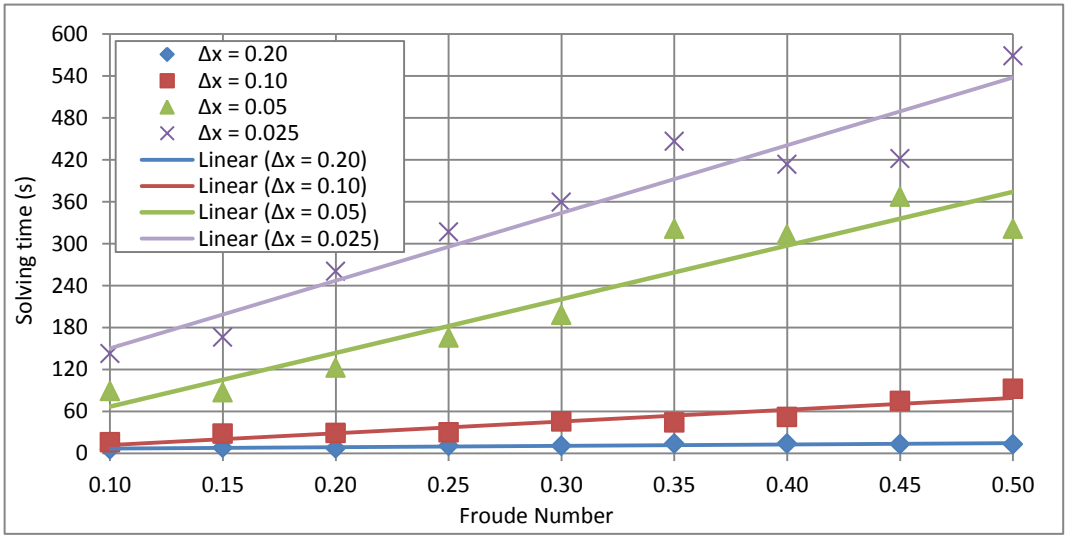

Figure 23: *Variation of the solving time with Froude number.*

The solving time also appears be proportional to the number of elements N, and not N^3 as expected [30], as shown in Figure 24.

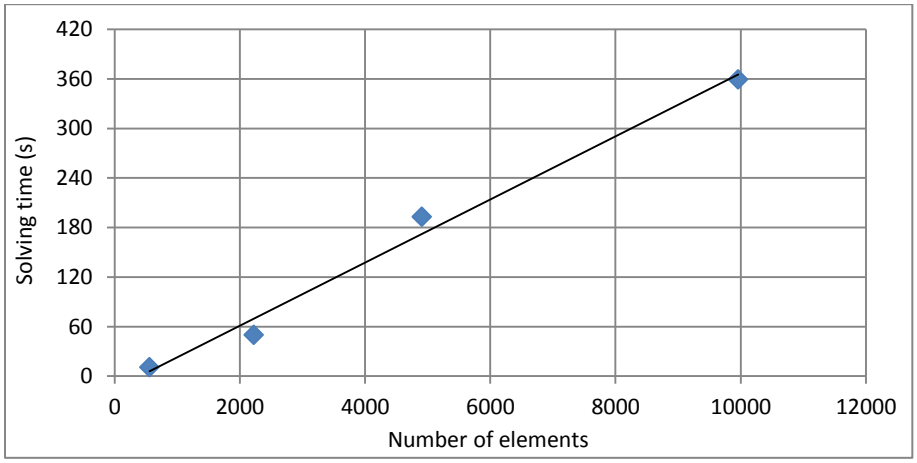

Figure 24: *Variation of the solving time with the number of elements at Fn = 0.30.*

From a user perspective, the compromise between solving time and error is critical, and it presented in Figure 25.

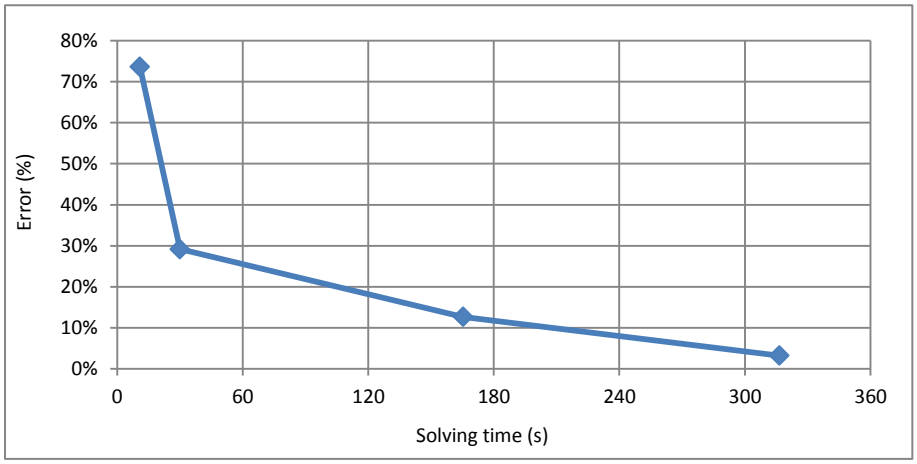

Figure 25: *Variation of solving time with error at Fn = 0.30.*

Improved accuracy requires significant increase in solving time. However, the panel code enables to keep the solving time very reasonable (in the order of minutes when RANSE solver would be hours). As a result, the finest mesh (Δx=0.025) will be used in this instance in order to maximise the accuracy.

4.3.7 Results

The results for the Sysser 62, performed with a mesh density of Δx = 0.025 and a domain size 5L by 2L will be detailed and compared with the experimental data as well as the DSYHS in this section.

4.3.7.1 Upright

Up to a Froude number of 0.35 (where the panel code is stable) a very good fit with the experimental data is achieved. Past this point, the difference in resistance is increasingly greater, and does not provide a particularly accurate estimate of the total resistance, as shown in Figure 26. Regarding the frictional resistance, both are based on the same theory (ITTC 1957 frictional line, and Reynolds length of 70% of the Lwl), the only difference being that the DSYHS is based on the static wetted surface area whereas FS-Flow inputs the dynamic wetted surface area as the wave pattern evolves.

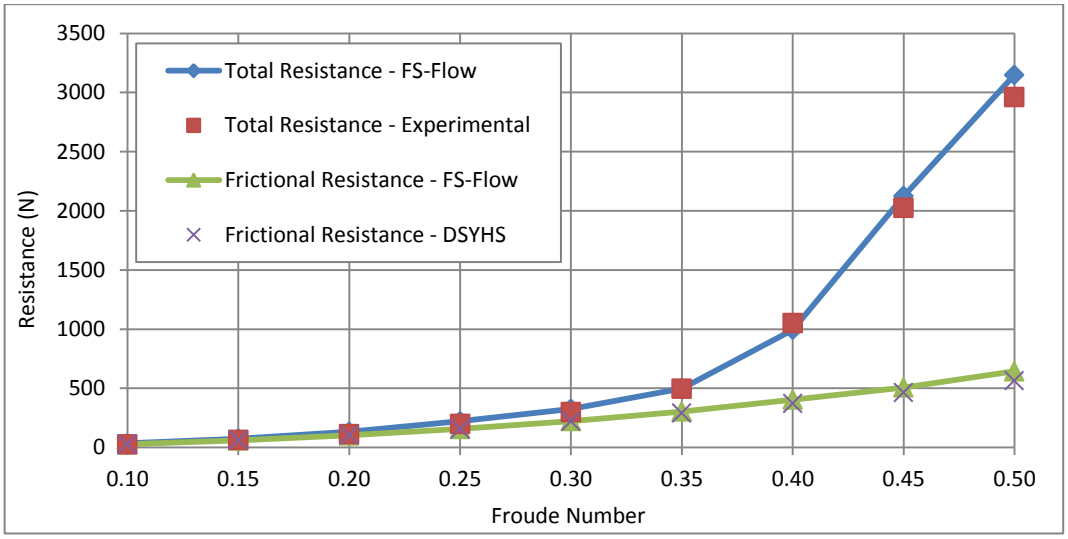

Figure 26: *Bare hull upright resistance of the Sysser 62.*

The bare hull is a good starting point to ensure appropriate use of the code, it is however not representative of a sailing yacht, fitted with appendages and that will operate at heel and yaw angles.

4.3.7.2 Heeled and Yawed

The Sysser 62 was tested at 3 heel angles, namely 10°, 20° and 30° and for 2 yaw angles: 3.1° and 6.1° in order to provide a comparison with the experimental data. The DSYHS calculations are presented for 10° of heel in Figure 27. Further detail and results at 20° and 30° of heel are to be found in Appendix D.

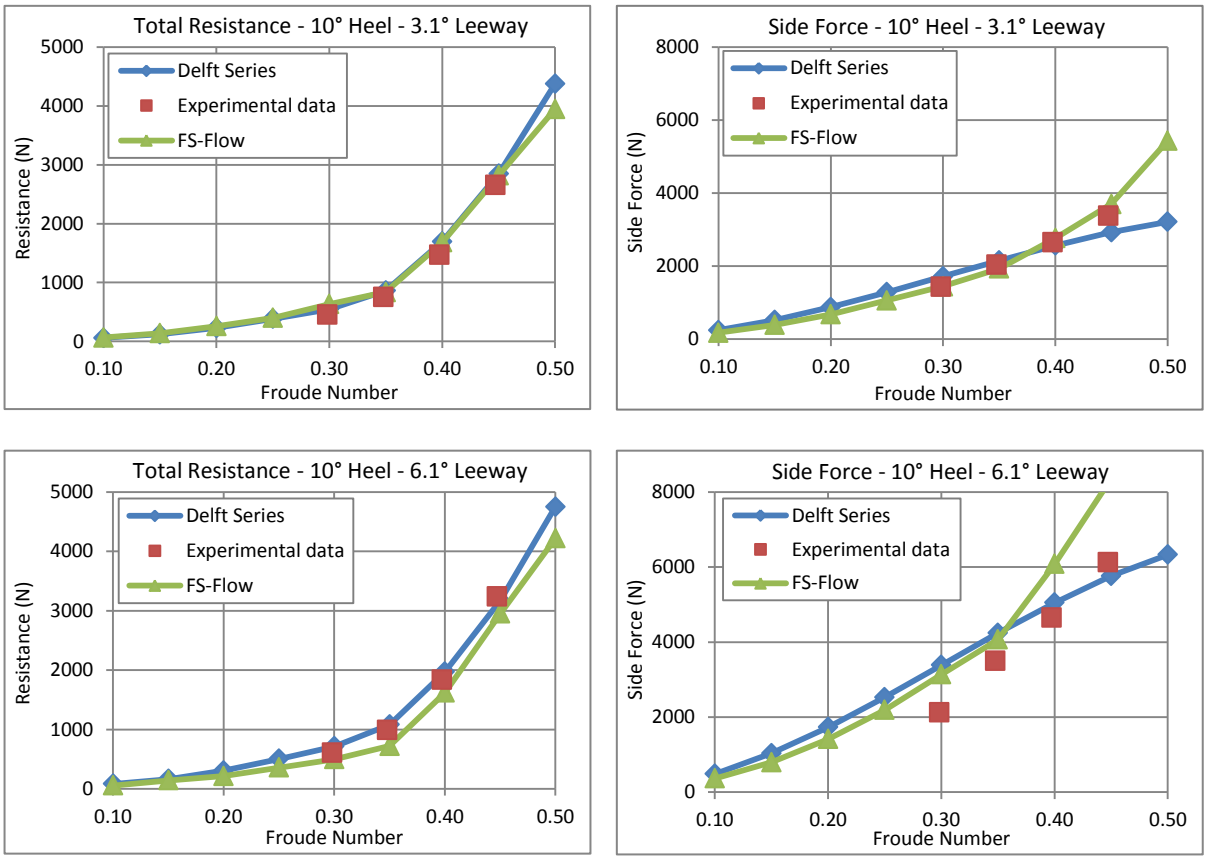

Figure 27: *DSYHS, experimental data and CFD comparison at 10° of heel.*

At moderate yaw angle (3.1°), the resistance and side force prediction appear to be good estimates in comparison with the experimental data, especially below a Froude number of 0.40, where the panel code remains stable; some discrepancies are exhibited at higher Froude numbers.

At high yaw angle (6.1°), the prediction appears incoherent: the resistance is under-estimated while a higher side force is generated. Trials to improve the accuracy of the results (modifying mesh densities, keel wake mesh or convergence parameters) proved unsuccessful.

Possible explanations for the over-predicted lift generated by the appendages are incorrect modelling of the automatically generated keel wake (over which very little control is allowed by FS-Flow), or the absence of separation due to the Kutta condition. A higher lift should generate a larger induced drag, the total resistance is however clearly under predicted. There are therefore some clear limitations to the use of FS-Flow for the modelling of sailing yachts.

4.3.8 Conclusions

A validation of the panel code FS-Flow has been undertaken against the experimental results of the Sysser 62 in order to assess the reliability of the panel code for the hydrodynamic model of sailing yachts. The setup and use of the software have been presented, and the analysis conducted revealed that the behaviour of the panel code can be dived into 3 distinct ranges of Froude number:

- Up to Fn = 0.35, the panel code is stable, convergence is always achieved, few iterations are required, no particular issue has been noticed. In addition, the discretization error has been proven to be minimal.

- From Fn = 0.40 to Fn = 0.50, some instabilities have been noted. Decreasing the relaxation factor, slowly increasing the speed to reach the desired one and reducing the convergence criteria proved to help achieve convergence. A much larger number of iterations are however required, and many attempts are usually necessary to achieve convergence. The results are generally not as accurate as those generate in the stable region of the code, with a much larger error associated with them.

- Higher than Fn = 0.50, no convergence proved to be possible, the panel code being too unstable to carry out iterations. It is unknown whether the use of a greater computational power would enable to achieve convergence at the highest Froude numbers. Further investigation on the origin of the instabilities and possible way to remedy this issue would be advised as future work to be undertaken.

At 3.1° of leeway, good correlation with experimental data was achieved upright and up to 30° of heel for both the resistance and side force, particularly in the stable zone of the code. Conversely, the results at 6.1° of leeway are incoherent and are inappropriate for VPP use; the DSYHS is however valid for the resistance prediction.

FS-Flow presents some clear restrictions at high Froude numbers and high leeway angles. The restricted amount of experimental data does not enable to precisely ascertain at which point the prediction starts being inaccurate, and therefore should not be considered valid past a yaw angle of 3.1°.

The limitations of the panel code can be linked to its intended use. Indeed, FS-Flow was primarily developed for comparison of ship resistance. Since ships operate at low Froude number, without leeway, the panel code is appropriate for such analysis, but not as relevant for sailing yacht at high Froude numbers and yaw angles.

The hydrodynamic model of the Stewart 34 will now be developed using FS-Flow. The analysis can only be as accurate as the model of the Stewart 34 is, hence the need to create an accurate 3 dimensional model of the yacht. This has been performed via 3D lofting: the original table of offsets [84] has been converted into metric (see Appendix E), to then loft the boat in 3 dimensions using Maxsurf [9]. The process is detailed and illustrated in Appendix F. The model of the Stewart 34 has then been used to perform the CFD simulations.

4.4 Application to the Stewart 34

Having evaluated the reliability of the panel code, the CFD analysis of the Stewart 34 can be undertaken; the test matrix will be defined before performing the simulations.

4.4.1 Test Matrix

The analysis of the Stewart 34 must thoroughly cover the sailing conditions of the vessel while keeping the number of CFD simulations to be realised to a manageable amount, hence the need to ascertain the appropriate range and interval of parameters to consider.

In this instance, an empirical 4 degrees of freedom VPP has been developed at an early stage of the project to establish the appropriate range of Froude numbers, heel and yaw angles. The process is presented in Section 5.2 and detailed in Appendix G. The results led to the following test matrix:

- Froude number from 0.10 to 0.50 in 0.05 increments.
- Heel angles of 0°, 7.5°, 15°, 22.5°, 28° and 35°.
- Leeway angles of 0°, 2.5°, 5° and 7.5°.

A total of 9 Froude numbers, 6 heel angles and 4 yaw angles will be taken into account, resulting in 216 CFD simulations, a number deemed appropriate given the relatively quick solving time of panel codes. The hydrodynamic model of the Stewart 34 can now be developed.

4.4.2 Analysis of the Stewart 34

For the analysis of the Stewart 34, the same procedure as presented for the Sysser 62 has been followed. The IGES geometry has been imported into FS-Flow, meshes and intersections were then generated, and the same analysis setup was applied. The influence of the domain size and mesh density have been studied to ensure consistent results with the analysis of the Sysser 62 were achieved. Identical conclusions have been drawn and the domain size (5L long by 2L wide) and mesh density (Δx = 0.025) were conserved for the analysis of the Stewart 34. The same regions of stability and instability of the panel code have been identified, and once again no convergence past a Froude number 0.50 proved to be possible.

Sample results for the hydrodynamic resistance and side force of the Stewart 34 at 7.5° of heel are presented in Figure 28, together with the DSYHS calculations. The complete results for the entire test matrix are to be found in Appendix H.

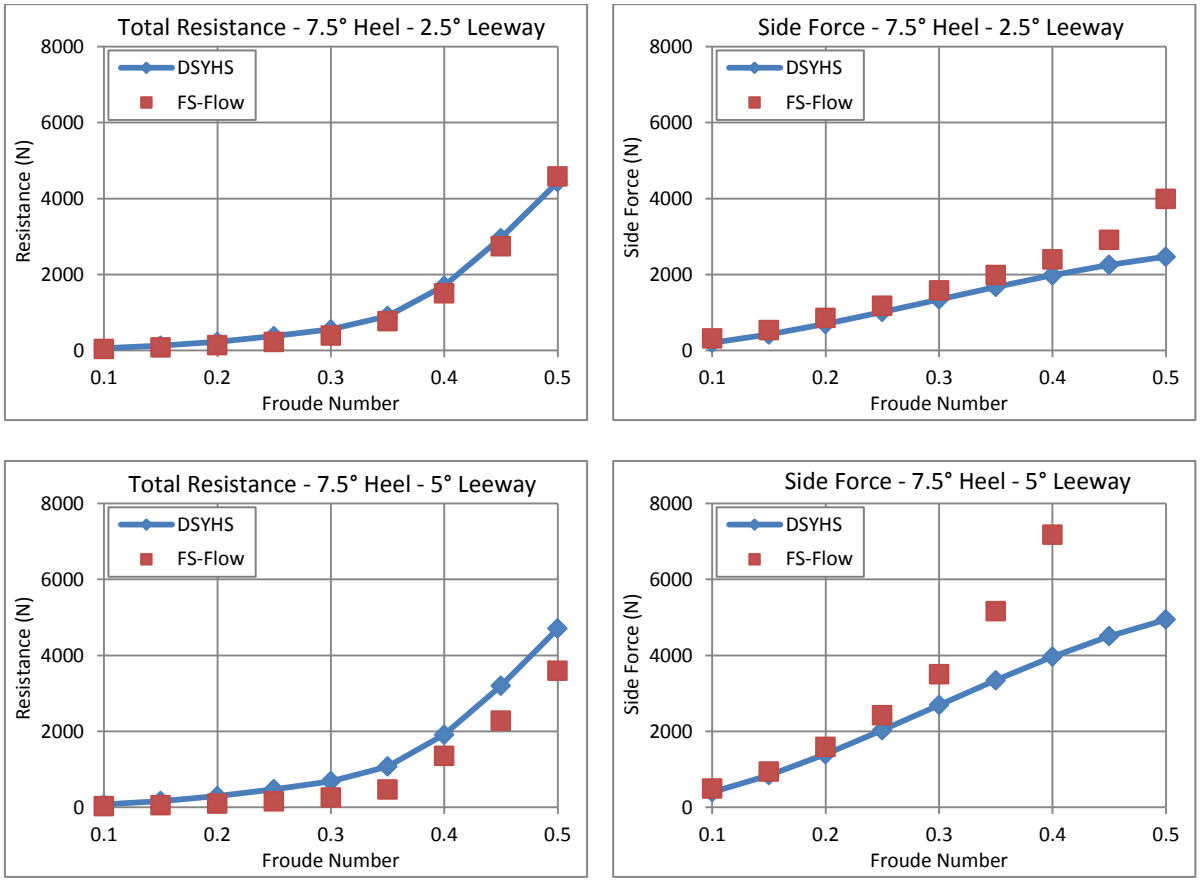

Figure 28: *Typical example of FS-Flow results for the hydrodynamic model of the Stewart 34.*

Similar conclusions as drawn from the Sysser 62 validation can be made. The resistance and side force prediction are valid for small angle of yaw (less than 3°), and discrepancies are likely to occur at high Froude numbers, especially for the side force.

4.4.3 Conclusions

The test matrix developed in accordance with the empirical VPP enabled to minimize the number of simulations to be performed and therefore the computation time, while focussing the analysis on the relevant range of parameters for the purpose of the VPP.

The hydrodynamic model developed using FS-flow can be judge appropriate over the range of heel angle tested up to 2.5° of yaw. At higher angles of yaw (respectively 5 and 7.5°), the resistance is under-estimated and the side force over-estimated.

4.5 Conclusions

A Rankine source panel code has been chosen over a RANSE solver for the much faster solving time. In this instance, FS-Flow has been used. The panel code setup has been presented in order to provide future reference for the use of FS-Flow. The absence of literature related to the panel code made the understanding and setup a major part of the project.

The hydrodynamic model of the Sysser 62 was developed to verify the correct use of the software, validate the hydrodynamic model against experimental results, and conduct optimisation studies.

The domain size did not prove to have any significant impact on the results. Conversely, the mesh density revealed that a finer mesh tends to minimize the error. Indeed, the convergence study proved that as the mesh is refined, the code tends to a precise solution.

The panel code is stable up to a Froude number of 0.35, past this point, convergence is harder to achieve and the accuracy of the results decreases. No convergence past a Froude number of 0.50 was achieved.

The validation against experimental results revealed a good fit for both the resistance and side force at low yaw angles (3° or less) in the stable region of the code, which represents an improvement compared to the DSYHS, particularly for the side force. However, at larger yaw angles, the results are not appropriate, with the resistance significantly under estimated while the side force is largely over estimated.

This behaviour can be related to the intended development of FS-Flow: the comparison of ships design, thus explaining the stability and accuracy of the code at low Froude number and none or very little yaw angle, representative of a ship. Care should therefore be taken when using FS-Flow for sailing yachts at high angles of leeway. The hydrodynamic model of the Stewart 34 was finally developed; comparison with the DSYHS supports the limitations inherent to high yaw angles.

The FS-Flow hydrodynamic model will be used as part of the VPP for the Stewart 34. The hydrodynamic forces will be balanced against the aerodynamic forces; there is however a crucial component of the VPP missing: the transverse stability of the Stewart 34, assessed and fully detailed in Appendix I.

Chapter 5: Velocity Prediction Program

Predicting the performance of yachts has become a crucial part of the design. In the last 4 years, VPP is the area of yacht design that progressed the most, and where all the attention has been focussed, with new challenges such has VPP for the foiling catamarans of the America's Cup [13]. But performance is not only restricted to the racing yacht industry: cruiser/racers have to be more and more performant under handicap rules, and even cruising boats are now expected to be fast cruisers. Velocity prediction programs are therefore relevant to all yachts, and can be performed at various levels, from empirical 3 degrees of freedom to advanced 6 degrees of freedom ones relying on experimental hydrodynamic and aerodynamic data.

The 6 degrees of freedom of yachts will be introduced. Three VPPs and their inherent principles will then be presented:

- An empirical 4 degrees of VPP for the purpose of ascertaining the required CFD test matrix.
- A 4 degrees of freedom VPP realised with WinDesign [97] to provide a reference and comparison while performing the final VPP.
- A 6 degrees of freedom VPP using FS-Equilibrium [23] relying on the experimental hydrodynamic and aerodynamic data.

The complete performance prediction of the Stewart 34 for all 6 degrees of freedom will eventually be achieved, thus completing the primary objective this project.

5.1 Six Degrees of Freedom

Yachts are subject to 6 degrees of freedom, 3 forces (surge x, sway y and heave z) and 3 moments (roll φ, pitch θ and yaw β); some are of vital importance, while others can sometimes be neglected. The degrees of freedom are illustrated in Figure 29 and presented hereafter.

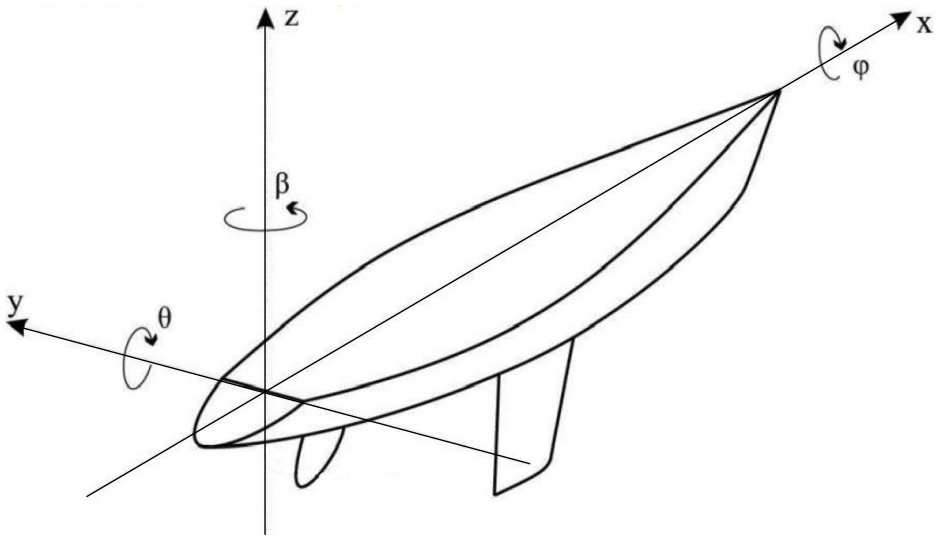

Figure 29: *Six degrees of freedom illustration, edited from [51].*

5.1.1 Forces

5.1.1.1 Surge (x)

Surge is the fore and aft movement of the yacht, i.e. the boat speed, and is the most important parameter as the speed of the vessel is the major point of interest of a VPP.

5.1.1.2 Sway (y)

Sway refers to the transverse movement of the boat, and is better known as the leeway. This is a primary component as the leeway angle constitutes the angle of attack of the flow on the keel that has to generate lift to counter act the sail side force.

5.1.1.3 Heave (z)

Heave denotes the vertical movement. On monohulls, such as the Stewart 34, heave is self-adjusted: the weight on the boat has to equal the buoyancy force. As a result, the impact of heave is minimal, and can often be neglected.

5.1.2 Moments

5.1.2.1 Roll (φ)

The rolling, or heeling moment occurs about the longitudinal axis, and is directly linked to the stability of the vessel, making it a primary component to be considered in a VPP.

5.1.2.2 Pitch (θ)

Pitch, or trim, is the moment about the transverse axis of the yacht. For monohulls, having a very large longitudinal stability, pitch is generally very small and has little effect on the boat speed.

5.1.2.3 Yaw (β)

The yaw moment about the vertical axis is relatively important to the sailing behaviour of the vessel, that can either experience lee-helm (boat heading away from the wind) or weather-helm (boat heading into to wind). This moment needs to be corrected using the rudder, which will result in an increase in drag that is quite small, but yet non-negligible.

5.1.3 VPP and Degrees of Freedom

A velocity prediction program for a monohull needs to consider at least 3 degrees of freedom: boat speed, heel and leeway angle. The rudder angle can also be added, giving a 4 degrees of freedom VPP that neglects heave and pitch, which are both very small and having minimum impact on the performance of the vessel. This is the approach taken for the preliminary empirical VPP. More advanced software will consider all 6 degrees of freedom, as it is the case for FS-Equilibrium [23] that will be used for the final VPP of the Stewart 34.

5.2 Empirical 4 Degrees of Freedom VPP

Early in the project, an empirical VPP has been performed for the Stewart 34. The primary objective being to establish the operating range of the boat for various parameters (boat speed, heel and yaw angle) in order to focus the CFD analysis on the relevant range of values, and therefore avoid unnecessary calculations. The aspects relevant to this empirical VPP are introduced hereafter.

5.2.1 Principle

The empirical VPP developed relies on the DSYHS hydrodynamic model previously introduced in Chapter 3 for the resistance and hydrodynamic side force. The aerodynamic model is based on the sail coefficients published by the Offshore Racing Congress (ORC) [69] and used as part of their VPP-based rating rule, thus providing the aerodynamic side force and drive force. The righting lever curve ascertained for the Stewart 34 in Appendix I has been used to assess the heel angle of the vessel. Furthermore, the rudder angle required to align the longitudinal centre of lateral resistance of the underwater body and the centre of effort of the sails has been considered. Finally, reef and flat have been used for the depowering of the sails.

The underpinning theory inherent to VPPs in general and the equations involved in the empirical 4 degrees of freedom VPP are fully presented and described in Appendix G.

In an iterative process, the VPP solves for the boat speed, heel angle, yaw angle and rudder angle of the Stewart 34 from a limited number of design inputs.

5.2.2 Results

The proposed empirical VPP has been used for wind speeds up to 8 m/s, equivalent to 16 knots of true wind speed or a Beaufort 4, which is the typical wind speed for which sailing yachts are designed: Martin's formula, the Dellenbaugh angle and the wind pressure coefficient all assume a wind speed of 16 knots [95].

A maximum upwind speed of 3.75 m/s has been ascertained, giving a Froude number of 0.39: this is typical of yachts sailing upwind, unable to climb over their bow wave, leading to a large resistance increase occurring at a Froude number of 0.4 where the wave making length equals the waterline length [54]. However, in the downwind case, a maximum speed of 4.42 m/s is reached, giving a Froude number of 0.46. In terms of heeling angle, the maximum value obtained is 29.78°, while the leeway does not exceed 6.27°.

The maximum values are summarised in Table 5, and then used to define the range of parameters to be taken into account for the hydrodynamic test matrix.

Maximum values	
Parameter	Empirical VPP
Froude Number	0.46
Heel angle (°)	29.78
Leeway angle (°)	6.27

Table 5: *Maximum values ascertained using the empirical VPP.*

5.2.3 Conclusions

As previously stated, the primary aim of the empirical VPP is to establish the parameters to be considered for the CFD analysis in order to cover the operating range of the Stewart 34 without performing irrelevant simulations. The test matrix is defined as follows:

- In terms of Froude number, given the maximum of 0.46, the proposed range to be tested for is from 0.10 to 0.50 in increments of 0.05. Ideally, higher Froude number would be considered (up to 0.60). However, as introduced in Section 4.3.7, no convergence was achieved past a Froude number of 0.50.
- The heel angles will match those used for the upwind wind tunnel testing [99], namely: 0°, 7.5°, 15°, 22° and 28°. Furthermore, 35° will be added to extend the range beyond the actual sailing conditions of the vessel, thus avoid to extrapolate data.
- Finally, leeway angles of 0°, 2.5°, 5° and 7.5° will be considered, once again, those values encapsulate the sailing conditions of the vessel, while the highest value enables to extend the range beyond the actual behaviour of the boat.

From an empirical 4 degrees of freedom VPP, the performance of the Stewart 34 has been assessed. The final VPP of the Stewart 34 will be based on the CFD analysis presented in Chapter 4 and the experimental aerodynamic model [12, 99]; all 6 degrees of freedom will be considered in FS-Equilibrium [23].

As an intermediate step, a VPP of the Stewart 34 has been realised using WinDesign [97]. The use of WinDesign requires inputs not available at the start of the project, hence the use of the empirical approach in the first place.

5.3 WinDesign

WinDesign is the most widely used VPP software [97], undergoing constant validation and updates, and therefore has a recognised validity that explains its popularity. The main motivation behind the realisation of this VPP is to provide a reference VPP to ensure the correct use of FS-Equilibrium and believability of the results.

5.3.1 Principle

WinDesign enables to perform 4 degrees of freedom VPPs based on a wide range of semi-empirical hydrodynamic and aerodynamic models.

The hydrodynamic model is essentially based on DSYHS with the hull measurements being based on the actual yacht, i.e. the geometry needs to be input. The Maxsurf model of the hull must be exported into Hydrolink, were it is divided into a large number of sections and converted into an IMS LPP (.lpp) file. The file can then be open in the Wolfson Unit lines processing program WinLPP [96], where the hull is regenerated and the appendages can be modelled. Finally, the file can be exported into WinDesign. The use of the lines processing program enables to assess the hydrostatics of the vessel at various heel angles, thus providing a more accurate definition of the yacht.

The stability is modelled from the $\overline{Gz}$ values presented in Appendix I.3, input for a given range of angles of heel, and then used to calculate the righting moment.

Sails and rig dimensions have been defined according to the sailplan and sails measurements stated in the class rules [85] in order for both the windage and sail forces to be established. The aerodynamic lift and drag are based on Hazen's coefficient [34], frequently used in VPPs and aerodynamic models [54].

In windy conditions, depowering the sails can results in improved performance, hence the use of depowering parameters in the VPP; WinDesign being based on the traditional reef and flat [33].

The reef function r reduces the sail area in a manner that keeps the sail aspect ratio constant; while the lift and drag are reduced due to the smaller sail area; reef also contributes to lower the centre of effort of the sails.

On the other hand, the flat parameter f does not impact on the sail area but reduces the lift coefficient, and consequently the induced drag; the parasitic drag however remains constant, as well as the height of the centre of effort.

The mathematical implications of those depowering parameters are described in Appendix G.5.

5.3.2 Results

The best boat speed for the Stewart 34 has been ascertained at true wind speeds of 4, 8, 12, 16, 20 and 25 knots and for both the jib (up to 120° TWA) and the spinnaker (from 80° TWA). It is to be noted that WinDesign does not enable to specify a precise wind speed value or unit (knots being a sensible choice for a VPP compared to meters per second).

The analysis considers 4 degrees of freedom (all but pitch and heave); results for the boat speed (in knots) are presented in Figure 30, where the jib is shown in black and the spinnaker in red; the cross over between the jib and spinnaker can be observed (intersection of the two lines). Furthermore, the angle for best Velocity Made Good (VMG) is depicted by a square.

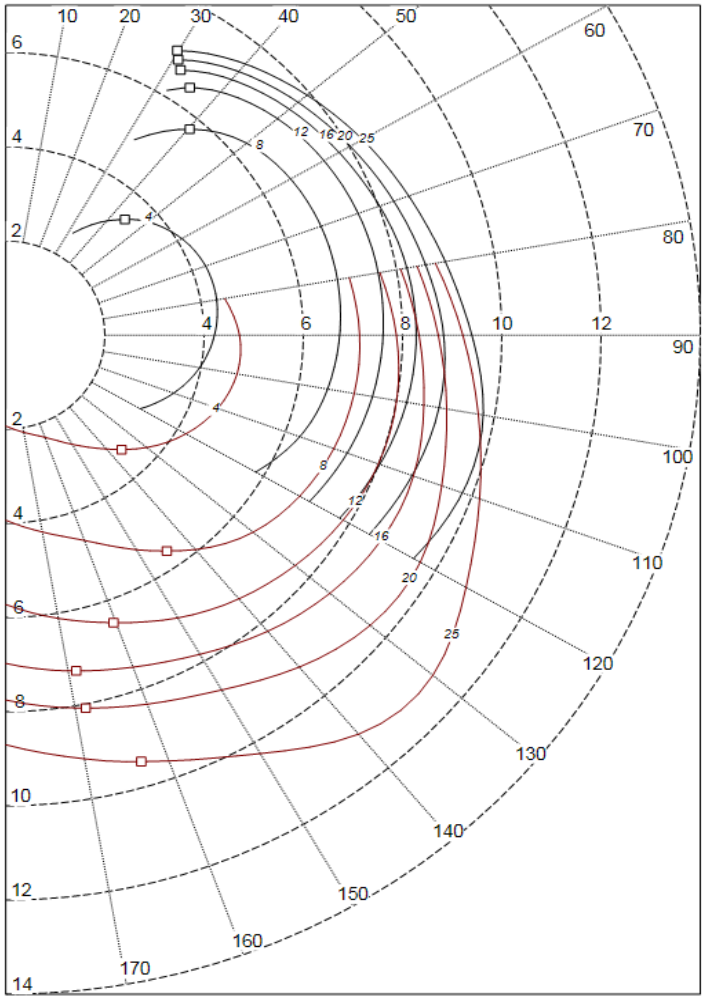

Figure 30: *Stewart 34 VPP using WinDesign.*

5.3.3 Conclusions

The sailing performance of the Stewart 34 has been assessed using WinDesign in order to ensure the reliability of the VPP later realised using FS-Equilibrium. The present VPP relies on advanced application of the DSYHS through the use of a lines processing program. A similar analysis can be conducted in FS-Equilibrium. As a result, an empirical analysis will be performed using FS-Equilibrium in order to ensure appropriate use of the program before performing the experimental VPP.

5.4 FS-Equilibrium: Setup

Part of the FutureShip suite, FS-Equilibium is a semi-empirical 6 degrees of freedom VPP that enables to input experimental data, such as the hydrodynamic and aerodynamic models in this instance. Similarly to FS-Flow, the user manual [25] is the main literature relative to FS-Equilibrium; a limited number of technical publications do however mention the use of FS-Equilibrium [14, 11]. The program and inherent setup will be presented in this section.

5.4.1 Principle

As any velocity prediction program, FS-Equilibrium relies of the balance of forces and moments to ascertain the performance of the vessel, as detailed in Appendix G. The steady state analysis iterates until convergence is achieved, and can assess all 6 degrees of freedom (provided sufficient inputs are provided). Manoeuvring can also be considered, this is however beyond the scope of this project.

A wide range of modules can be defined to perform a VPP based on either empirical or experimental data. Firstly, empirical aerodynamic and hydrodynamic modules have been defined, trying to achieve a similar setup and identical inputs as the WinDesign analysis is order to validate the use of the program. A comparison between FS-Equilibrium and WinVPP is presented in Appendix J. The CFD hydrodynamic model has then been input to ensure its reliability. Finally, the aerodynamic data resulting from wind tunnel tests has been considered in order to realise the final VPP of the Stewart 34 based on experimental data.

5.4.2 Coordinate system

The coordinate system needs to be clearly defined in order to bring together the hydrodynamic data with the upwind [99] and downwind [12] aerodynamic data. The origin has been set at the forward perpendicular on the design waterline. The forces and moments obey the following convention (previously illustrated in Figure 29):

- F_X positive forward.
- F_Y positive to port.
- F_Z positive upwards.
- M_X positive to starboard.
- M_Y positive downwards.
- M_z is positive to port.

FS-Equilibrium assumes that the boat is sailing on a starboard tack. Due to the sign convention, the heel angles ascertained are therefore negative. In addition, the lift generated by the rudder is negative to windward: a negative rudder angle therefore corresponds to weather helm.

5.4.3 Modification of Experimental Data

It is no be noted that some experimental CFD data have been modified from the FS-Flow analysis for the purpose of the VPP. Indeed, the lower resistance at high leeway angles and the higher side force at high Froude number and leeway angles previously highlighted proved to impact on the quality of the VPP. As a result, and in order to refine the quality of the VPP, some values of the resistance and side force have been modified.

5.4.3.1 Resistance

At high leeway angles, characteristic of upwind sailing, the resistance in under-predicted by FS-Flow. As a result, for a given aerodynamic drive force, a much higher boat speed will be achieved, as presented in Figure 31.

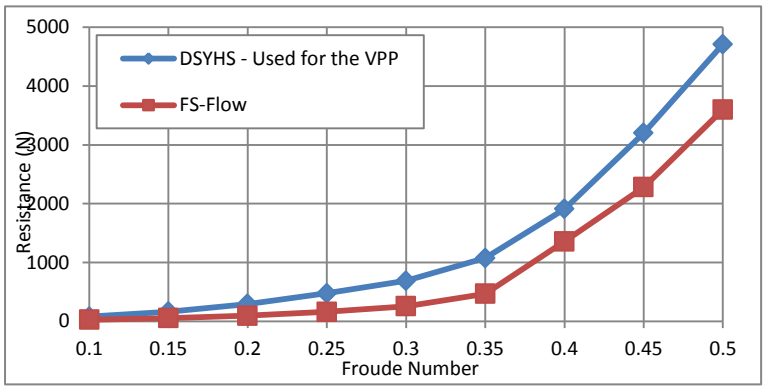

Figure 31: *Typical example of modified resistance values.*

This is however not a realistic behaviour, and speeds significantly higher than ascertained using WinDesign were achieved. The resistance ascertained using the DSYHS has therefore been used at high leeway angles to remedy the issue and achieve more reasonable speeds upwind.

5.4.3.2 Side Force

On the other hand, the inaccurate side force prediction in the unstable region of the panel code (Froude number of 0.40 and above) highlighted in Section 4.4.2 has been replaced by a linear extrapolation in order to provide more realistic values. For the small range of speeds considered, the assumption that side force will vary linearly can be deemed valid. A typical example of modified values is presented in Figure 32.

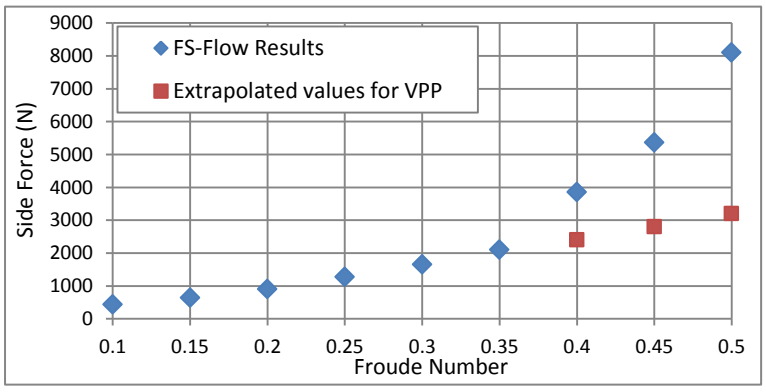

Figure 32: *Typical example of modified side force values.*

5.4.4 Experimental Hydrodynamic Module

The hydrodynamic model of the Stewart 34 has been input into FS-Equilibrium using the *Hydro Volume* module, which comprises response volumes for: lift, drag, roll moment, yaw moment and rudder angle. The forces (lift and drag) and moments (roll and yaw) are all direct outputs from the FS-Flow analysis conducted, and are to be divided by the dynamic pressure q:

$$q = \frac{1}{2} \times \rho \times V^2 \qquad \textbf{Equation 26}$$

Since no rudder angle was tested for, no CFD data is available. The use of the empirical rudder module did not prove to be a viable solution, thus preventing the rudder angle to be taken into account in the VPP. In this instance, the rudder angle will be a vital piece of information to ascertain the cross over between the jib, gennaker and spinnaker. Indeed, the gennaker or spinnaker might provide a high boat speed, but it must be ensured that the rudder has not stalled yet, hence the need to account for the rudder angle.

As a result, the rudder angle required to keep a steady course has been calculated empirically (see Appendix G.6) over a range of speeds, heel and yaw. The data was then used as part of the experimental module.

All variables for the response surfaces are expressed as a function of the boat speed, heel angle and yaw angles, effectively resulting in a 4 dimensional response surfaces to be fitted through the data. The 4D nature of the response surfaces does not enable graphical representations to be presented in this report.

Note that the *Hydro Volume* module does not allow the pitch to be factored in. The restoring pitching moment is accounted for thanks to the value of the longitudinal metacentric radius BM_L ascertained in the *Buoyant Volume* module.

5.4.5 Buoyant Volume Module

The *Buoyant Volume* module enables to input the hull geometry, thus allowing the hydrostatics to be evaluated. Furthermore, the transverse stability is assessed based on the location of the centre of gravity; this constitutes a critical part of the VPP. The VCG position has been ascertained based on a previously conducted inclining experiment [79]. The data gathered was deemed satisfactory, the interpretation however did not correct for the presence of the inclining weights. The theory inherent to transverse stability and inclining experiments and the detailed calculations of the VCG are to be found in Appendix I.

The use of the *linearize hydrostatics* functions lead to the automatic creation of a *Hydrostatics* module, resulting in significant reduction in solving time.

5.5 Application to the Stewart 34

Once setup, FS-Equilibrium has been used to perform a 6 degrees of freedom VPP of the Stewart 34. The results and inherent analysis will be presented in this section. It is to be noted that the scope of the project being restricted to the hydrodynamic side, the impact of aerodynamic factor (such as depowering modes) will not be discussed. The results have been generated using the experimental aerodynamic data and the inherent power depowering mode since it better represents the actual behaviour of sailing yachts [33] compared to traditional reef and flat.

5.5.1 VPP Results

The VPP was solved considering 25 iterations; indeed, the default value of 10 revealed some inconsistencies: slightly different values were achieved for the same conditions due to the limited number of iterations.

The results for 8, 12 and 16 knots of TWS are presented for all 6 degrees of freedom; the boat speed is illustrated in Figure 33, other degrees of freedom are introduced and discussed in Appendix K.

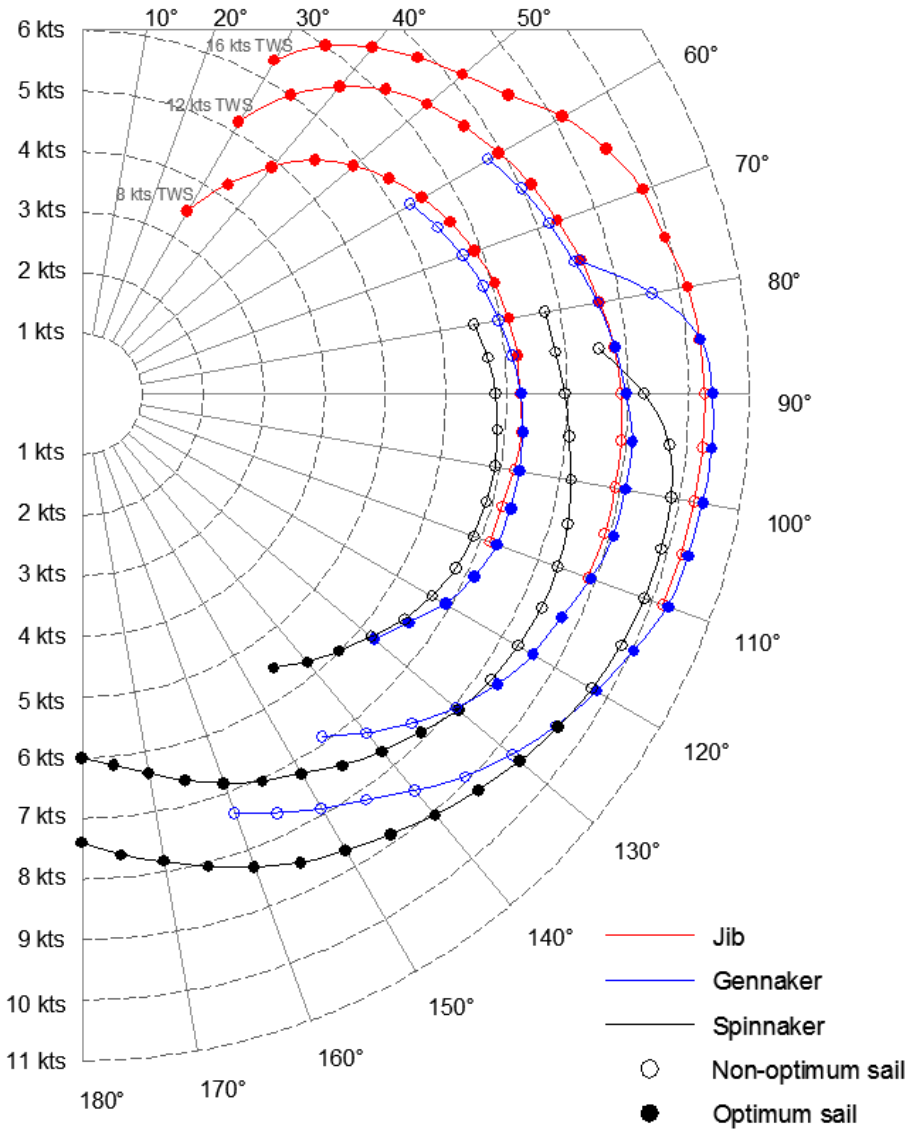

Figure 33: *Fs-Equilibrium VPP, boat speed (knots).*

The velocity prediction enables to assess the best fore sail among the 3 considered (jib, gennaker and spinnaker) as well as the best VMG upwind and downwind. Planning behaviour is not accounted for, as a result, higher downwind speeds can be expected once the boat starts to plane.

Note that issues in the upwind aerodynamic depowering mode (power parameter) have been noticed and are highlighted in Appendix K, and have also been identified in previous work [99]. This therefore represents a limitation of the VPP realised. Investigations into the origin of the problem and potential ways to fix it proved unsuccessful.

5.5.2 Impact of the Rudder

One of the limitations to how far up a downwind sails can be carried will be the rudder; hence particular attention has been paid to this degree of freedom. At the highest wind speed, the spinnaker and gennaker can be seen to experience a sudden reduction in speed, followed by failure of the VPP to solve the particular condition, indicating that the rudder has stalled and that the sail cannot be used so high.

In this instance, stall has been defined as a rudder angle greater than 15°. It is to be noted that the Stewart 34 class recently voted a new rudder design, having a much larger thickness/chord ratio, thus leading to a delayed stall angle and resulting in ability to carry the spinnaker and gennaker closer to the wind.

5.5.3 Impact of Pitch and Heave

Heave and pitch are generally not taken into account for standard monohulls since they are generally very small. In order to assess the impact of those two degrees of freedom on the boat speed of the Stewart 34, the VPP has been realised excluding alternatively the pitch, the heave, and finally both. The boat speeds where then compared to the reference 6 degrees of freedom VPP; results at a TWS of 6 m/s are presented in Figure 34.

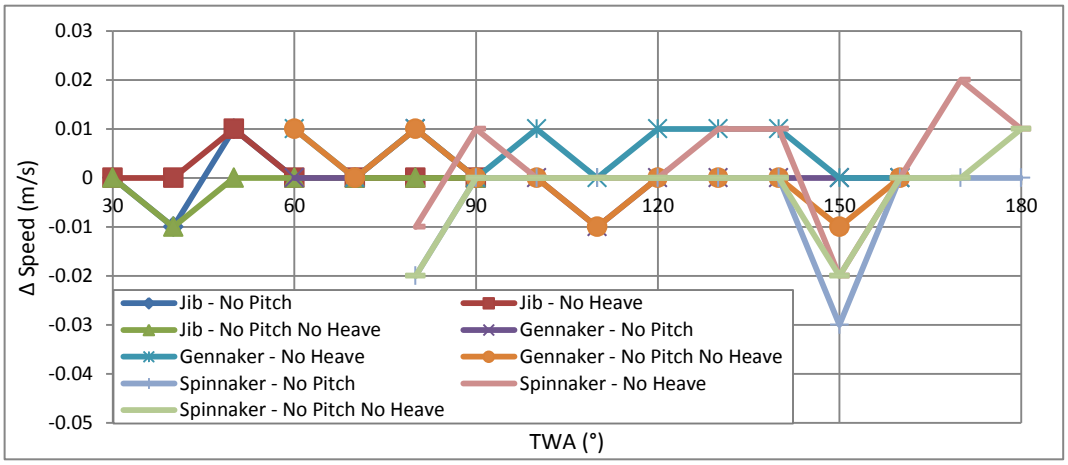

Figure 34: *Impact of pitch and heave on boat speed.*

The impact of pitch and heave proved to be very limited, and justifies the assumption that they are not of primary importance in this case. Greater differences occur for the spinnaker since the largest changes in pitch are induced by this particular sail.

5.5.4 Validation

In order to evaluate the uncertainties inherent to the VPP realise and quantify it accuracy, comparison between experimental full size data [10] and the velocity prediction have been compared.

The performance of the Stewart 34 *Pride*, on which this project is focussed, has been recorded for upwind sailing in true wind speed ranging from 9.2 to 13.8 knots in order to investigate rig tension [10]. As a result, actual sailing data is available. The boat speed, apparent wind angle and apparent wind speed recorded during the experiment have been used to ascertain the true wind speed and true wind angle of the vessel (using Velocity triangle, see Appendix G2). Those conditions were then input in FS-Equilibrium. Comparison of the boat speeds is presented in Figure 35 in increasing order of TWA.

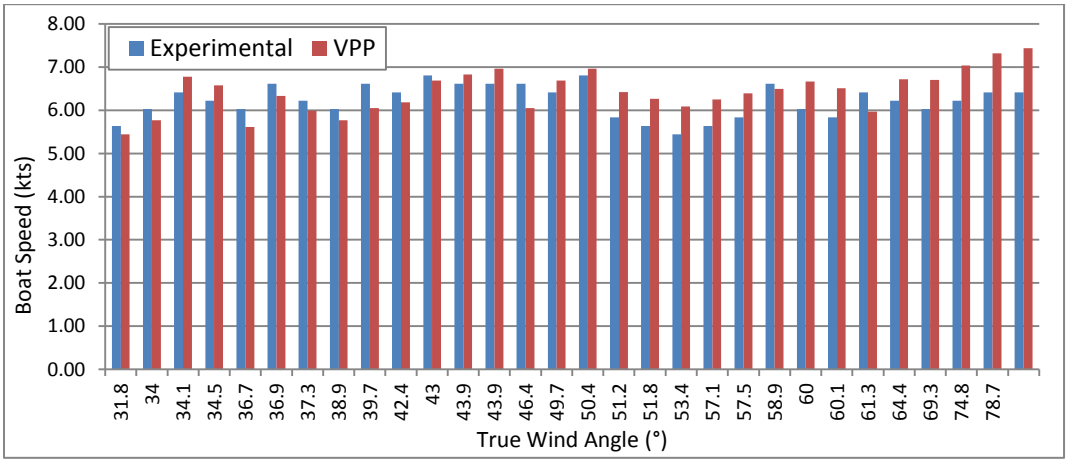

Figure 35: *Experimental [10] and VPP comparison.*

An overall degree of agreement can be observed; the data can however be divided into two main categories, related to the true wind angle.

On the one hand, the VPP slightly under-estimates the speed up to 43° of true wind angle. The VPP being a theoretical speed, it would have been expected to be higher than the actual value. This is however understood as the presence of the crew to windward, providing additional righting moment and thus boat speed. Since no crew weight was modelled in the VPP, it is a plausible interpretation.

On the other hand, a much larger over-prediction of the VPP is exhibited at higher TWA. A possible explanation is the fact that the data gathered during the experiment was not aiming at achieving the highest possible speed. As a result, the full performance of the boat may not have been exploited, hence the differences.

There is however a large degree of uncertainties inherent to the full size data, for which very little detail is provided [10], hence the differences with the VPP.

5.5.5 Conclusions

Uncertainties related to the velocity prediction of the Stewart 34 have been highlighted by the validation undertaken; the amount of difference between the VPP and experimental speeds is however reasonable, especially considering that the full size data was not intended for VPP comparison.

Speed trials aiming at providing an accurate VPP benchmark coupled with a recorded position of the crew (to then be used in combination with a *crew* module in FS-Equilibrium) would be advised, and will provide a more relevant validation, with an expected increased accuracy. Finally, the validation was restricted to upwind sailing in this instance, the gennaker and spinnaker would have to be considered for a full validation

5.5 Conclusions

A total of 3 VPPs have been developed for the Stewart 34. First of all, a preliminary 4 degrees of freedom one enables to ascertain the hydrodynamic test matrix. Secondly, the use of WinDesign enabled to better evaluate the performance of the vessel, and provide a reference VPP to compare with FS-Equilibrium. Finally, a 6 degrees of freedom VPP has been realised based on the experimental aerodynamic and hydrodynamic data, also combining some of the DSYHS in areas where FS-Flow proved to have limitations (high Froude numbers and high leeway angles).

The coordinate system of the VPP has been presented as well as the hydrodynamic and hydrostatic modules considered. The additional drag generated by the rudder proved to be accounted for and the stall angle successfully modelled. In addition, the negligible contribution of heave and pitch has been demonstrated. However, potential discrepancies in the upwind experimental depowering have been noticed, leading to some incoherent results at the highest wind speeds.

The VPP of the Stewart 34 enables optimisation of the sailing performances, considering the best fore sail of VMG angle for instance. A preliminary validation of the VPP against experimental data has been undertaken, and qualitatively validates the analysis. However, speed trials to ascertain a more accurate benchmark (also considering additional factors such as the heel, leeway and rudder angle as well as downwind sails) would be advised; the additional righting moment provided by the crew can then be modelled in FS-Equilibrium, providing a more relevant and accurate validation.

Chapter 6: Conclusions and Recommendations

The conclusions drawn from the development and validation of an hydrodynamic model of the Stewart 34 using both the Delft Systematic Yacht Hull Series and the Rankine source panel code FS-Flow and the inherent applications in the 6 degrees of freedom velocity prediction program FS-Equilibrium are summarised in this chapter. In addition, recommendations for further refinement of the work conducted in this project as well as future work will be made.

6.1 Conclusions

In order to apply a velocity prediction program to the Stewart 34, the hydrodynamic model had to be developed. The use of the Delft Systematic Yacht Hull Series provided an empirical hydrodynamic model, then refined using the Rankine source panel code FS-Flow. Both methods have been validated against the experimental towing tank results of the Sysser 62, selected as a benchmark for its resemblance with the Stewart 34. The available wind tunnel aerodynamic data for the yacht has then been used for the realisation of a 6 degrees of freedom velocity prediction using FS-Equilibrium.

6.1.1 Delft Systematic Yacht Hull Series

The use of the Delft Systematic Yacht Hull Series revealed multiple limitations. On the one hand, those inherent to the method, i.e. the need for the vessel to fit within a given range of parameters, a maximum Froude number of 0.60 and a maximum heel angle of 30°. On the other hand, the validation of the method highlighted further limitations, such as the invalidity of the side force prediction at large angles of yaw, and issues at high Froude number for modern designs, once the vessel reaches semi-displacement mode.

Indeed, different hull shapes will exhibit different behaviours at high Froude numbers, and thus semi-displacement mode cannot be properly assessed from the main dimensions and regressions coefficients.

Nevertheless, the method is suitable in displacement mode and offers a complete hydrodynamic model over a wide range of sailing conditions for common hull shapes in a very short amount of time and at no cost since the calculation method is fully published. In addition, the limited number of design inputs required enables to consider the resistance of the yacht at a very early stage of the design, even prior to the actual linesplan drawing.

The Delft Systematic Yacht Hull Series is therefore an appropriate preliminary design tool.

6.1.2 Computational Fluid Dynamics: FS-Flow

The Rankine source panel code FS-Flow was considered to refine the hydrodynamic model. In the absence of literature relative to the panel code, the setup and use have been defined to enable future use. The panel code appears to be stable and provide accurate results up to a Froude number of 0.35. Past this point and up to 0.50, the code develops some instabilities resulting in harder convergence and loss of accuracy. Past a Froude number of 0.50, no convergence was achieved.

The code proved to be accurate for both resistance and side force at small yaw angles, especially in the stable region of the code. However, at higher yaw angles (5° and above), the resistance is significantly under-estimated whilst the side force is over-predicted. Care should therefore be taken when using the hydrodynamic model developed for upwind VPP where large yaw angles are exhibited.

The limitations of the panel code can be traced to its original development and intended use: the comparison of ships' forebody, which implies low Froude number and no yaw angle. The particular panel code used in this instance does not provide a clear improvement from the Delft Systematic Yacht Hull Series in terms of resistance since its accuracy only holds up to a Froude number of 0.35. It however appears to provide a more accurate side force, provided the leeway angle remains small.

High Froude numbers and high leeway angles are the main limitations to the hydrodynamic model developed using FS-Flow.

6.1.3 Velocity Prediction Program: FS-Equilibrium

A total of three velocity prediction programs have been used for the Stewart 34. An initial empirical 4 degrees of freedom has been developed early in the project to ascertain the range of sailing conditions of the vessel and thus refine the CFD test matrix, leading to narrowing down the range of parameters to be tested for. The second VPP was realised using WinDesign; the 4 degrees of freedom analysis was this time aiming at providing a reference velocity prediction to ensure appropriate use of FS-Equilibrium, used for the final 6 degrees of freedom of the Stewart 34.

The coordinate system use by FS-Equilibrium is critical when bringing together different sets of experimental data, which led to significant modifications to the aerodynamic models (both upwind and downwind) in order to match the hydrodynamic one and achieve sensible results. Note that the use of the FS-Flow hydrodynamic model had to be modified using DSYHS values at high Froude numbers and high leeway angles in order to achieve a coherent and accurate VPP. One of the limitations proved to be the upwind depowering mode; as a result, care should be taken when considering the upwind results at high wind speeds. Furthermore, discrepancies in the depowering of the upwind aerodynamic model have been noticed.

The 6 degrees of freedom VPP was validated against upwind full size data, and showed relatively accurate results considering clear limitations of the validation, such the absence of crew in the VPP, the absence of downwind data or degrees of freedom other than boat speed, and the fact that the benchmark was not developed for this particular purpose. Further validation would appear essential.

A complete 6 degrees of freedom VPP of the Stewart 34 based on experimental data was achieved using FS-Equilibrium.

6.1.4 Conclusions

The objectives set for this project have been met: the hydrodynamic model of the Stewart 34 was developed and validated for the purpose of velocity prediction program applications. The Delft Systematic Yacht Hull Series proved to be a useful and efficient preliminary design tool despite its limitations. On the other hand, the panel code FS-Flow revealed some degree of improvement; but its application to sailing yachts at high leeway angle is questionable. It however appears perfectly suitable for ship design, its intended use. Finally, a complete upwind and downwind 6 degrees of freedom VPP of the Stewart 34 is now available. A number of interesting points highlighted in this project led to the recommendations for future work made in the following section.

6.2 Recommendations for Future Work

The results of the work undertaken raised additional opportunities for further investigation and future work. Those aspects have not been tackled as most are beyond the scope of the project or have been revealed as area of further research by the conclusions of this project. Some of the suggestions made hereafter would appear as suitable future projects.

- A very significant part of the project was dedicated to understanding and using FS-Flow. The panel code has been set up to a satisfactory level of accuracy and enabled to generate the hydrodynamic model of the Sysser 62 and Stewart 34. With the panel code now functioning, further investigations can be carried out to further refine the accuracy and optimise the use of FS-Flow.

- Preliminary investigations into the use of RANSE to ascertain the upright hydrodynamic resistance of the Sysser 62 revealed encouraging accuracy, particularly at high Froude numbers. The development of a complete hydrodynamic model of both the Sysser 62 and Stewart 34 in the conditions taken into account in this instance would enable to compare the accuracy and reliability of both methods, as well as the trade off in computation time in order to assess the most appropriate tool for the resistance and side force prediction of sailing yachts.

- The Sysser 62 has been elected has a benchmark for the Stewart 34 due to the availability of the towing tank results. However, the use of a DSYHS model for the purpose of validating the DSYHS calculation method is debatable, and validation using a non-DSYHS model would be advised. Furthermore, a greater set of experimental data, particularly in heeled and yawed conditions would enable to better assess the reliability of empirical and CFD results in sailing conditions. This is however restricted by the availability of both experimental towing tank data and associated model geometry.

- A number of resistance components have been either approximated, or ignored. The shaft/propeller drag has been empirically added to the resistance of the Stewart 34; the arrangement could be modelled an added to the CFD model in order to refine the resistance. Furthermore, environmental factors such as added resistance due to waves have not been taken into account. The water never being perfectly flat and the significant impact added resistance due to waves can have would be another area of further refinement of the resistance and resulting VPP for the Stewart 34.

- A steady state VPP has been realised in this instance; FS-Equilibrium offers the possibility to consider manoeuvring. A dynamic VPP could therefore be realised, with two main outcomes. On the one hand, the manoeuvring model of FS-Equilibrium could be compared with actual manoeuvres realised on the boat, thus providing further insights into the semi-empirical modelling of manoeuvres in VPPs. On the other hand, the dynamic VPP could be coupled with the race course and meteorological conditions to ascertain the optimum course of the boat on the water to complete the race in the shortest possible time. This aspect would result in enhanced racing and strategic capabilities.

- In order to validate the VPP realised and quantify the various uncertainties, speed trials on the actual Stewart 34 considered in this instance could be realised, trying to achieve the maximum boat speed while recording the sailing conditions to provide data for an accurate comparison of the VPP with the performance of the boat. Furthermore, the realisation of a complete FS-Equilibrium VPP aiming at maximising the accuracy could constitute a project in itself. Indeed, the VPP realised in this instance was restricted by both the dongle availability and the need to extend the scope of the research to the use of wind tunnel data to obtain aerodynamic coefficients in order to achieve a functioning aerodynamic model.

- Finally, the most relevant further work to be undertaken would be towing tank testing of a Stewart 34 model. This would provide an experimental benchmark for the validation of the DSYHS as well as the FS-Flow prediction developed in this project and any further CFD analysis. There are however physical and financial constraints, such as the absence of towing tank facilities in New Zealand, and the high costs associated with the experiment.

The results of this project led to a range of possible enhancements and suitable areas for future work, among which three would constitute relevant projects, namely the realisation of a dynamic VPP for racing optimisation applications, the use of RANSE for the hydrodynamic model of the Sysser 62 and Stewart 34, and towing tank testing of the Stewart 34. The last two aiming at ascertaining the balance between reliability and accuracy on the one hand, and time and cost implications of the other hand, to assess the most appropriate use of each of the resistance predictions tools (DSYHS, panel code, RANSE and towing tank) in modern yacht design and optimisation.

References

[1] Baba E. (1975). Blunt bow forms and wave breaking. *The 1st STAR symposium on ship technology and research*. The society of naval architects and marine engineers.

[2] Backhus G. (2009). *Stewart 34 yachting: the first fifty years*. Published by the Author, Auckland.

[3] Barkley G. (2012). *Resistance of displacement sailing yachts and the Gerritsma series*. Southampton Solent University, Southampton.

[4] Barkley G. (2012). *Calculating the components of drag and scaling up drag to full size*. Southampton Solent University, Southampton.

[5] Barkley G. (2012). *The three main components of drag acting on a hull*. Southampton Solent University, Southampton.

[6] Barkley G. (2011). *Froude Number: towing tank testing pictures*. Southampton Solent University, Southampton.

[7] Bentley Systems (2012). *Hydrolink* (Version 19.0 V8i) [Software].

[8] Bentley Systems (2012). *Hydromax – Maxsurf stability* (Version 19.0 V8i) [Software].

[9] Bentley Systems (2012). *Maxsurf modeller* (Version 19.0 V8i) [Software].

[10] Bergsma F. (2012). *Effect of rig tension on sailing yacht performance*. The University of Auckland, Auckland.

[11] Binns J. R., Hochkirch K., De Board F. and Burns I. A. (2008). The development and use of sailing simulation for IACC starting manoeuvre training. *3rd high performance yacht design conference*, Auckland.

[12] Boscarino M. (2014). *Development of a downwind aerodynamic model and velocity prediction program for a Stewart 34 class yacht*. Master of yacht engineering research project. The University of Auckland, Auckland.

[13] Burns F. (2014). *North sails design system*. The University of Auckland, Auckland.

[14] Capdeville J. D., Nicolopoulos D. and Hansen H. (2013). Easy-to-use advanced performance prediction analysis for yacht racing teams. *3rd international conference on innovation in high performance sailing yacht*, Lorient.

[15] Celik I. B. (Undated). *Procedure for estimation and reporting of discretization error in CFD applications*. West Virginia University.

[16] Coleman H. W. and Stern F. (1997). Uncertainties in CFD code validation. *ASME journal of fluids engineering*. 119:785-803.

[17] Curtis E. G, Ilie M. and Schallhorn P. A. (2012). *Comprehensive approach to verification and validation of CFD simulations applied to backward facing step – Application of CFD uncertainty analysis*. University of central Florida.

[18] Delft Systematic Yacht Hull Series (2014). *DSYHS database*. Retrieved from: http://dsyhs.tudelft.nl/ [March 20th, 2014]

[19] Firth G. (2010). *Naval architecture principles*. Southampton Solent University, Southampton.

[20] Fossati F., Muggiasca S. and Viola I. M. (Undated). An investigation of aerodynamic force modelling for IMS rule using wind tunnel techniques. *19th HISWA symposium*, Amsterdam.

[21] Froude W. (1872). *Experiments of the surface-friction experienced by a plane moving through water*. Report to the British Association for the Advancement of Science, London.

[22] Froude W. (1874). *Report to the Lords Commissioners of the Admiralty on experiments for the determination of the frictional resistance of the water on a surface under various conditions*. Report to the British Association for the Advancement of Science, London.

[23] FutureShip (2009). *FS-Equilibrium* (Rel14.0228) [Software].

[24] FutureShip (2009). *FS-Flow* (Rel14.0228) [Software].

[25] FutureShip (2014). *FS-Equilibrium – User manual*. FutureShip GmbH, Postdam.

[26] FutureShip (2014). *FS-Flow – User Manual*. FutureShip GmbH, Postdam.

[27] Gerristma J., Moeyes G. and Onnink R. (1997). Test results of a systematic yacht hull series. *5th HISWA symposium yacht architecture*.

[28] Gerritsma J., Onnink R. and Versluis A. (1981). Resistance and stability of the Delft systematic yacht hull series. *International shipbuilding progress* (Vol. 28).

[29] Gerritsma J., Onnink R. and Versluis A. (1996). The bare hull resistance of the Delft systematic yacht hull series. *The International HISWA symposium on yacht design and yacht construction*.

[30] Gropp W. D, Kaushik D. K., Keyes D. E and Smith B. F (2000). *Performance modelling and tuning of an unstructured mesh – CFD applications*. IEEE.

[31] Groves C. E. (2014). *Computational fluid dynamics uncertainty analysis for payload fairing spacecraft environmental control systems*. PhD thesis, University of centre Floria, Orlando.

[32] Hadler J. B. (1958). *Coefficient for international towing tank conference 1957 model-ship correlation line*. DTMB Report 1185.

[33] Hansen H., Richard P. J. and Jackson P. S (2010). Reef and flat or twist and ease: an improved trim parameter model for yacht sails. *Royal Institution of Naval Architects, international journal of small craft technology*.

[34] Hazen G. S. (1980). *A model of sail aerodynamics for diverse rig types*. New England sailing yacht symposium.

[35] Hess J. L. (1974). The problem of three dimensional lifting potential flow and its solution by means of surface singularity distributions. *Computer methods in applied mechanics and engineering*, pp 283-319.

[36] Hoekstra M. and Eça L. (Undated). An example of error quantification of ship-related CFD results. Instituto Superior Tecnico, Lisboa.

[37] Hoerner S. F. (1965). *Fluid-dynamic drag: theoretical, experimental and statistical information*. Published by the Author, Great Britain.

[38] Huetz L. and Guillern P. E. (2013). Database building and statistical methods to predict sailing yachts hydrodynamics. *The 3rd international conference on innovation in high performance sailing yachts*, Lorient.

[39] International Organisation for Standardisation (2002). *ISO 12217: Small craft – Stability and buoyancy assessment and categorization. Part 2: Sailing boats of hull length greater or equal to 6m*. Ref. n° ISO 12217-2:2002.

[40] International Sailing Federation (2013). *Racing rules of sailing: 2013-2016*. ISAF.

[41] International Towing Tank Conference (1978). Report of the Resistance Committee. *15th International Towing Tank Conference*, The Hague.

[42] International Towing Tank Conference (1999). ITTC recommended procedures: performance, propulsion, 1978 ITTC performance prediction method. *22th International Towing Tank Conference*, Seoul.

[43] International Towing Tank Conference (1999). ITTC recommended procedures: testing and extrapolation methods, resistance, resistance test. *22th International Towing Tank Conference*, Seoul.

[44] International Towing Tank Conference (1999). ITTC recommended procedures: testing and extrapolation methods, uncertainty analysis, example of resistance test. *22th International Towing Tank Conference*, Seoul.

[45] International Towing Tank Conference (2002). ITTC recommended procedures and guidelines: model manufacture, ship models. *23th International Towing Tank Conference*, Venice.

[46] International Towing Tank Conference (2002). ITTC recommended procedures and guidelines: uncertainty analysis in CFD verification and validation methodology and procedures. *23th International Towing Tank Conference*, Venice.

[47] International Towing Tank Conference (2006). *ITTC recommended procedures and guidelines: testing and extrapolation methods, general density and viscosity of water*. International Towing Tank Conference.

[48] Jacquin E., Roux Y., Guillerm P. E. and Alessandrini B. (2005). Towards numerical VPP with the full coupling of hydrodynamics and aerodynamic solvers for ACC yacht. *17th Chesapeake sailing yacht symposium*, Annapolis.

[49] Johnson F. T., Tinoco E. N. and Yu N. J. (2005). *Thirty years of development and application of CFD at Boeing commercial airplanes*. Boeing, Seattle.

[50] Jones P. and Korpus R. (2001). International America's cup class yacht design using viscous flow CFD. *15th Chesapeake sailing yacht symposium*.

[51] Katgert M. and Den Ouden J. (2013). *Manual DSYHS*. Delft University of Technology, Delft.

[52] Keuning J. A. and Binkhorst B-J. (1997). Appendage resistance of a sailing yacht hull. *13th Chesapeake sailing yacht symposium,* Amsterdam.

[53] Keuning J. A., Katgert M. and Vermeulen K. J. (2007). *Further analysis on the forces on keel and rudder of a sailing yach*t. Delft University of Technology, Delft.

[54] Keuning J. A. and Katgert M. (2008). *A bare hull resistance prediction method derived from the results of the delft systematic yacht hull series extended to higher speeds*. Delft University of Technology, Delft.

[55] Keuning J. A. and Katgert M. (2010). *The influence of heel on the bare hull resistance of a sailing yacht*. Delft University of Technology, Delft.

[56] Keuning J. A. and Sonnenberg U. B. (1998). Approximation of the hydrodynamic forces on a sailing yacht based on the Delft systematic yacht hull series. *15th International symposium on yacht design and construction*, Amsterdam.

[57] Keuning J. A. and Sonnenberg U. B. (1998). Development in the velocity prediction based on the Delft systematic yacht hull series. *International conference on the modern yacht*. The royal institution of naval architects, Portsmouth.

[58] Keuning J. A. and Sonnenberg U. B. (1999). *Approximation of the calm water resistance on a sailing yacht based on the Delft systematic yacht hull series*. Delft University of Technology, Delft.

[59] Keuning J. A., Onnink R., Versluis A. and Van Gulik A. A. M. (1996). The Bare hull resistance of the Delft systematic yacht hull series. *The international HISWA symposium on yacht design and yacht construction*, Amsterdam.

[60] Keuning J. A. and Verwerft B. (2009). A new method for prediction of the side force on keel and rudder of a sailing yacht based on the results of the Delft systematic yacht hull series. *The 19th Chesapeake sailing yacht symposium*, Annapolis.

[61] Knudsen S. S and Wedersoe K. (2008). *Velocity prediction of a sailing yacht*. Technical University of Denmark.

[62] Kristensen H. O. and Lützen M. (2013). *Prediction of resistance and propulsion power of ships*. Technical University of Denmark and University of Southern Denmark.

[63] Kuethe A. M. and Schetzer J. D. (1959). *Foundations of aerodynamics*. 2nd edition, John Willey and Sons.

[64] Larsson L. and Eliasson R. E. (2000). *Principles of yacht design*. Adlard Coles Nautical, 2nd edition, London.

[65] Lavini G, Pedone L and Genuzio D. H. (2009). Applications of fully viscous CFD codes in the design of non cavitating propellers for passenger vessels. *1st international symposium on marine propulsor,* Trondheim .

[66] Mac Kenzie P. M. and Forrester M. A. (2008). *Sailboat propeller drag*. Ocean Engineering, University of Strathclyde, Glasgow.

[67] Mantzaris D. A. (1998). *A Rankine panel method as a toll for the hydrodynamic design of complex marine vehicles*. PhD thesis, Massachusetts institute of technology.

[68] Mason A. and Philpott A. (2000). *Optimising yacht routes under uncertainty*. The University of Auckland, Auckland.

[69] Offshore Racing Congress (2013). *ORC VPP Documentation*. Updated 4th July 2013.

[70] Philpott A. and Mason A. (2002). Advances in optimisation in yacht performance analysis. *High performance yacht design conference*, Auckland.

[71] Prince M. and Claughton A. R. (2013). Estimating a yacht's hull-sailplan balance and sailing performance using experimental results and VPP results. *3rd international conference on innovation in high performance sailing yachts*, Lorient.

[72] Prohaska C. W (1966). A simple method for the evaluation of the form factor and low speed wave resistance. *11th International Towing Tank Conference*, Tokyo.

[73] Pulliam T. H. (1986). *Solution methods in computational fluid dynamics*. NASA ames research centre, California.

[74] Remmlinger U. (2014). *Bare hull resistance prediction based on the Delft Systematic Yacht Hull Series*. Ulirch Remmlinger, Germany.

[75] Remmlinger U. (2013). *The influence of sand grain strip on boundary layer transition in the towing tank*. Ulrich Remmlinger, Germany.

[76] Reynolds O. (1883). *An experimental Investigation of the circumstances which determine whether the motion of water shall be direct or sinuous, and of the law of resistance in parallel channels*. Philosophical transactions of the Royal Society of London.

[77] Rhinoceros (2012). *Rhinoceros - Modelling tools for designers* (Version 5.1.20927.2230) [Software]

[78] Roache P. J. (1997). *Quantification of uncertainty in computational fluid dynamics*. Annual review of fluid mechanics 29:123-60

[79] Sammour Y. (2012). *Development of a VPP for the Stewart 34 sailing yacht*. Master of yacht engineering research project. The University of Auckland, Auckland.

[80] Silverberg J. P. and Miller P. H. (Undated). *A comparison of parametric analysis, tank testing and CFD methods as part of an advanced sailboat velocity prediction program*. United States naval academy.

[81] Smith P. and Harvey B. (2007). *Boat hull modelling using terrestrial laser scanners*. School of surveying and spatial information systems, the University of New South Wales.

[82] Stern F., Wilson R. V, Coleman H. W. and Paterson E.G (2001). Comprehensive approach to verification and validation of CFD simulations – Part 1: methodology and procedure. *ASME journal of fluids engineering*. 123:793-802.

[83] Stern F., Wilson R. and Shao J. (2006). Quantitative V&V of CFD simulations and certification of CFD codes. *International journal for numerical methods in fluid*.

[84] Stewart R. (1959). *Stewart 34 Linesplan* [Drawing]. Conserved at the New Zealand Maritime Museum, Auckland.

[85] Stewart R. (1959). *Stewart 34 Sailplan* [Drawing]. Conserved at the New Zealand Maritime Museum, Auckland.

[86] Souppez J-B. R. G. (2012). *Structural analysis: mast and rigging case study*. Southampton Solent University, Southampton.

[87] Souppez J-B. R. G. (2011). *Resistance and Power estimate of a Halmatic lookalike*. Southampton Solent University, Southampton.

[88] Van Oossanen P. (1993). Predicting the speed of sailing yachts. *SNAME transactions*. Vol. 101, pp 337-397. Wageningen.

[89] Viola I. M., Bot P. and Riotte M. (2013). On the uncertainty of CFD in sail aerodynamics. *International journal for numerical methods in fluids*. 72:1146-1164.

[90] Viola I. M. and Enlender J. (2013). On the hydrodynamics of a skiff at different crew positions. *21st Chesapeake sailing yacht symposium*, Annapolis.

[91] Viola I. M., Flay R. G. J. and Ponzini R. (2009). CFD analysis of the hydrodynamic performance of two candidate America's Cup AC33 hulls. *Royal Institution of Naval Architects, International journal of small craft technology*.

[92] Wallis S. (2013). *Aero-hydrodynamics: keels, hulls, side for and drag*. Southampton Solent University, Southampton.

[93] Wallis S. (2013). *Aero-hydrodynamics: sailing equilibrium and VPPs*. Southampton Solent University, Southampton.

[94] Wallis S. (2013). *Marine craft design and development: estimating Keels and Ballast*. Southampton Solent University, Southampton.

[95] Wallis S. (2013). *Marine craft design and development: Wind pressure, Martin's formula and Beaufort scale.*. Southampton Solent University, Southampton.

[96] Wolfon Unit (2009). *Lines processing program* (Version 20.04.10/FV-25). [Software].

[97] Wolfon Unit (2009). WinDesign 4.0 (Version 4.2.29N). [Software].

[98] Wolfson Unit (2014). *WinDesign[6]: advanced yacht performance solutions*. Wolfson Unit.

[99] Yu L. (2014). *Upwind testing of the Stewart 34*. Master of yacht engineering research project. The University of Auckland, Auckland.

Appendices

A. DSYHS Calculation Method

The calculations inherent to the DSYHS resistance model [56] will be presented for the hull and appendages in upright, heeled and heeled and yawed conditions.

A.1 Upright: Bare Hull

The hull friction resistance Rfh considered by the DSYHS is given by [56]:

$$Rfh = \frac{1}{2} \times \rho \times V^2 \times Sc \times Cf \qquad \textbf{Equation 27}$$

The ITTC 57 friction coefficient (Equation 4) is used in this instance, with however a slight modification: only 70% of the waterline length Lwl is taken into account in the Reynolds number Rn:

$$Rn = \frac{\rho \times V \times 0.7 \times Lwl}{\mu} \qquad \textbf{Equation 28}$$

The ITTC 57 coefficient has been derived for ships, which feature a parallel midbody that yachts do not have, and therefore a higher waterplane area coefficient. The DSYHS therefore proposes to use 70% of the Lwl as a correction factor for yachts [3]; the reduced Lwl increases the Reynolds number and therefore the friction coefficient.

Note that if still unknown at a preliminary design stage, the wetted surface area Sc can be approximated as [56]:

$$Sc = \left(1.97 + 0.171 \times \frac{Bwl}{Tc}\right) \times \sqrt[3]{\frac{0.65}{Cm}} \times \sqrt{\nabla c \times Lwl} \qquad \textbf{Equation 29}$$

On the other hand, the hull residuary resistance Rrh is defined as [56]:

$$\frac{Rrh}{\nabla c \times \rho \times g} = a_0 + \left(a_1 \times \frac{LCB_{fpp}}{Lwl} + a_2 \times Cp + a_3 \times \frac{\nabla c^{2/3}}{Aw} + a_4 \times \frac{Bwl}{Lwl}\right) \times \frac{\nabla c^{1/3}}{Lwl} + \left(a_5 \times \frac{\nabla c^{2/3}}{Sc} + a_6 \times \frac{LCB_{fpp}}{LCF_{fpp}} + a_7 \times \left(\frac{LCB_{fpp}}{Lwl}\right)^2 + a_8 \times Cp^2\right) \times \frac{\nabla c^{1/3}}{Lwl} \qquad \textbf{Equation 30}$$

Where a_0 to a_8 are regression coefficients given in Table 6.

Fn	a_0	a_1	a_2	a_3	a_4	a_5	a_6	a_7	a_8
0.10	-0.0014	0.0403	0.0470	-0.0227	-0.0119	0.0061	-0.0086	-0.0307	-0.0533
0.15	0.0004	-0.1808	0.1793	-0.0004	0.0097	0.0118	-0.0055	0.1721	-0.1728
0.20	0.0014	-0.1071	0.0637	0.0090	0.0153	0.0011	0.0012	0.1021	-0.0648
0.25	0.0027	0.0463	-0.1263	0.0150	0.0274	-0.0299	0.0110	-0.0595	0.1220
0.30	0.0056	-0.8005	0.4891	0.0269	0.0519	-0.0313	0.0292	0.7314	-0.3619
0.35	0.0032	-0.1011	-0.0813	-0.0382	0.0320	-0.1481	0.0837	0.0223	0.1587
0.40	-0.0064	2.3095	-1.5152	0.0751	-0.0858	-0.5349	0.1715	-2.4550	1.1865
0.45	-0.0171	3.4017	-1.9862	0.3242	-0.1450	-0.8043	0.2952	-3.5284	1.3575
0.50	-0.0201	7.1576	-6.3304	0.5829	0.1630	-0.3966	0.5023	-7.1579	5.2534
0.55	0.0495	1.5618	-6.0661	0.8641	1.1702	1.7610	0.9176	-2.1191	5.4281
0.60	0.0808	-5.3233	-1.1513	0.9663	1.6084	2.7459	0.8491	4.7129	1.1089

Table 6: *DSYHS upright hull residuary resistance regression coefficients [56].*

This equation was developed for the first 40 models tested, but did not prove to be suitable for the more recent ones at high Froude numbers. In 2008, Delft suggested an alternative formula (Equation 31) for the bare hull residuary resistance [54], with new regression coefficients (Table 7) updated with the results of the latest series.

$$\frac{Rrh}{\nabla c \times \rho \times g} = a_0 + \left(a_1 \times \frac{LCB_{fpp}}{Lwl} + a_2 \times Cp + a_3 \times \frac{\nabla c^{2/3}}{Aw} + a_4 \times \frac{Bwl}{Lwl} + a_5 \times \frac{LCB_{fpp}}{LCF_{fpp}} + a_6 \times \frac{Bwl}{Tc} + a_7 \times Cm\right) \times \frac{\nabla c^{1/3}}{Lwl} \qquad \textbf{Equation 31}$$

Fn	a_0	a_1	a_2	a_3	a_4	a_5	a_6	a_7
0.15	-0.0005	0.0023	-0.0086	-0.0015	0.0061	0.0010	0.0001	0.0052
0.20	-0.0003	0.0059	-0.0064	0.0070	0.0014	0.0013	0.0005	-0.0020
0.25	-0.0002	-0.0156	0.0031	-0.0021	-0.0070	0.0148	0.0010	-0.0043
0.30	-0.0009	0.0016	0.0337	-0.0285	-0.0367	0.0218	0.0015	-0.0172
0.35	-0.0026	-0.0567	0.0446	-0.1091	-0.0707	0.0914	0.0021	-0.0078
0.40	-0.0064	-0.4034	-0.1250	0.0273	-0.1341	0.3578	0.0045	0.1115
0.45	-0.0218	-0.5261	-0.2945	0.2485	-0.2428	0.6293	0.0081	0.2086
0.50	-0.0388	-0.5986	-0.3038	0.6033	-0.0430	0.8332	0.0106	0.1336
0.55	-0.0347	-0.4764	-0.2361	0.8726	0.4219	0.8990	0.0096	-0.2272
0.60	-0.0361	0.0037	-0.2960	0.9661	0.6123	0.7534	0.0100	-0.3352

Table 7: *New hull residuary resistance coefficients [54].*

The sum of the frictional and residuary resistance gives the total upright hull resistance Rth [56]:

$$Rth = Rfh + Rrh \qquad \textbf{Equation 32}$$

To the bare hull resistance, appendages resistance can be added.

A.2 Upright: Appendages

For appendages, whether keel or rudder, the frictional resistance can be calculated as described in Equation 27, using the appendage wetted surface area and the mean chord length of the foil to ascertain the Reynolds number. The viscous resistance can then be calculated [56]:

$$Rv_{app} = Rf \times (1 + k) \qquad \textbf{Equation 33}$$

Indeed, if the form factor cannot be mathematically calculated for a hull, it can be for a foil based on Hoerner formula [37]:

$$1 + k = 1 + 2 \times \frac{t}{c} + 60 \times \left(\frac{t}{c}\right)^4 \qquad \textbf{Equation 34}$$

The residuary resistance, only applicable to the keel (the rudder residuary resistance being neglected) is then given by [58]:

$$\frac{Rr_{keel}}{\nabla_{keel} \times \rho \times g} = A_0 + A_1 \times \frac{T}{Bwl} + A_2 \times \frac{Tc + Zcb_{keel}}{\nabla_{keel}{}^{1/3}} + A_3 \times \frac{\nabla c}{\nabla_{keel}} \qquad \textbf{Equation 35}$$

Where A_0 to A_3 are regression coefficients presented in Table 8.

Fn	A_0	A_1	A_2	A_3
0.20	-0.00104	0.00172	0.00117	-0.00008
0.25	-0.00550	0.00597	0.00390	-0.00009
0.30	-0.01110	0.01421	0.00069	0.00021
0.35	-0.00713	0.02632	-0.00232	0.00039
0.40	-0.03581	0.08649	0.00999	0.00017
0.45	-0.00470	0.11592	-0.00064	0.00035
0.50	0.00553	0.07371	0.05991	-0.00114
0.55	0.04822	0.00660	0.07048	-0.00035
0.60	0.01021	0.14173	0.06409	-0.00192
Coefficient are multiplied by 1000				

Table 8: *DSYHS upright appendages residuary resistance regression coefficients [58].*

The formula considers the volume of the keel ∇_{keel}, and the location of its vertical centre of buoyancy Zcb_{keel}. Those values can be estimated thanks to [94]:

$$\nabla_{keel} = SAC \times \frac{t}{c} \times \frac{b}{3} \times (Cr^2 + Cr \times Ct + Ct^2) \qquad \textbf{Equation 36}$$

$$Zcb_{keel} = \frac{b}{4} \times \left(\frac{1 + 2 \times Tr + 3 \times Tr^2}{1 + Tr + Tr^2} \right) \qquad \textbf{Equation 37}$$

The total upright resistance Rt of the hull and appendages can then be calculated:

$$Rt = Rth + Rv_{keel} + Rr_{keel} + Rv_{rudder} \qquad \textbf{Equation 38}$$

This upright resistance approach would be suitable to ascertain the engine power required to achieve a target speed. However, when sailing and for VPP applications, the resistance must be assessed over a range of heel and yaw angles.

A.3 Heeled: Bare Hull

In heeled and yawed cases, the DSYHS assumes that the change in frictional resistance is due to the new heeled wetted surface area $Sc\varphi$ [56]:

$$Sc\varphi = Sc_{(\varphi=0°)} \times \left(1 + \frac{1}{100} \left(s_0 + s_1 \times \frac{Bwl}{Tc} + s_2 \times \left(\frac{Bwl}{Tc} \right)^2 + s_3 \times Cm \right) \right) \qquad \textbf{Equation 39}$$

The regression coefficient s_0 to s_3 apply from 5° to 35° in 5° increment, as shown in Table 9.

φ	s_0	s_1	s_2	s_3
5°	-4.112	0.054	-0.027	6.329
10°	-4.522	-0.132	-0.077	8.738
15°	-3.291	-0.389	-0.118	8.949
20°	1.850	-1.200	-0.109	5.364
25°	6.510	-2.305	-0.066	3.443
30°	12.334	-3.911	0.024	1.767
35°	14.648	-5.182	0.102	3.497

Table 9: *DSYHS heeled wetted surface area regression coefficients [56].*

For heel angles in between, the wetted surface area can be interpolated from the values of the two adjacent heel angles. Many yacht hulls tend to have a smaller wetted surface area when heeled; as a result the heeled frictional resistance is likely to be less than in upright condition.

Equation 40, based on the regression coefficient u_0 to u_5 presented in Table 10, enables to establish the difference (delta) in residuary resistance $\Delta Rrh_{(\varphi=20°)}$ between 20° of heel and the upright condition [56]:

$$\frac{\Delta Rrh_{(\varphi=20°)}}{\nabla c \times \rho \times g} = u_0 + u_1 \times \frac{Lwl}{Bwl} + u_2 \times \frac{Bwl}{Tc} + u_3 \times \left(\frac{Bwl}{Tc}\right)^2 + u_4 \times LCB + u_5 \times LCB^2 \qquad \textbf{Equation 40}$$

Fn	u_0	u_1	u_2	u_3	u_4	u_5
0.25	-0.0268	-0.0014	-0.0057	0.0016	-0.0070	-0.0017
0.30	0.6628	-0.0632	-0.0699	0.0069	0.0459	-0.0004
0.35	1.6433	-0.2144	-0.1640	0.0199	-0.0540	-0.0268
0.40	-0.8659	-0.0354	0.2226	0.0188	-0.5800	-0.1133
0.45	-3.2715	0.1372	0.5547	0.0268	-1.0064	-0.2026
0.50	-0.1976	-0.1480	-0.6593	0.1862	-0.7489	-0.1648
0.55	1.5873	-0.3749	-0.7105	0.2146	-0.4818	-0.1174
Coefficients multiplied by 1000						

Table 10: *DSYHS 20° of heel hull delta residuary resistance regression coefficients [56].*

Hence the hull residuary resistance at 20°:

$$Rrh_{(\varphi=20°)} = Rrh + \Delta Rrh_{(\varphi=20°)} \qquad \textbf{Equation 41}$$

For any other heel angle φ up to 30°, the delta in residuary resistance can be estimated [56]:

$$\Delta Rrh_{\varphi} = \Delta Rrh_{(\varphi=20°)} \times 6 \times \varphi^{1.7} \qquad \textbf{Equation 42}$$

Finally, the total heeled resistance of the bare hull $Rth\varphi$ is simply:

$$Rth\varphi = Rfh\varphi + Rrh\varphi \qquad \textbf{Equation 43}$$

In terms of side force, it is to be noted that the impact of the rudder or the asymmetry of the heeled waterplane is not directly considered by the DSYHS, but incorporated in the extended keel method presented hereafter.

A.4 Extended Keel Method

Foils experience tip losses at both ends, however, keels and rudders suffer tip losses at one end only since the other is in contact with the hull. This leads to idea of a mirror boundary effect [92] that doubles the aspect ratio of the foil. The DSYHS presents a slightly modified approach: the extended keel method [60]. In order to consider the effect of the hull and rudder on the side force, the keel is extended to and mirrored about the waterline, as shown in Figure 36:

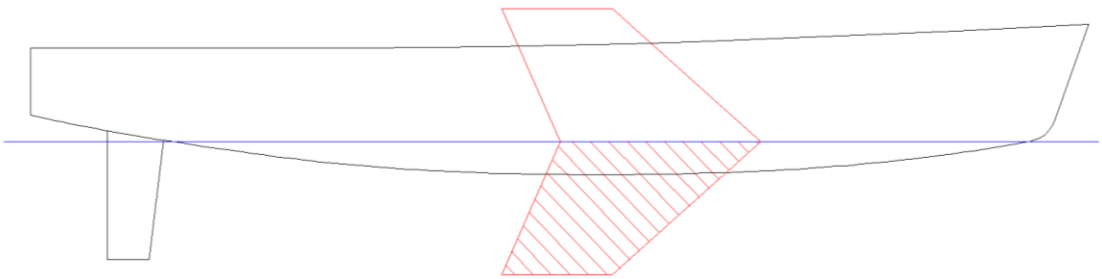

Figure 36: *Extended keel method illustration, edited from [60].*

This method will be applied in heeled and yawed conditions.

A.5 Heeled: Appendages

First of all, the viscous resistance remains unchanged provided that the appendages remain fully immersed, a situation that could happen with bilge keels or canting keels, but those are beyond the scope of the DSYHS, and irrelevant to the Stewart 34.

On the other hand, the change in keel residuary resistance $\Delta Rr\varphi k$ is [58]:

$$\frac{\Delta Rr\varphi k}{\nabla_{keel} \times \rho \times g} = \left(H_1 \times \frac{Tc}{T} + H_2 \times \frac{Bwl}{Tc} + H_3 \times \frac{Tc}{T} \times \frac{Bwl}{Tc} + H_4 \times \frac{Lwl}{\nabla_{keel}^{1/3}} \right) \times Fn^2 \times \varphi \qquad \textbf{Equation 44}$$

The regression coefficients H_1 to H_4 are to be found in Table 11.

H_1	H_2	H_3	H_4
-3.5837	-0.0518	0.5958	0.2055

Table 11: *DSYHS heeled appendages delta residuary resistance regression coefficients [58].*

The total resistance of a hull with keel and rudder in heeled conditions is therefore:

$$Rt\varphi = Rth\varphi + Rv_{keel} + Rr\varphi_{keel} + Rv_{rudder} \qquad \textbf{Equation 45}$$

Finally, for the appendages to develop sufficient lift to counteract the sail side force, yachts sail at a yaw angle λ also known as leeway, a case considered by the DSYHS.

A.6 Yawed: Appendages

By generating lift, the appendages will also create an induced drag component as well as a side force. The calculations inherent to the induced drag and the side force are detailed in this section.

First of all, the effective draft Te of the keel is assessed [56]:

$$\frac{Te}{T} = \left(A_1 \times \frac{Tc}{T} + A_2 \times \left(\frac{Tc}{T}\right)^2 + A_3 \times \frac{Bwl}{Tc} + A_4 \times TR \right) \times (B_0 + B_1 \times Fn) \qquad \textbf{Equation 46}$$

The coefficient A_1 to A_4 and B_0 and B_1 are given in Table 12.

φ	A_1	A_2	A_3	A_4	B_0	B_1
0°	3.7455	-3.6246	0.0589	-0.0296	1.2306	-0.7256
10°	4.4892	-4.8454	0.0294	-0.0176	1.4231	-1.2971
20°	3.9592	-3.9804	0.0283	-0.0075	1.5450	-1.5622
30°	3.4891	-2.9577	0.0250	-0.0272	1.4744	-1.3499

Table 12: *DSYHS effective draft regression coefficients [56].*

Applying the extended keel method, the lateral area of the keel is given by [56]:

$$Alat = \bar{c} \times T \qquad \textbf{Equation 47}$$

The effective aspect ratio can then be calculated [56]:

$$AR_e = \frac{Te^2}{Alat} \qquad \textbf{Equation 48}$$

The lift and induced drag coefficients, C_L and C_{Di}, are respectively [56]:

$$C_L = \frac{2\pi \times \lambda}{1 + 2/AR_e} \qquad \textbf{Equation 49}$$

$$C_{Di} = \frac{C_L^2}{\pi \times AR_e}$$ ***Equation 50***

Leading to the side force Fh and the induced drag component Ri [56]:

$$Fh = C_L \times \frac{1}{2} \times \rho \times V^2 \times Alat$$ ***Equation 51***

$$Ri = C_{Di} \times \frac{1}{2} \times \rho \times V^2 \times Alat$$ ***Equation 52***

The induced drag is added to the viscous and residuary keel resistance to give the total keel resistance:

$$Rt_{keel} = Rv_{keel} + Rr\varphi_{keel} + Ri_{keel}$$ ***Equation 53***

A similar procedure is applied to the rudder, with a couple of corrections to take into account the fact that the rudder operates in the downwash of the keel [60]. Firstly, the flow velocity is reduced to 90% of the flow velocity of the keel (i.e. the boat speed). In addition, the leeway angle is halved.

The DSYHS therefore enables to estimate the resistance of both hull and appendages in upright, heeled, and heeled and yawed conditions, provided the design fits the range of parameters considered.

B. Wave Patterns

The respective wave patterns at high Froude numbers are illustrated in Figure 37 to Figure 39 for a recent yacht (on the left hand side) and a 1970's design (on the right hand side), tested at Southampton Solent University [6].

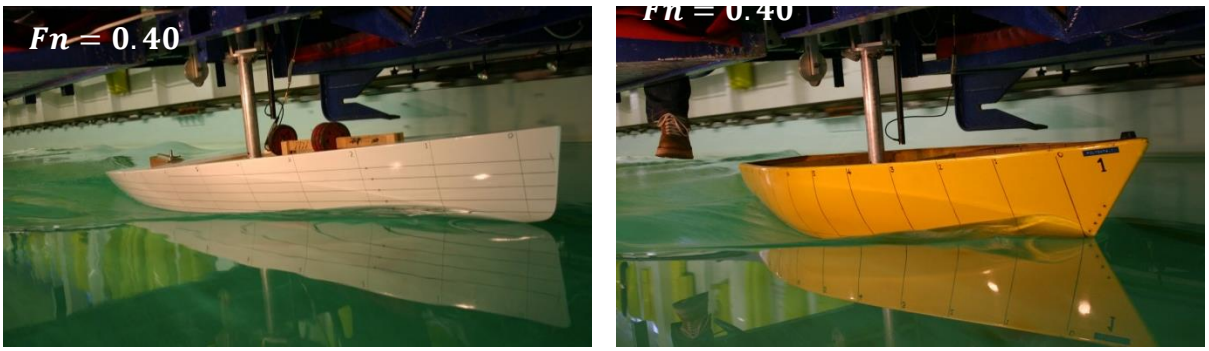

Figure 37: *Wave pattern at a Froude number of 0.40.*

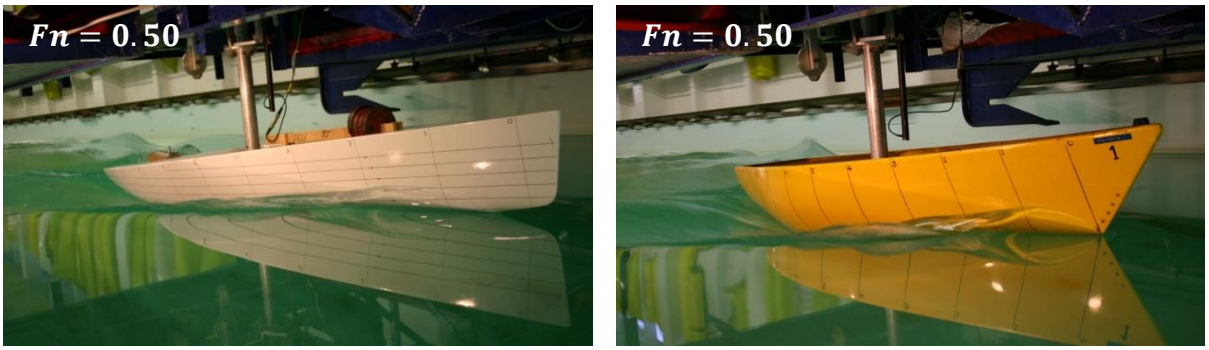

Figure 38: *Wave pattern at a Froude number of 0.50.*

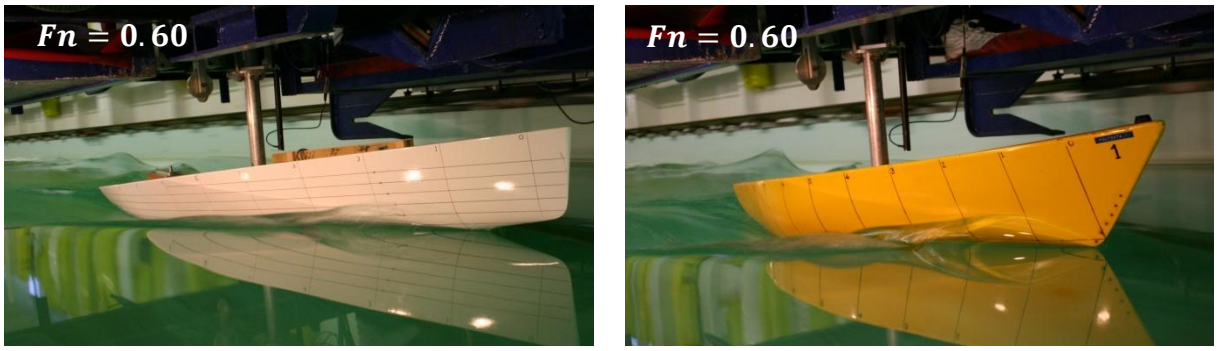

Figure 39: *Wave pattern at a Froude number of 0.60.*

C. DSYHS Examples of High Froude Number Resistance Prediction

Vessels able to reach semi-displacement mode early will see their resistance over predicted by the DSYHS, as illustrated in Figure 40.

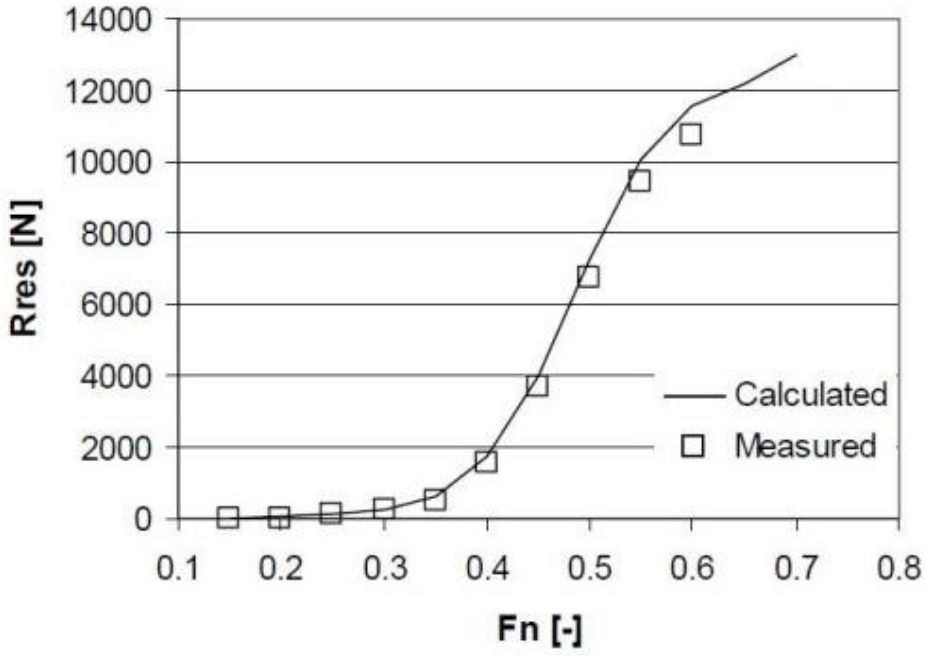

Figure 40: *Case of over-predicted resistance by the DSYHS (unknown model), from [54].*

Conversely, the resistance will be under-predicted for vessel reaching semi-displacement mode much later, such as the long and very slender model 329, as shown in Figure 41.

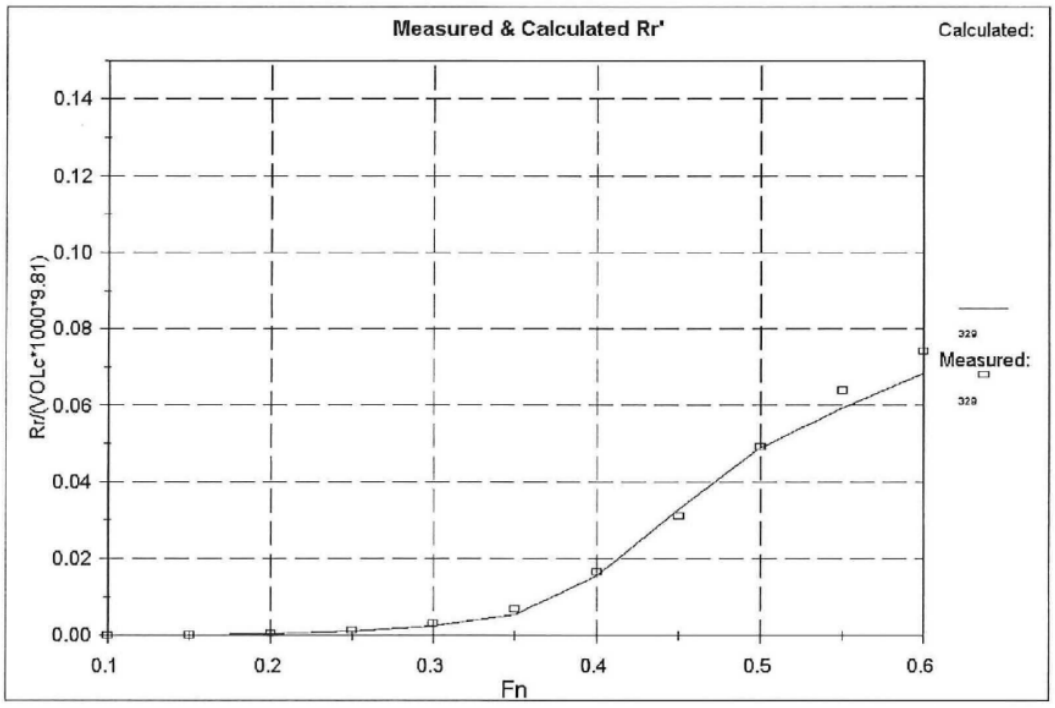

Figure 41: *Case of under-predicted resistance by the DSYHS (model 329), from [56].*

D. Validation of the Sysser 62 Hydrodynamic Model

D.1 10° Heel

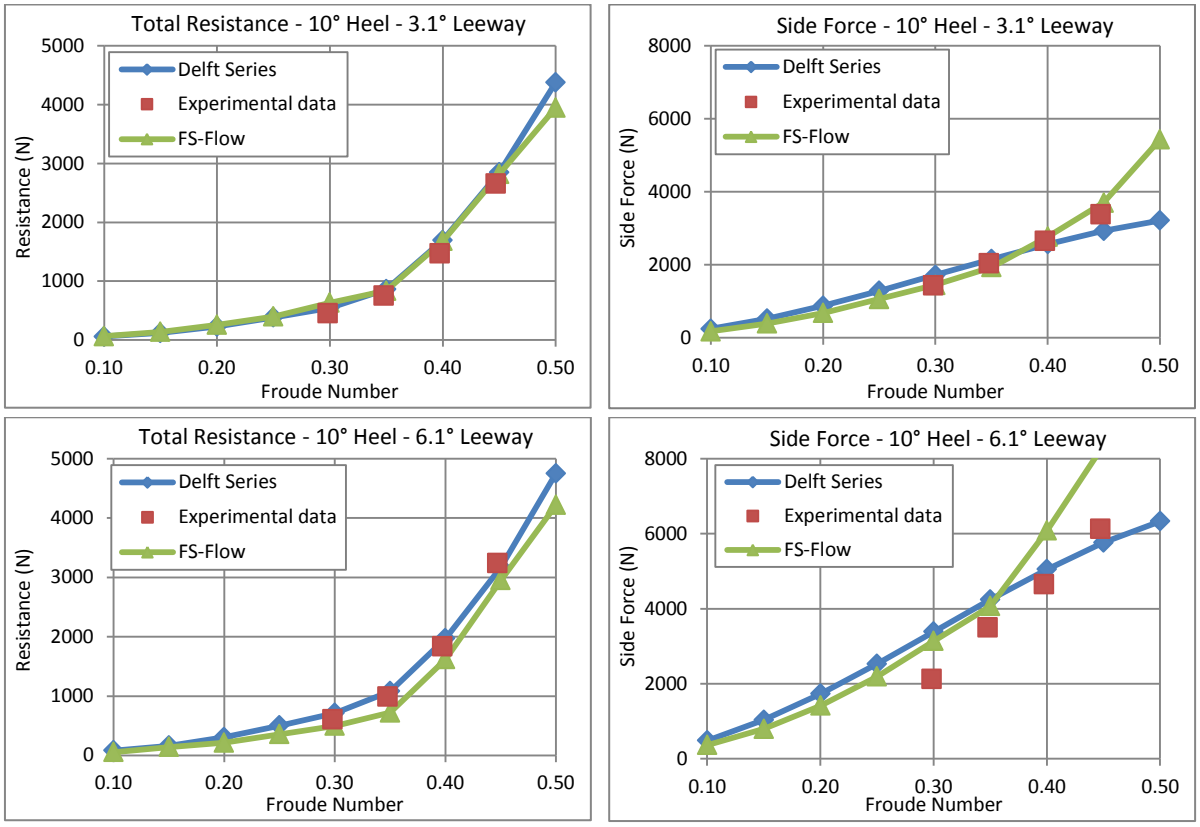

Figure 42: *DSYHS, experimental data and CFD comparison at 10° of heel.*

D.2 20° Heel

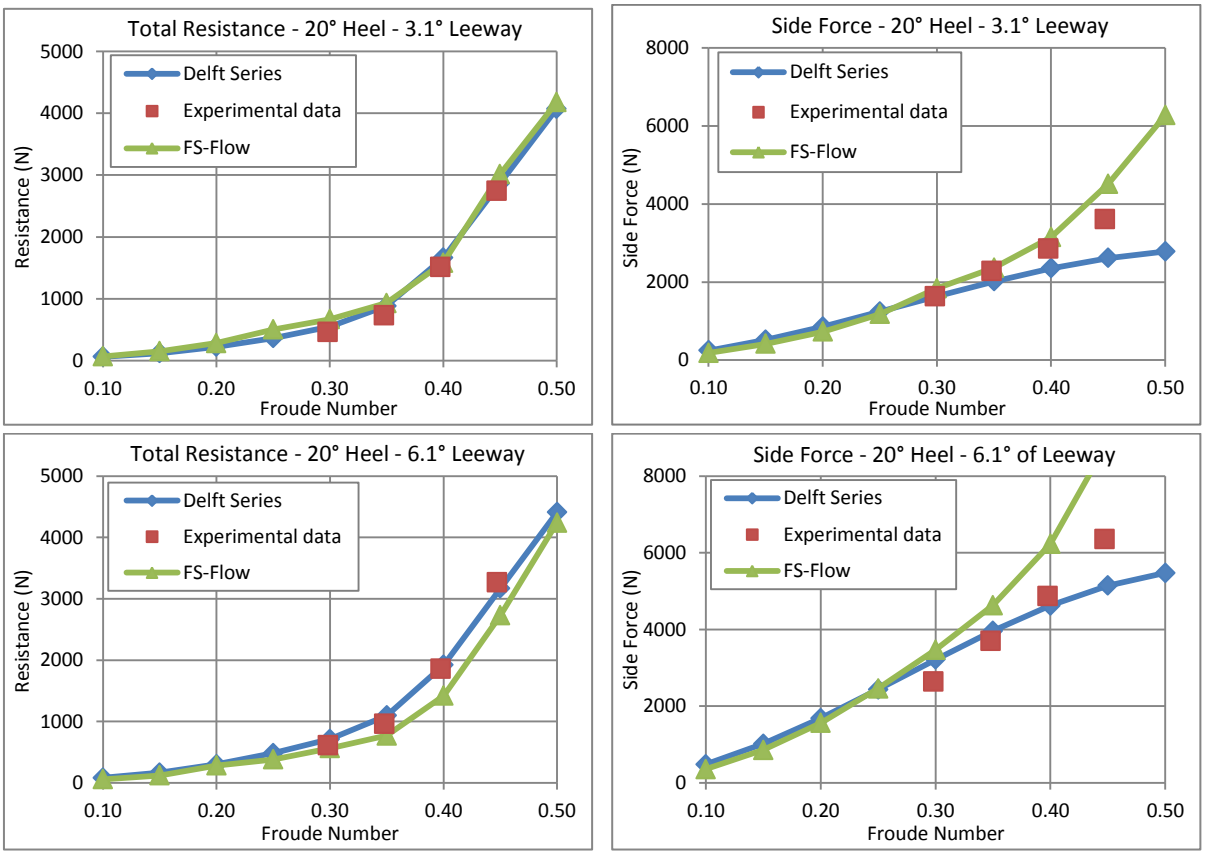

Figure 43: *DSYHS, experimental data and CFD comparison at 20° of heel.*

D.3 30° Heel

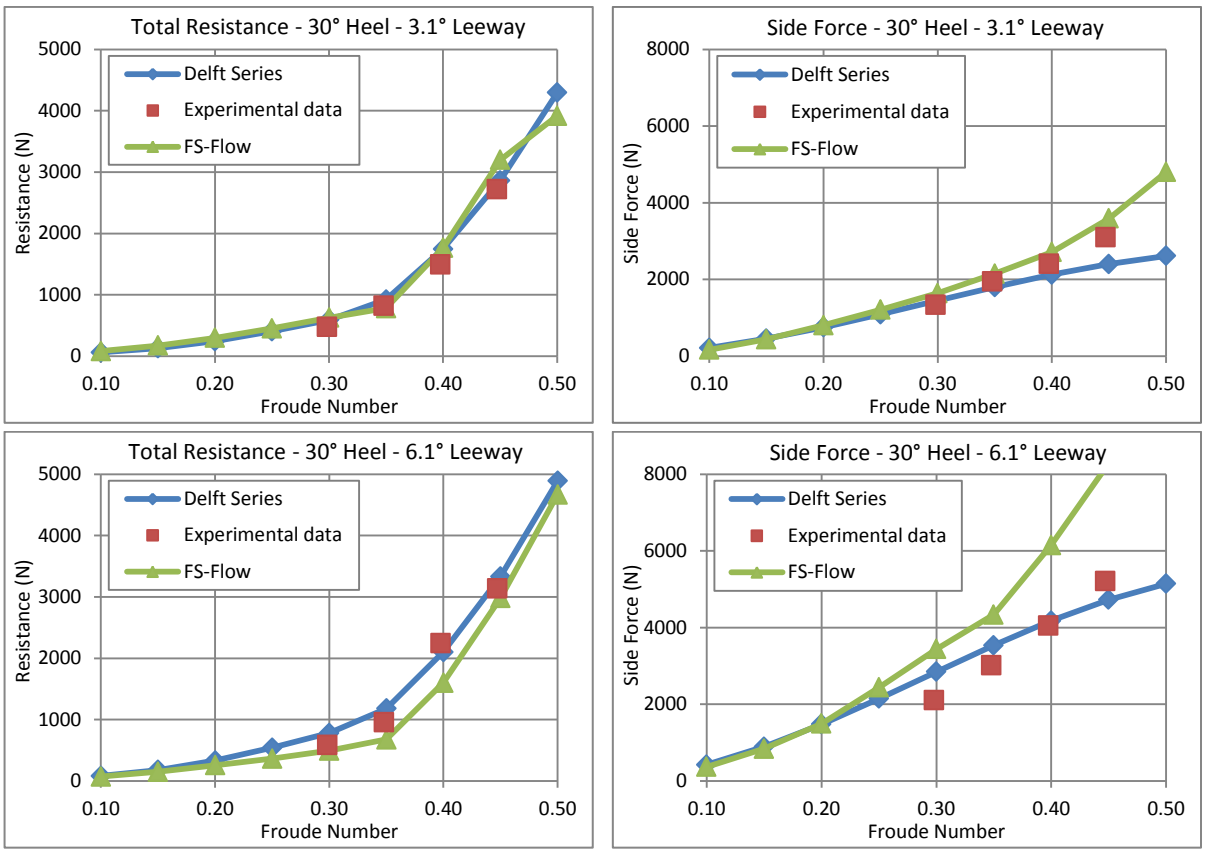

Figure 44: *DSYHS, experimental data and CFD comparison at 30° of heel.*

E. Table of Offsets of the Stewart 34

E.1 Original Imperial Measurements

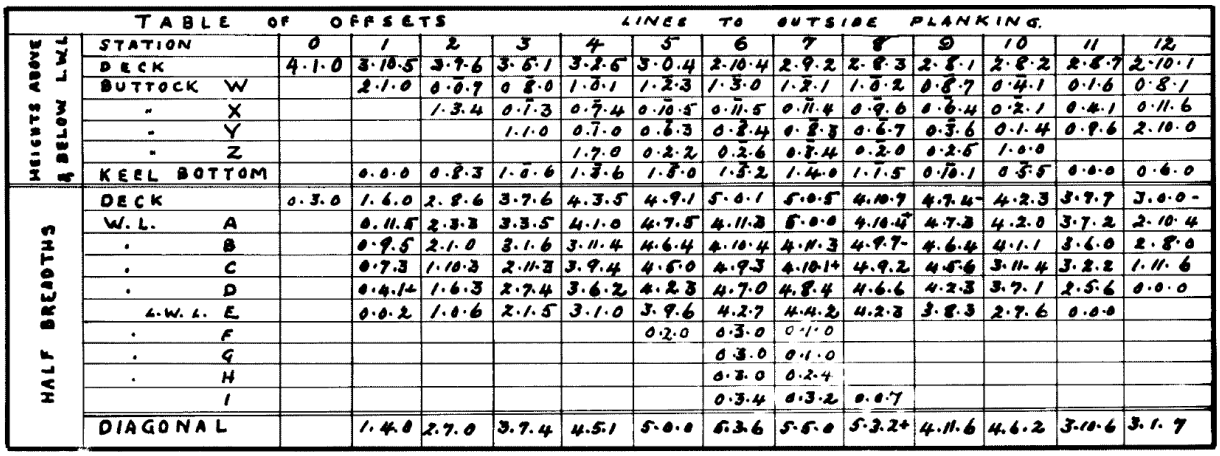

TABLE OF OFFSETS — LINES TO OUTSIDE PLANKING.

HEIGHTS ABOVE & BELOW LWL	STATION	0	1	2	3	4	5	6	7	8	9	10	11	12
	DECK	4·1·0	3·10·5	3·9·6	3·6·1	3·2·5	3·0·4	2·10·4	2·9·2	2·8·3	2·8·1	2·8·2	2·8·7	2·10·1
	BUTTOCK W		2·1·0	0·0·7	0 8·0	1·0·1	1·2·3	1·3·0	1·3·1	1·0·2	0·8·7	0·4·1	0·1·6	0·8·1
	" X			1·3·4	0·1·3	0·7·4	0·10·5	0·11·5	0·11·4	0·9·6	0·6·4	0·2·1	0·4·1	0·11·6
	" Y				1·1·0	0·1·0	0·6·3	0·3·4	0·3·3	0·6·7	0·3·6	0·1·4	0·9·6	2·10·0
	" Z					1·7·0	0·2·2	0·2·6	0·3·4	0·2·0	0·2·5	1·0·0		
	KEEL BOTTOM		0·0·0	0·8·3	1·0·6	1·3·6	1·3·0	1·3·2	1·4·0	1·1·5	0·10·1	0 3·5	0·0·0	0·6·0
HALF BREADTHS	DECK	0·3·0	1·6·0	2·8·6	3·7·6	4·3·5	4·9·1	5·0·1	5·0·5	4·10·7	4·7·4	4·2·3	3·9·7	3·0·0
	W.L. A		0·11·5	2·3·3	3·3·5	4·1·0	4·7·5	4·11·3	5·0·0	4·10·4	4·7·3	4·2·0	3·7·2	2·10·4
	" B		0·9·5	2·1·0	3·1·6	3·11·4	4·6·4	4·10·4	4·11·3	4·9·7	4·6·4	4·1·1	3·6·0	2·8·0
	" C		0·7·3	1·10·3	2·11·3	3·9·4	4·5·0	4·9·3	4·10·4	4·9·2	4·5·6	3·11·4	3·2·2	1·11·6
	" D		0·4·4	1·6·3	2·7·4	3·6·2	4·2·3	4·7·0	4·8·4	4·6·6	4·2·3	3·7·1	2·5·6	0·0·0
	L.W.L. E		0·0·2	1·0·6	2·1·5	3·1·0	3·9·6	4·2·7	4·4·2	4·2·3	3·8·3	2·7·6	0·0·0	
	" F						0·2·0	0·3·0	0·1·0					
	" G							0 3·0	0·1·0					
	" H							0·3·0	0·2·4					
	" I							0·3·4	0·3·2	0·0·7				
	DIAGONAL		1·4·0	2·7·0	3·7·4	4·5·1	5·0·0	5·3·6	5·5·0	5·3·2+	4·11·6	4·6·2	3·10·6	3·1·7

Table 13: *Original table of offsets of the Stewart 34 [84].*

E.2 Metric Conversion

TABLE OF OFFSETS OF THE STEWART 34 (CONVERTED FROM IMPERIAL TO METRIC - ALL UNITS ARE MILLIMETRE)														
Station number			0	1	2	3	4	5	6	7	8	9	10	11	12
Distance From FP			0	730	1614	2498	3382	4266	5150	6034	6918	7802	8686	9569	10446
Height above / below DWL	Sheer line		1245	1184	1162	1045	981	927	876	845	822	816	819	835	867
	Buttocks	W (300)		635	-22	-203	-308	-365	-381	-359	-311	-225	-105	44	206
		X (600)			394	-35	-191	-270	-295	-292	-248	-165	-54	105	298
		Y (900)				330	-25	-162	-216	-213	-175	-95	38	248	864
		Z (1200)					483	57	-70	-89	-51	67	305		
	Keel bottom				-213	-324	-400	-432	-438	-406	-346	-257	-143	0	152
Half breadth	Deck		76	457	832	1113	1311	1451	1527	1540	1495	1410	1280	1114	914
	Waterlines (from base)	A (2286)		295	695	1006	1225	1413	1508	1524	1486	1407	1270	1099	876
		B (2134)		244	635	959	1207	1384	1486	1508	1470	1384	1248	1067	813
		C (1981)		187	568	899	1156	1346	1457	1476	1454	1365	1207	972	603
		D (1829)		105	467	800	1073	1280	1397	1435	1391	1280	1095	756	
		E - Dwl (1676)		6	324	651	940	1162	1292	1327	1295	1127	806		
		F (1067)						51	76	25					
		G (762)							76	25					
		H (457)							76	64					
		I (152)							89	82	22				

Table 14: *Table of offsets of the Stewart 34, converted into metric units from [84].*

F. Three Dimensional Lofting

Before laser and CNC cutting, the linesplan of a yacht had to be drawn full size first, the various stations were then used to make the station moulds to be used to build the boat: this process is known as lofting.

The shape of the vessel is recorded in the table of offsets: stations, buttocks and waterlines offsets are listed, effectively providing the coordinates of points that joined together will form a given line of the linesplan. A batten tacked to the loft floor is traditionally used to fair the lines. Indeed, fairing is an essential part of lofting. Fortunately, the table of offsets of the Stewart 34 was available. Once converted from empirical to metric (see Appendix E), the table of offsets was used to loft the vessel in 3 dimensions using Maxsurf [9].

The starting point is a half cylinder surface, as shown in Figure 45.

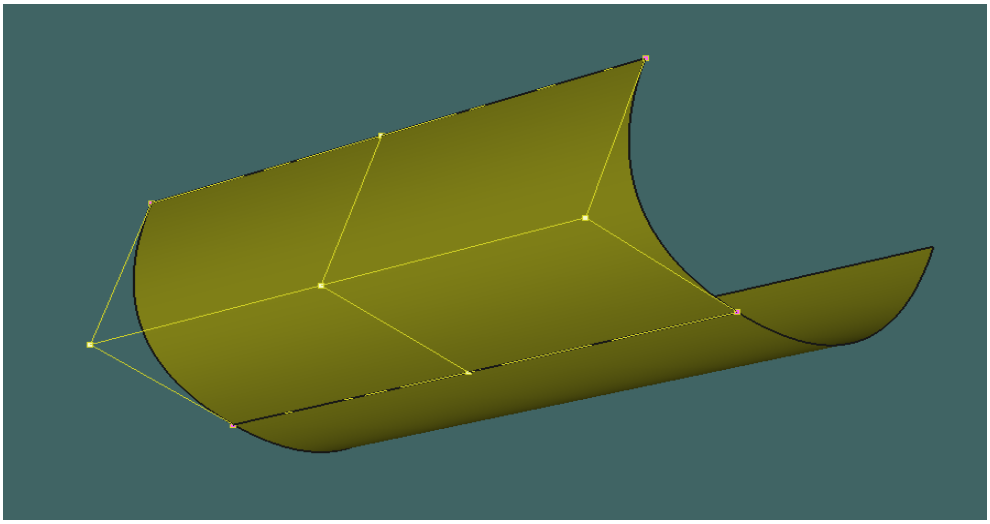

Figure 45: *Half cylinder, starting point of the 3D lofting.*

The table of offsets defines 12 stations, 5 waterlines and 4 buttock lines. Only 2 of those 3 sets of lines need to be combined to create a 3D model.

To maximise the accuracy, stations and waterlines have been selected as more are available than buttock lines. The net of the surface is modified to match the grid defined in the tables of offsets; the stations and waterlines can be seen in Figure 46.

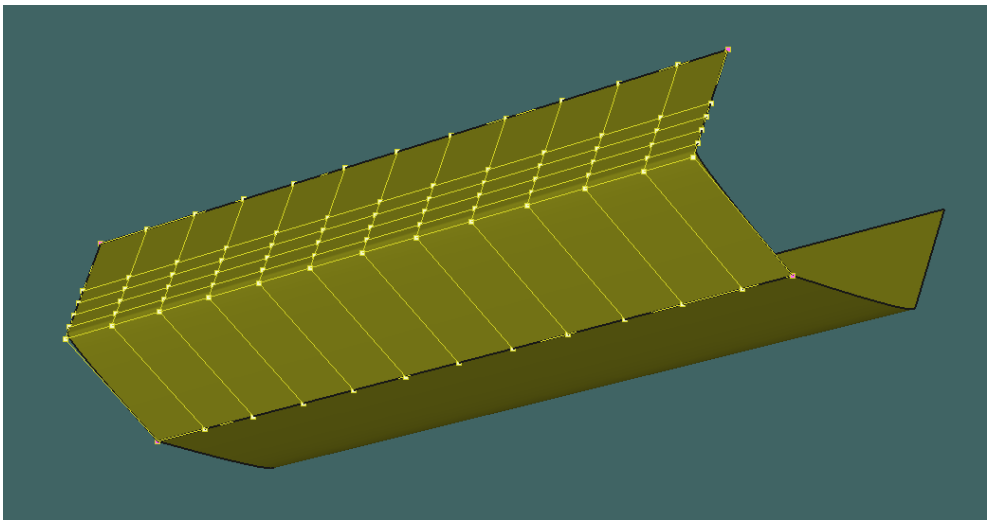

Figure 46: *Surface net matching the tables of offsets grid.*

Each node is then given its coordinate in space, quickly turning the surface into a 3D model of the Stewart 34, depicted in Figure 47.

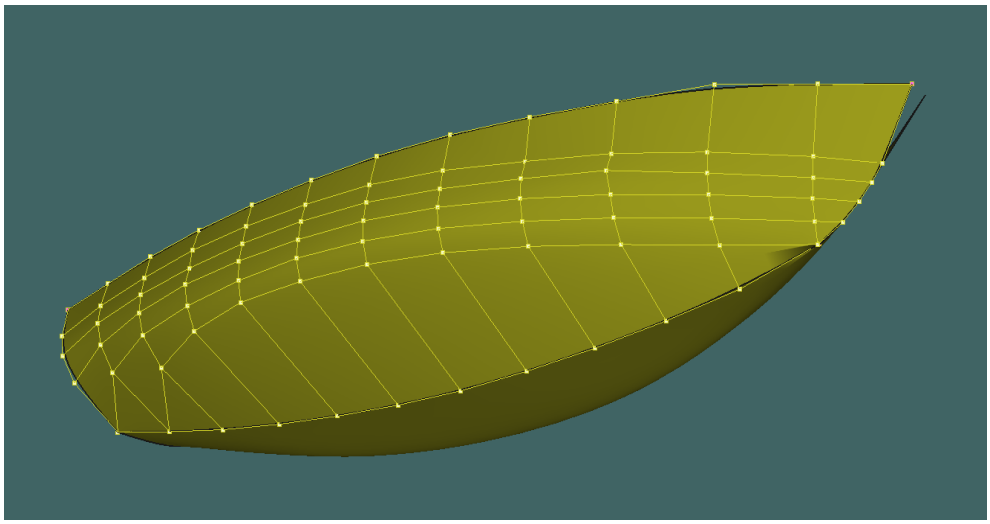

Figure 47: *Net of the 3D lofted Stewart 34*

The table of offsets aims at recreating the yacht's shape from the sheer line to the keel, and is therefore not particularly focused on the underwater shape. In the instance of the Stewart 34, no waterline below the design waterline was provided. In order to improve the definition of the underwater profile, an underwater waterline has been created from the linesplan, and the offsets have then been added to the 3D model, as illustrated in Figure 48.

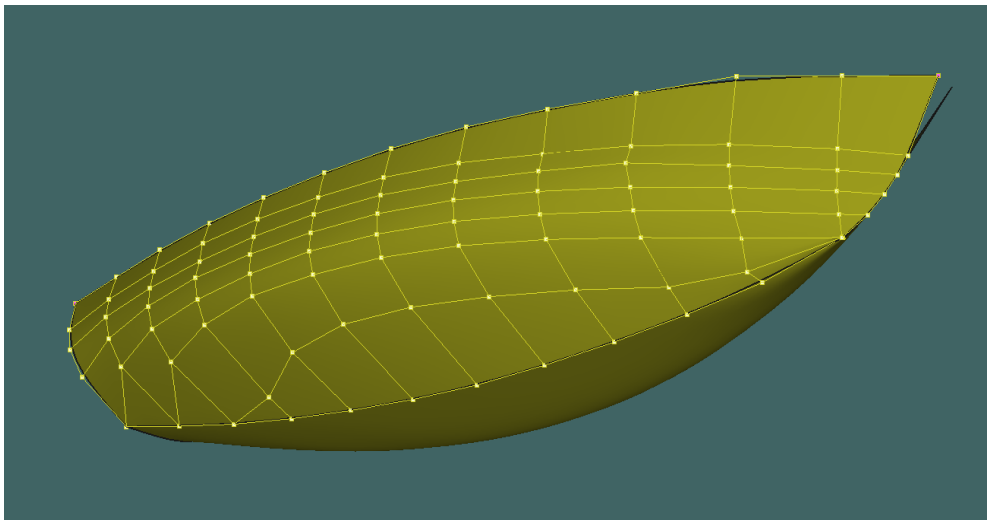

Figure 48: *Additional waterline added to the model of the Stewart 34.*

If the use of non-uniform radial B-splines (NURBS) produces a relatively fair finish, particular attention has been paid to achieve a model as fair as possible, eventually resulting in the final representation of the Stewart 34 presented in Figure 49.

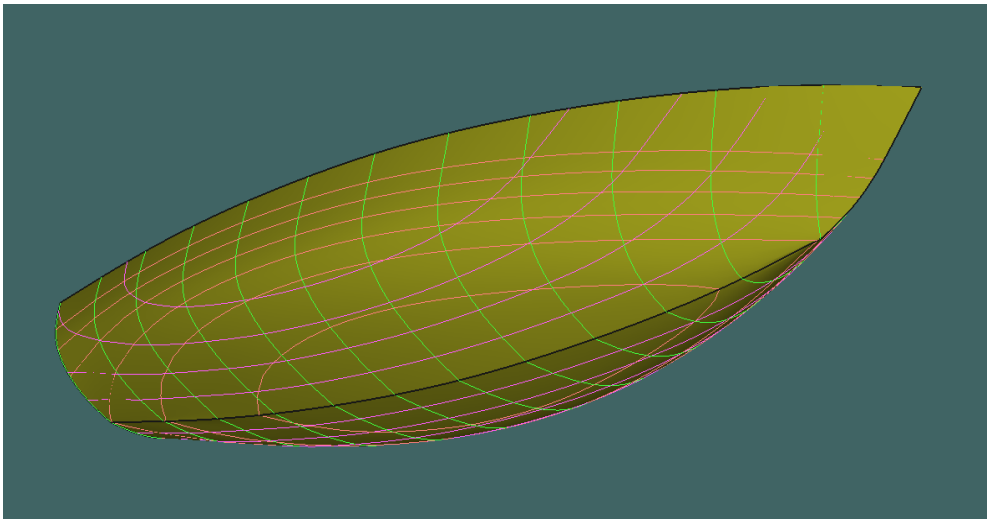

Figure 49: *Final model of the Stewart 34.*

The appendages were modelled combining information provided by the linesplan and measurements realised on the vessel. Deducing the appendages volumes, the hull was set to the appropriate depth to match the total 5100 kg displacement of the vessel considered, hence providing the relevant hydrostatics as well as the 3D model of the yacht used for the CFD analysis.

G. Empirical 4 Degrees of Freedom VPP

The theory being the empirical 4 degrees of freedom VPP program developed in order to ascertain the test matrix for the Stewart 34 is presented hereafter, also providing the underpinning theory to VPPs (such as WinDesign And FS-Equilibrium).

G.1 Hydrodynamic model

For the purpose of the empirical VPP, the hydrodynamic resistance and side force have been ascertained thanks to the DSYHS, as presented in Appendix A. Those two forces are then to be balanced with the aerodynamic drive and side force.

G.2 Velocity triangles

For a given true wind speed Vt and a true wind angle βt, and considering the boat speed Vs, the apparent wind speed Va and apparent wind angle βa can be found by solving:

$$Va \times \cos \beta a = Vs + Vt \times \sin \beta t \qquad \textbf{Equation 54}$$

$$Va \times \sin \beta a = Vt \times \sin \beta t \qquad \textbf{Equation 55}$$

For the purpose of the preliminary VPP, effective angle theory has been neglected: the impact of the heel angle on the effective wind speed and angle is not accounted for.

G.3 Aerodynamic model

The sail coefficients proposed by Hazen [34] have been (and still are) commonly used for the aerodynamic model of VPP. There are however some limitations to the use of those coefficients. Indeed, only 5 different angles for the main sail, 3 for the jib, and 4 for the spinnaker are considered. In this instance, another set of coefficients have been preferred for its greater number of angles, its more recent development, and its validated accuracy. Indeed, the coefficients presented in Table 15 are those established by the Offshore Racing Congress (ORC) [69] for their VPP-based handicap racing rules.

Main Sail			Jib			Spinnaker		
βa (°)	C_L	C_{Dp}	βa (°)	C_L	C_{Dp}	βa (°)	C_L	C_{Dp}
0	0.000	0.043	7	0.000	0.050	28	0.085	0.170
7	0.862	0.026	15	1.000	0.032	41	1.114	0.238
9	1.052	0.023	20	1.375	0.031	50	1.360	0.306
12	1.164	0.023	27	1.450	0.037	60	1.513	0.459
28	1.347	0.033	50	1.430	0.250	67	1.548	0.392
60	1.239	0.113	60	1.250	0.350	75	1.479	0.493
90	1.125	0.383	100	0.400	0.730	100	1.207	0.791
120	0.838	0.969	150	0.000	0.950	115	0.956	0.894
150	0.296	1.316	180	-0.100	0.900	130	0.706	0.936
180	-0.112	1.345				150	0.425	0.936
						180	0.000	0.936

Table 15: *Offshore Racing Congress sail coefficients [69].*

Unless stated otherwise, the following equations are defined in [54]. The lift and drag coefficients are ascertained for a given sail set thanks to:

$$C_{L\,main/jib} = \frac{C_{L\,main} \times A_{main} + C_{L\,jib} \times A_{jib}}{(A_{N\,main} + A_{N\,jib})} \quad \textit{Equation 56}$$

$$C_{Dp\,main/jib} = \frac{C_{Dp\,main} \times A_{main} + C_{Dp\,jib} \times A_{jib}}{(A_{main} + A_{N\,jib})} \quad \textit{Equation 57}$$

Where the jib area is defined as a function of the height I, the base J and the luff perpendicular LP:

$$A_{jib} = 0.5 \times \sqrt{I^2 + J^2} \times LP \quad \textit{Equation 58}$$

While its nominal area is:

$$A_{N\,jib} = 0.5 \times I \times J \quad \textit{Equation 59}$$

On the other hand, the mainsail luff P and foot E give the main area as:

$$A_{main} = A_{N\,main} = 0.5 \times P \times E \quad \textit{Equation 60}$$

And the spinnaker area is given based on the spinnaker luff SL:

$$A_{spi} = A_{N\,spi} = 1.15 \times SL \times J \quad \textit{Equation 61}$$

Finally, the lift and drag are given by:

$$Lift = \frac{1}{2} \times \rho \times A_N \times Va^2 \times C_L \quad \textit{Equation 62}$$

$$Parasitic\ Drag = \frac{1}{2} \times \rho \times A_N \times Va^2 \times C_{Dp} \quad \textit{Equation 63}$$

For apparent wind angle where both the jib and spinnaker could be used, the sail which would perform best (i.e. achieve the best boat speed) is automatically selected.

The induced drag of the sails can then be calculated based on the aspect ratio, defined for close hauled as:

$$AR = \frac{\left(1.1 \times (EMH + FA)\right)^2}{A_N} \quad \textit{Equation 64}$$

Where EMH is the mast height and FA the freeboard. This definition of the aspect ratio takes into account the mirror effect of the deck on the jib when sailing close to the wind.

This aspect ratio has been assumed to apply up to 30° apparent wind angle. For other courses, the aspect ratio is given by:

$$AR = \frac{\left(1.1 \times (EMH)\right)^2}{A_N} \quad \textit{Equation 65}$$

The induced drag coefficient is then established:

$$C_{Di} = {C_L}^2 \times \left(\frac{1}{\pi \times AR} + 0.005\right) \quad \textit{Equation 66}$$

Where 0.005 represent the separation drag. The coefficient is eventually incorporated into the induced drag equation:

$$Ri = \frac{1}{2} \times \rho \times A_N \times Va^2 \times C_{Di} \quad \textit{Equation 67}$$

Finally, the windage of the sails and rigging needs to be established from first principles. For each component, the frontal and lateral area are assessed, and then combined with their respective coefficients presented in Table 16 to give the windage of the element:

$$Dw = \frac{1}{2} \times \rho \times Va^2 \times (A_{lat} \times C_{D\,lat} \times \sin \beta a + A_{front} \times C_{D\,front} \times \cos \beta a) \quad \textbf{Equation 68}$$

Element	C_D front	C_D lat
Rigging and mast (circular)	1	1
Hull	0.4	0.9

Table 16: *Windage coefficients, as defined in [93].*

The elements considered in the windage analysis are: the hull, mast, forestay, back stay, vertical and diagonal shrouds and spreaders. Note that the shrouds and stays diameters have been estimated from the rig dimensions in a first principles mast scantlings analysis [86].

The sum of the parasitic, induced (inclusive of the separation) and windage drag gives the total aerodynamic drag.

Based on recognised sail coefficients, the aerodynamic lift and drag have been ascertained, leading to the two main aerodynamic outputs: drive and side force, respectively given by:

$$Drive = Lift \times \sin(\beta a - \lambda) - Drag \times \cos(\beta a - \lambda) \quad \textbf{Equation 69}$$

$$Side\ force = Lift \times \cos(\beta a - \lambda) - Drag \times \sin(\beta a - \lambda) \quad \textbf{Equation 70}$$

Note that the side force needs to be corrected to solve for the side force in the horizontal plane by multiplying by the cosine of the heel angle.

So far, the resistance, hydrodynamic side force, drive and sail side force have been established, and the boat speed and leeway angle could therefore be assessed. However, an additional degree of freedom must be considered to solve for the heel angle, hence the need to calculate both the heeling and righting moment.

G.4 Stability

The heeling arm, vertical distance between the centre of lateral resistance CLR and the centre of effort CE is required to calculate the heeling moment. Both will be assumed to remain in the same location despite the various sailing conditions of the vessel.

The centre of lateral resistance in simply taken as 45% of the total draft.

On the other hand, the centre of effort of each sail is established as follows:

$$CE_{main} = 0.39 \times P + BAD + FA \quad \textbf{Equation 71}$$

$$CE_{jib} = 0.39 \times I + FA \quad \textbf{Equation 72}$$

$$CE_{spi} = 0.59 \times I + FA \quad \textbf{Equation 73}$$

Where BAD is the boom above deck. The centre of effort of a sail set is given in a similar manner as the combined lift coefficient presented previously:

$$CE_{main/jib} = \frac{CE_{main} \times A_{N\,main} + CE_{jib} \times A_{N\,jib}}{(A_{N\,main} + A_{N\,jib})} \quad \textbf{Equation 74}$$

And therefore the heeling arm HA is:

$$HA = CLR + CE \quad \textit{Equation 75}$$

Finally, the heeling moment HM is:

$$HM = HA \times SSF \quad \textit{Equation 76}$$

The heeling moment is then balanced with the righting moment ascertained in Appendix I.3 to give the heel angle.

All the elements required for a 3 degrees of freedom are now available. However, the performance of the yacht can be improved in some circumstances thanks to the depowering of the sails.

G.5 Depowering

Despite not being as appropriate as ease and twist or the power parameter [33], the effects of reef r and flat f have been considered for their ease of computation coupled with their wide use in various VPP softwares [93].

Reef enables to reduce the sail area while conserving the aspect ratio. As a result, the lift and drag are reduced, and the centre of effort is lowered, thus reducing the heeling arm. On the other hand, flat allows to flatten the sail, which reduced the lift and induced drag generated, while the parasitic drag, sail area and centre of effort height remain unchanged.

Those two parameters impact on both the lift and drag coefficients of the sails [33]:

$$C_L = C_{L\,opt} \times r^2 \times f \quad \textit{Equation 77}$$

$$C_{Di} = \frac{{C_{L\,opt}}^2 \times r^2 \times f^2}{\pi \times e \times AR} \quad \textit{Equation 78}$$

Where e is an efficiency factor. The optimum performance can now be assessed by the empirical 3 degrees of freedom VPP proposed.

Finally, a fourth degree of freedom will be considered: the yaw moment, that has to be corrected with the rudder angle.

G.6 Rudder Angle

The yaw moment is created due to the yaw lever between the sail side force acting at the longitudinal centre of effort, and the hydrodynamic side force acting at the longitudinal centre of lateral resistance. Those two centres must therefore be aligned to achieve equilibrium so that no moment is generated. This is done by adding some rudder angle that will shift the centre of lateral resistance aft until equilibrium is achieved.

The DSYHS does not consider the lift generated by the rudder in its analysis (the rudder lift being incorporated as part of the extended keel method presented Appendix A.4), hence the need to ascertain the lift and inducted drag generated. In addition, the location of the centre of effort and the centre of lateral resistance must be known. The simplified approach taken is presented in this section.

G.6.1 Vertical centre of effort

The centre of effort is based on the geometric centre of area. Treating the jib as a triangle, its centre of effort will be located two thirds of the way aft from the tack, hence:

$$CE_{jib} = \frac{2}{3} \times J$$ ***Equation 79***

Also considering the main sail as a triangle, the centre of effort is given as:

$$CE_{main} = \frac{1}{3} \times E$$ ***Equation 80***

This is the centre of effort of the main relative to its luff, the centre of effort relative to the tack (or forward extent) is:

$$CE_{main} = J + MD + \frac{1}{3} \times E$$ ***Equation 81***

Where MD is the mast diameter. The combined centre of effort is then ascertained based on the respective areas of each sails. Note that the proposed model is only valid with the jib, at reasonable heel angle, and not applicable downwind.

G.6.2 Centre of lateral resistance

Horizontally projecting the centre of area of the keel onto the quarter chord line has been used to establish the centre of lateral resistance [94]. The same technique has been used for the rudder.

The DSYHS assumes that the lift is generated by the keel only (thanks to the extended keel method): the centre of lateral resistance with no rudder angle on has therefore been assumed to be the centre of lateral resistance of the keel, thus neglecting the lift generated by the rudder on centreline due to the leeway. As the rudder angle increases, lift L is generated, shifting the combined centre of lateral resistance aft:

$$CLR_{combined} = \frac{L_{Keel} \times CLR_{keel} + L_{Rudder} \times CLR_{rudder}}{L_{Total}}$$ ***Equation 82***

G.6.3 Rudder Lift

An important factor to take into account is that the rudder evolves in the downwash of the keel. Recent work undertaken by Delft University [53] suggests that the rudder only experiences 90% of the boat speed and 50% of the leeway angle, hence the lift generated by the rudder at an angle of attack α is:

$$L_{Rudder} = \frac{1}{2} \times \rho \times A_{lat} \times (0.9 \times V)^2 \times \frac{2\pi \times \left(\frac{\lambda}{2} + \alpha\right)}{1 + \frac{2}{AR_e}}$$ **Equation 83**

The single rudder being located under the boat, it is very unlikely to ventilate, hence the effective aspect ratio has been taken has twice the geometric aspect ratio:

$$AR_e = 2 \times AR_g$$ ***Equation 84***

Since lift is generated, the induced drag must be taken into account:

$$C_{Di} = \frac{{C_L}^2}{\pi \times AR_e}$$ ***Equation 85***

$$Ri = \frac{1}{2} \times \rho \times A_{lat} \times (0.9 \times V^2) \times C_{Di}$$ ***Equation 86***

The induced resistance is then added to the total resistance of the vessel.

G.6.4 Equilibrium

In order to achieve equilibrium, there must be no yaw lever between the longitudinal centre of effort of the sails and the longitudinal centre of lateral resistance of the appendages, mathematically:

$$CE = CLR \qquad \textbf{Equation 87}$$

Inputting the definition of the combined CLR defined in Equation 82:

$$CE = \frac{L_{Keel} \times CLR_{keel} + L_{Rudder} \times CLR_{rudder}}{L_{Keel} + L_{Rudder}} \qquad \textbf{Equation 88}$$

And solving for the rudder lift:

$$L_{Rudder} = \frac{L_{Keel} \times (CLR_{keel} - CE)}{CE - CLR_{rudder}} \qquad \textbf{Equation 89}$$

This gives the amount of lift to be generated by the rudder for the two centres to align. The rudder angle required to generate such lift is given by:

$$\alpha = \frac{L_{Rudder} \times \left(1 + \frac{2}{AR_e}\right)}{\frac{1}{2} \times \rho \times A_{lat} \times (0.9 \times V)^2 \times 2\pi} - \frac{\lambda}{2} \qquad \textbf{Equation 90}$$

Balancing the CE and the CLR thanks to the rudder angle to avoid any yaw moment constitute a fourth degree of freedom.

This is however a very simplified estimation, based on the centre of area of the sails as a centre of effort, and assuming that it remains constant as the boat heels and as the sails are trimmed. Nevertheless, it constitutes a suitable simplification for a preliminary VPP aiming at establishing the operating speeds, heel and leeway angles of the Stewart 34.

H. Hydrodynamic Model of the Stewart 34

H.1 Upright

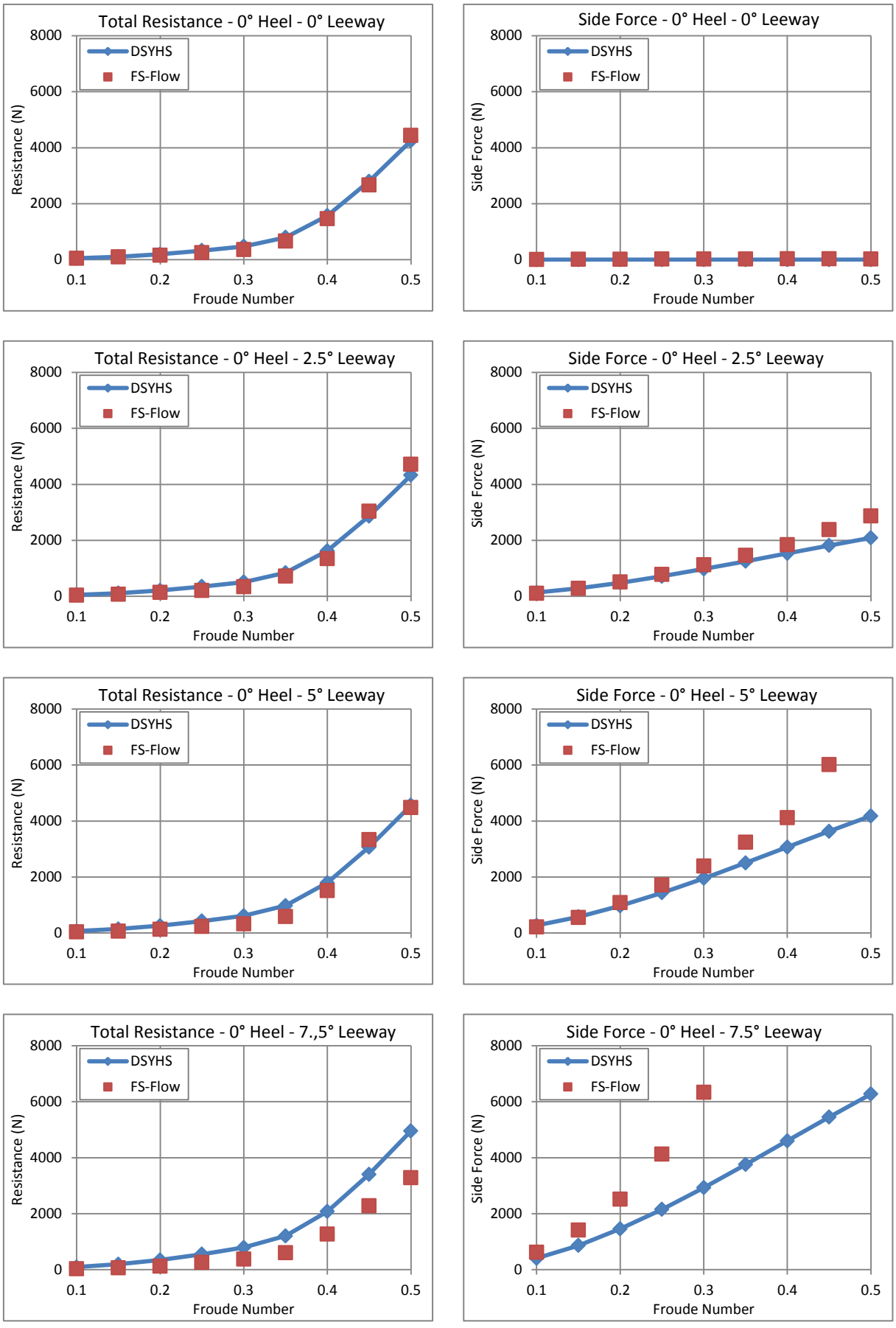

Figure 50: *Stewart 34 hydrodynamic model: FS-Flow and DSYHS comparison, 0° Heel.*

H.2 7.5° Heel

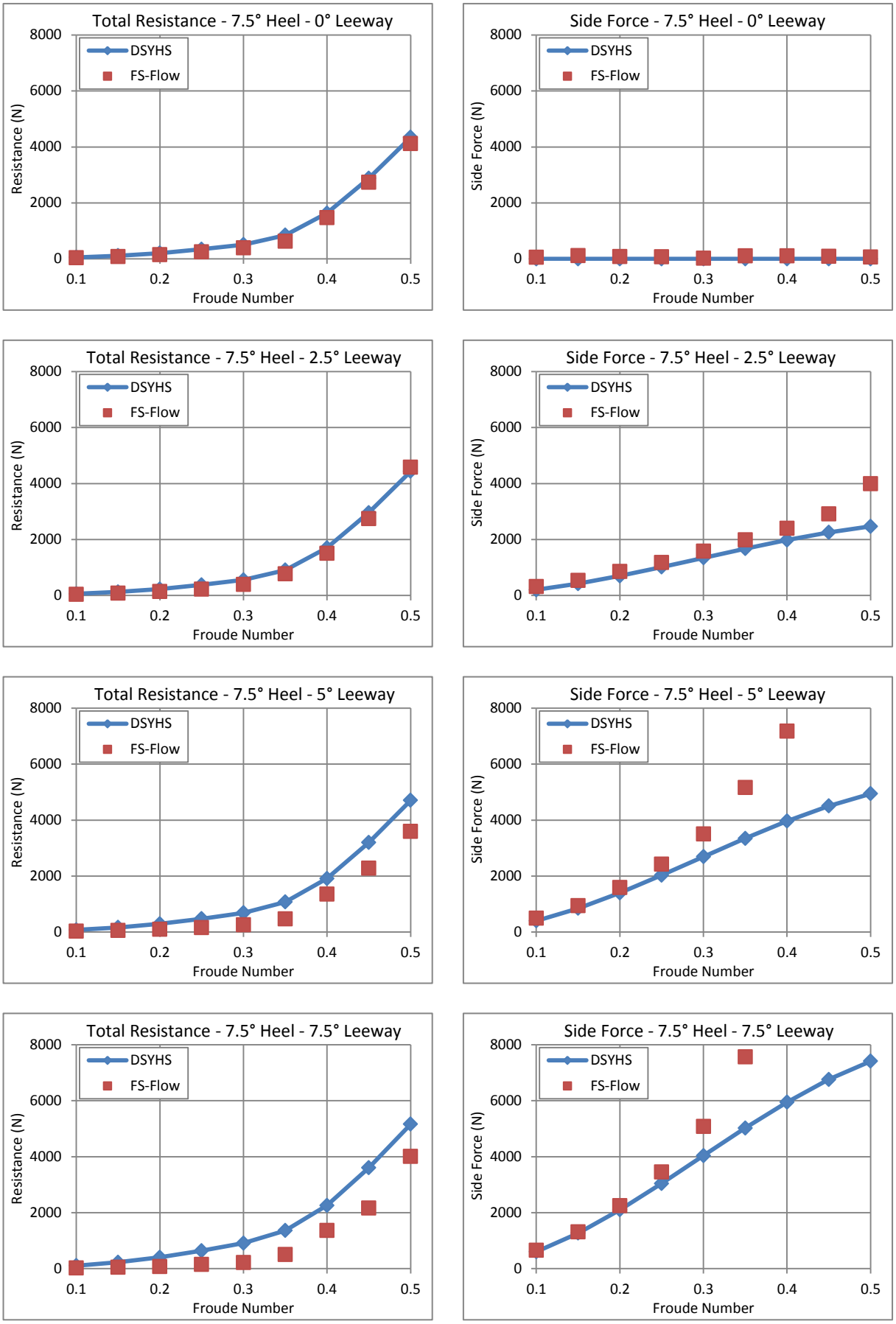

Figure 51: *Stewart 34 hydrodynamic model: FS-Flow and DSYHS comparison, 7.5° Heel.*

H.3 15° Heel

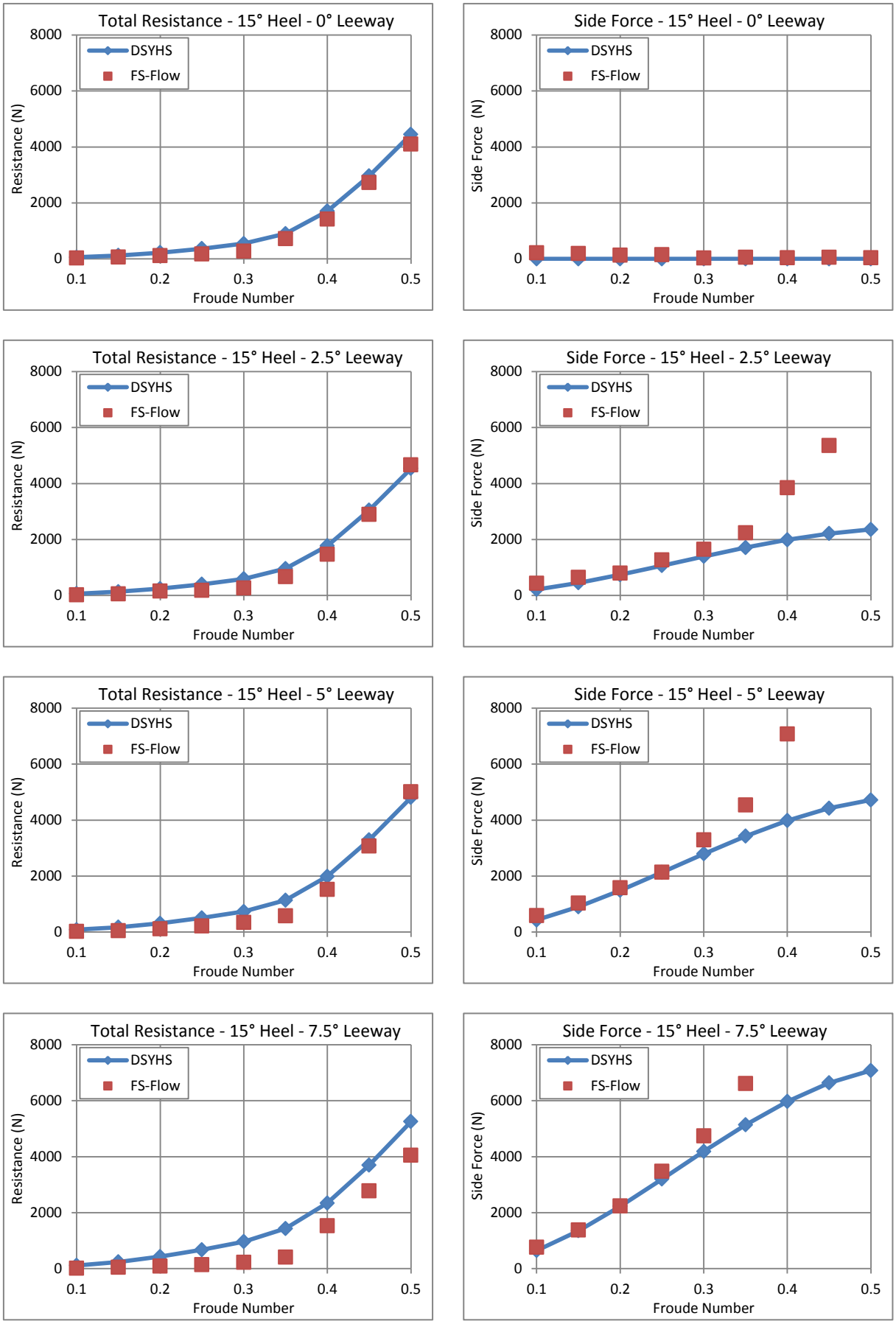

Figure 52: *Stewart 34 hydrodynamic model: FS-Flow and DSYHS comparison, 15° Heel.*

H.4 22.5° Heel

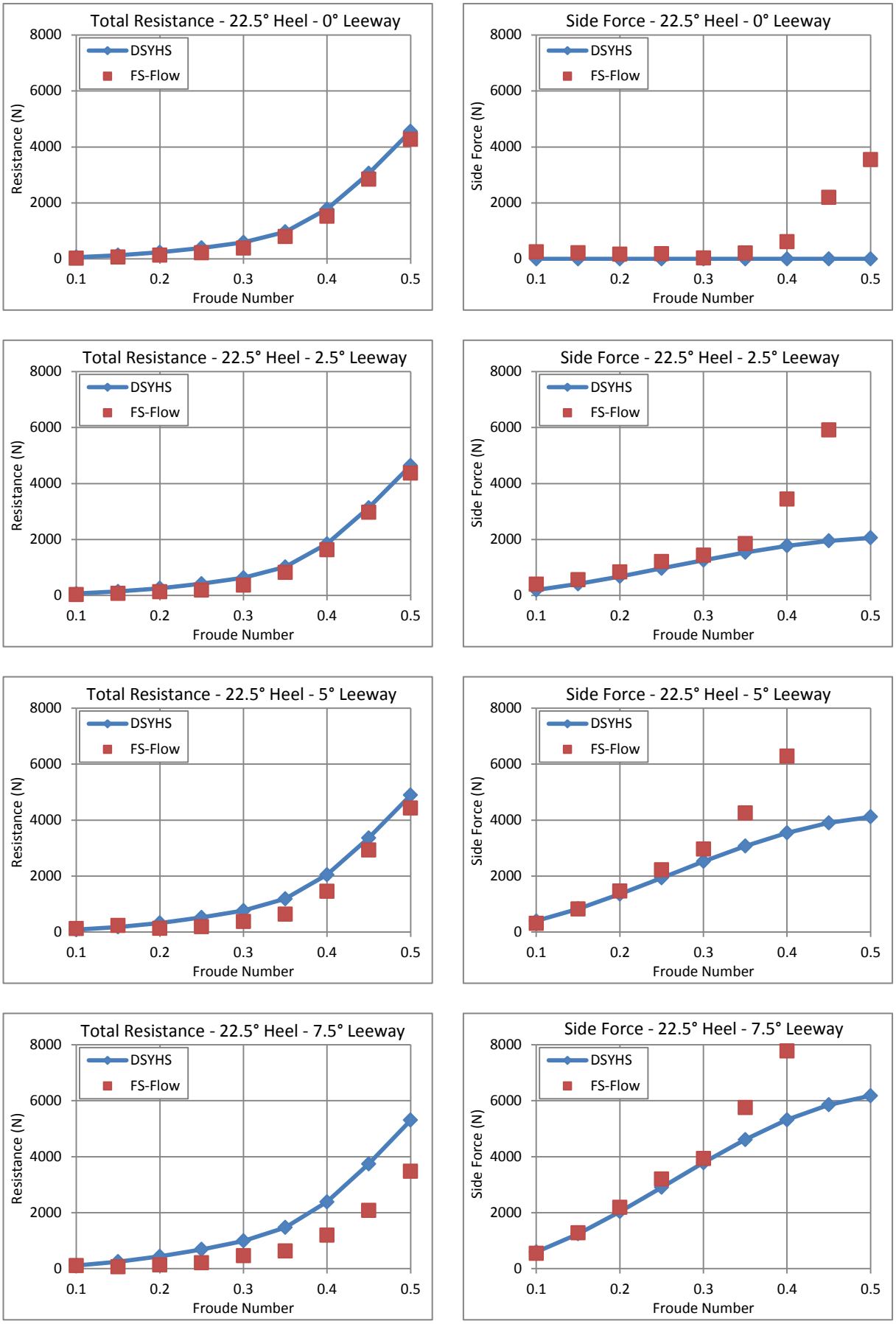

Figure 53: *Stewart 34 hydrodynamic model: FS-Flow and DSYHS comparison, 22.5° Heel.*

H.5 28° Heel

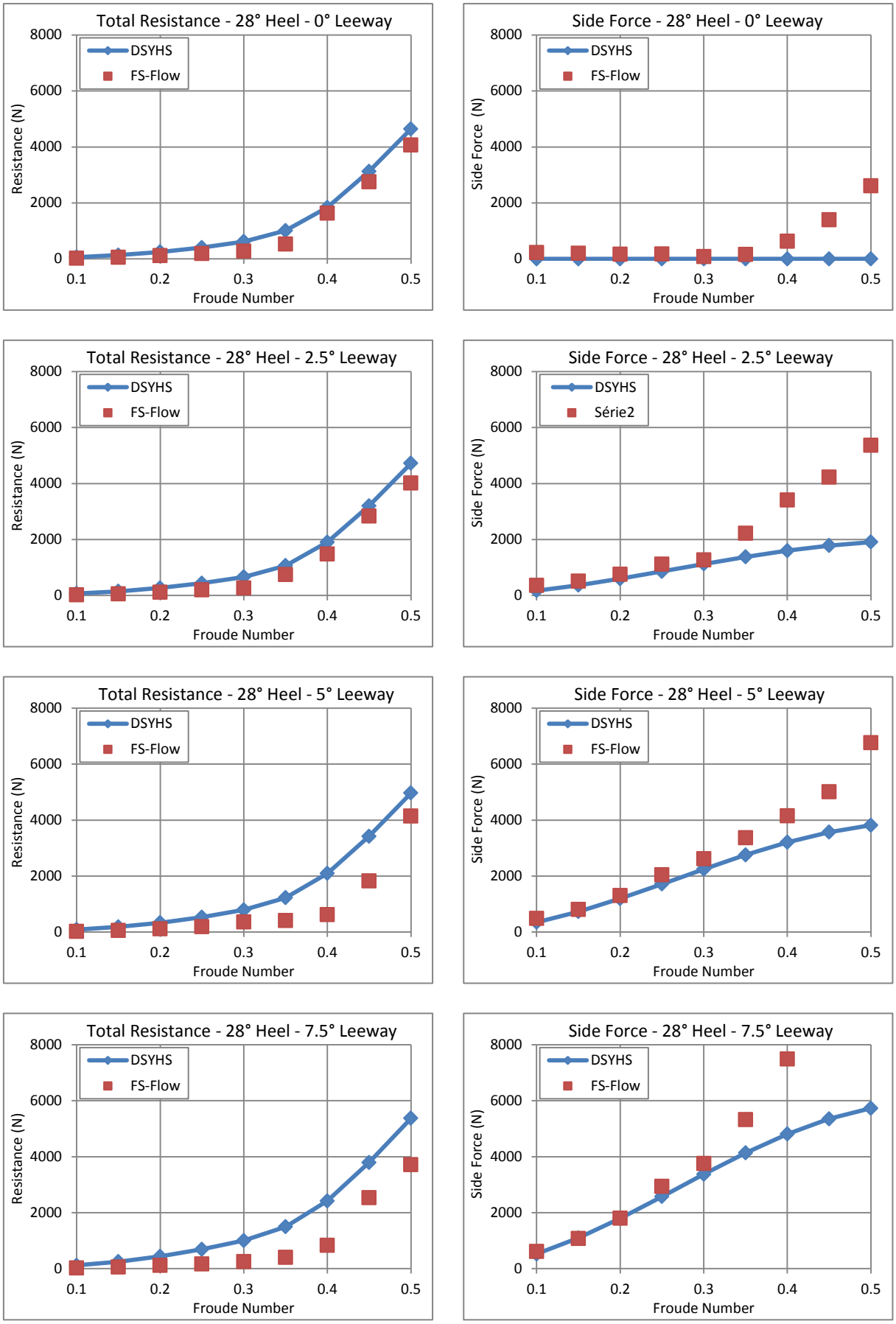

Figure 54: *Stewart 34 hydrodynamic model: FS-Flow and DSYHS comparison, 28° Heel.*

H.6 35° Heel

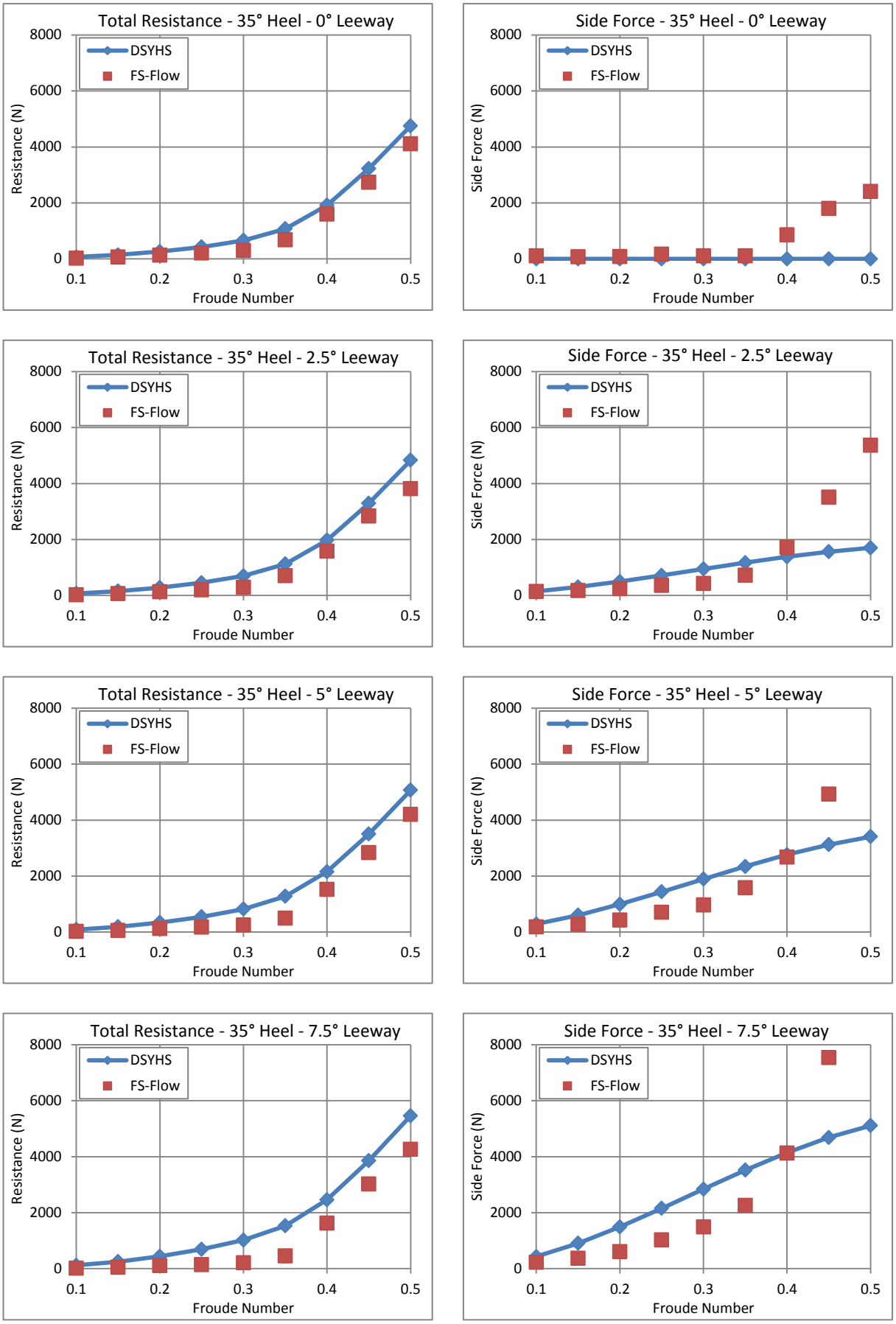

Figure 55: *Stewart 34 hydrodynamic model: FS-Flow and DSYHS comparison, 35° Heel.*

I. Transverse Stability Assessment

The transverse stability is a predominant component of a VPP as the balance of the heeling moment and the righting moment will define the heel angle at which the yacht is sailing. Assessing the stability of boats has been greatly enhanced by the development of specialised software, such as Hydromax [8] that will be used for the stability assessment of the Stewart 34. The difficulty in establishing the stability of a vessel is to locate the Vertical Centre of Gravity (VCG). Despite the increasing accuracy of weight estimates, the position of the VCG can only be found through an inclining experiment once the vessel has been built. Such experiments rely on the principles of small angle stability. Once known, the VCG will be used for the large angle stability of the vessel. The main sources of inaccuracy will be identified to comment the reliability of the stability model. The ascertained stability of the Stewart 34 will then be used for the VPP of the vessel.

I.1 Small Angle Stability

For the stability of yachts, four key points need to be located: the vertical centre of buoyancy B, the vertical centre of gravity G, the transverse metacentre M, and the reference point K, as shown in Figure 56. The distance $\overline{BM}$ is known as the metacentric radius, while $\overline{GM}$ is the metacentric height. For small angles of heel φ, typically less than 3°, the position of the metacentre is assumed to be fixed [54].

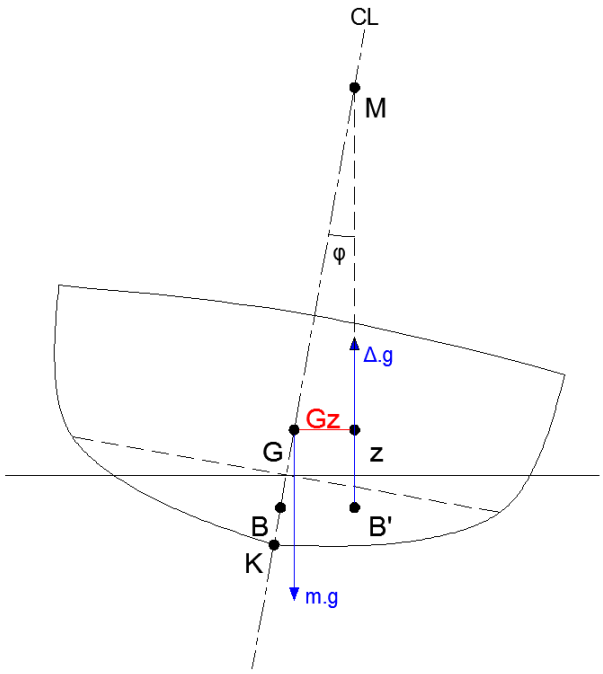

***Figure 56**: Transverse stability at small heel angles.*

As the yacht heels, the centre of buoyancy shifts to a new position B', where the upward buoyancy force is applied, while the downward force due to the mass of the vessel is applied through the centre of gravity.

The righting moment is $\Delta . g . \overline{Gz}$, where the lever arm $\overline{Gz}$ is given by:

$$\overline{Gz} = \overline{GM} \times \sin\varphi \qquad \textbf{Equation 91}$$

The metacentric height $\overline{GM}$ is indirectly found using:

$$\overline{GM} = \overline{KB} + \overline{BM} - \overline{KG} \qquad \textbf{Equation 92}$$

Where:

$\overline{KB}$ is the height of the centre of buoyancy above the reference point K; mathematically:

$$\overline{KB} = Tc - VCB \qquad \textbf{Equation 93}$$

$\overline{BM}$ is defined as the transverse second moment of area of the waterplane I_{xx} divided by the immersed canoe body volume ∇c [54], mathematically:

$$\overline{BM} = \frac{I_{xx}}{\nabla c} \qquad \textbf{Equation 94}$$

And $\overline{KG}$ is the distance from the reference point K to the vertical centre of gravity that can be estimated thanks to a weight estimate. However, an accurate $\overline{GM}$ can only be ascertained through an inclining experiment.

I.2 Inclining Experiment

An inclining experiment has previously been conducted on the Stewart 34 [79]; if the experimental procedure has been carefully followed, the interpretation of the data was not deemed satisfactory. From the raw data of the experiment, the stability has been assessed. The procedure will be presented, and the uncertainties will be discussed.

I.2.1 Theory

An inclining experiment consists in measuring the heel angle φ resulting from a known mass m being shifted a known distance d across the deck. The heel angle is traditionally measured with a pendulum, as illustrated in Figure 57.

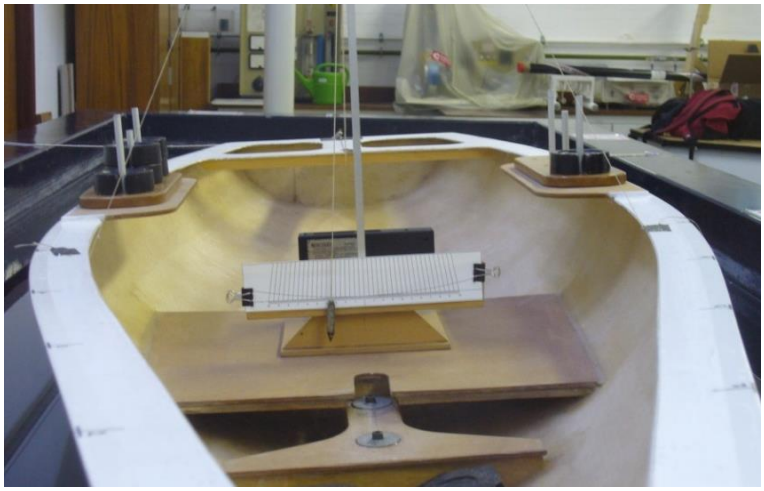

Figure 57: *Model scale inclining experiment illustrating a typical setup.*

In those conditions, the righting moment $\Delta . g . \overline{GZ}$ has to equal the created heeling moment $m . g . d$:

$$\Delta \times g \times \overline{GZ} = m \times g \times d \qquad \textbf{Equation 95}$$

Or:

$$\Delta \times g \times \overline{GM} \times \sin\varphi = m \times g \times d \qquad \textbf{Equation 96}$$

Solving for $\overline{GM}$:

$$\overline{GM} = \frac{m \times d}{\Delta \times \sin\varphi}$$ ***Equation 97***

Since the experiment is carried out at small angles of heel (less than 3°), $\sin\varphi$ can be approximated as $\tan\varphi$, and therefore:

$$\overline{GM} = \frac{m \times d}{\Delta \times \tan\varphi}$$ ***Equation 98***

Where the tangent of the heel angle can be expressed as a function of the pendulum length l and the recorded deflection x:

$$\tan\varphi = \frac{x}{l}$$ ***Equation 99***

Thus giving the metacentric height:

$$\overline{GM} = \frac{m \times d}{\Delta} \times \frac{l}{x}$$ ***Equation 100***

For the inclining experiment realised, four 70 kg masses have been used, hence a total displacement of the boat of $5100 + 4 \times 70 = 5380\ kg$.

In those conditions, a $\overline{GM}$ of 1.590 m has been ascertained. However, this is the metacentric height of the vessel with the inclining weights; since the vessel will not be sailing with those weights onboard, the height of the centre of gravity must be corrected thanks to a $\overline{GG'}$ shift [19]:

$$\overline{GG'} = -\frac{\overline{Gg} \times m}{\Delta - m}$$ ***Equation 101***

Where $\overline{Gg}$ represents the distance between the previously ascertained overall centre of gravity and the centre of gravity of the inclining weights on deck g; and m is the sum of the mass of the weights used, i.e. 280 kg. Numerically:

$$\overline{GG'} = -\frac{1.3 \times 280}{5380 - 280} = -0.033\ m$$

Hence the final $\overline{GM}$ is given by:

$$\overline{GM} = \overline{GM}_{initial} - \overline{GG'} = 1.590 + 0.033 = 1.623\ m$$ ***Equation 102***

Knowing the metacentric height, the position of the VCG has been ascertained at 206mm below the design waterline, which will later enable to carry a stability assessment at larger angles.

A full size inclining experiment includes various uncertainties that will be discussed in the following section.

I.2.2 Uncertainties

The inclining experiment of the Stewart 34 realised is described in [79], providing relevant information regarding the experimental procedure followed as well as an illustration of the pendulum set up (Figure 58). The procedure will be described and recommendations will be made based on best practice [19].

The experiment is to be realised in conditions as calm as possible, with flat sea, no wind and ideally slack tide, thus enabling to loosen the mooring lines so the vessel is not restricted in its ability to heel.

The bilges are also to be emptied, and any item able to switch side as the yacht heels must be secured. All tanks must be empty, or the amount of liquid must be recorded to account for free surface effect. The inclining experiment realised did not record the depth of the tanks; however, as later described in Appendix I.4.1, the impact of free surface effect is minimum in this instance and can therefore be neglected.

The position of all crew onboard were recorded and evenly distributed as to not create any heeling moment.

The major source of uncertainty results from the pendulum setup and reading. The setup used is illustrated in Figure 58.

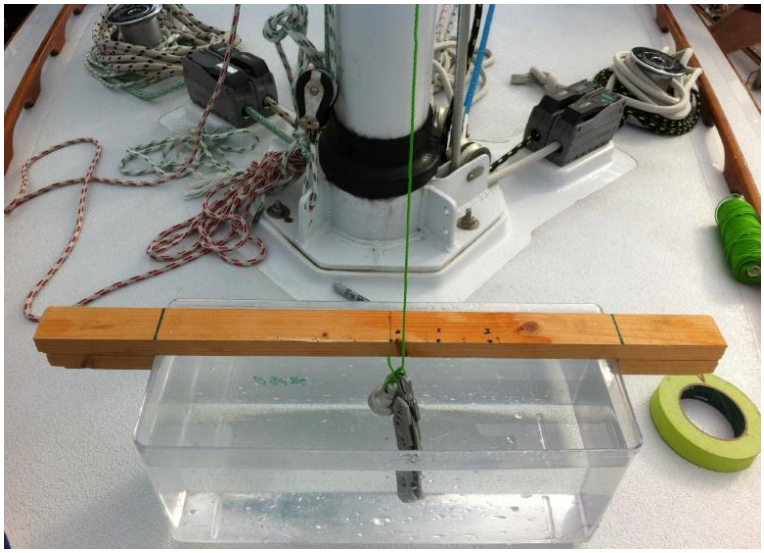

Figure 58: *Pendulum setup for the inclining experiment of the Stewart 34, illustration from [79].*

The presence of the water tank damps the motion of the pendulum, enabling more accurate readings. The pendulum is to be as long as possible to maximise the deflection and decrease the measuring error. A best practice approach suggests that the pendulum length is made a multiple of 57.3 cm [19]. For a 57.3 cm pendulum length, 1° of deflection will coincide with 1 cm. As a result, a ruler can be used to directly measure the deflection, thus improving the accuracy.

The experimental setup shows the use of a felt pen on wet wood to mark the position of the pendulum, then measured off at the end of the experiment: this will result in large uncertainties regarding the recorded deflection.

Finally, the freeboard was measured fore and aft in order to assess the vessel's displacement and hydrostatics from the 3D model of the vessel. It is to be noted that the model of the vessel used was developed by drawing over the linesplan. The use of the table of offsets would appear to be a more accurate way to capture the hull geometry, as previously presented in Appendix F.

There are therefore multiple uncertainties regarding the inclining experiment. Recommendations to improve the accuracy of the experiment have been made. If the use of the data has been questioned, there are no fundamental doubts about the quality of the experimental results themselves, as highlighted in the uncertainty analysis. As a result, the data has been deemed appropriate to be used for the assessing the VCG position, resulting in the large angle stability of Stewart 34.

I.3 Large Angle Stability

The stability of yachts is expressed by a $\overline{Gz}$ curve. At small angles of heel $\overline{Gz} = \overline{GM} \times \sin\varphi$ due to the assumption that the metacentre is fixed. However, this assumption is not valid at larger angles of heel, and therefore $\overline{Gz}$ cannot be ascertained as easily. Large angle stability is assessed via computational methods; in this instance the Hydromax software [8] has been used, and later validated thanks to the FS-Equilibrium [23] hydrostatics module.

A typical $\overline{Gz}$ curve would cover the whole range of heel angles, up to 180°; such an analysis would be required to prove compliance with a class rule for instance, and would involve careful modelling of the coachroof, cockpit and down-flooding points: a very time consuming process. Fortunately, for VPP applications, only the sailing heel angles are to be considered.

For the Stewart 34, deck-edge immersion has been ascertained at 31.6°, and the coachroof will not be in contact with the water until 37.7°. Given that the maximum heel angle considered is 35°, the analysis can be carried out on the hull only. In addition, if the static deckedge immersion occurs at 31.6°, the dynamic one is likely to be delayed due to the development of a midship trough as the yachts sails.

The $\overline{Gz}$ curve of the Stewart 34 is presented in Figure 59 and detailed in Table 17.

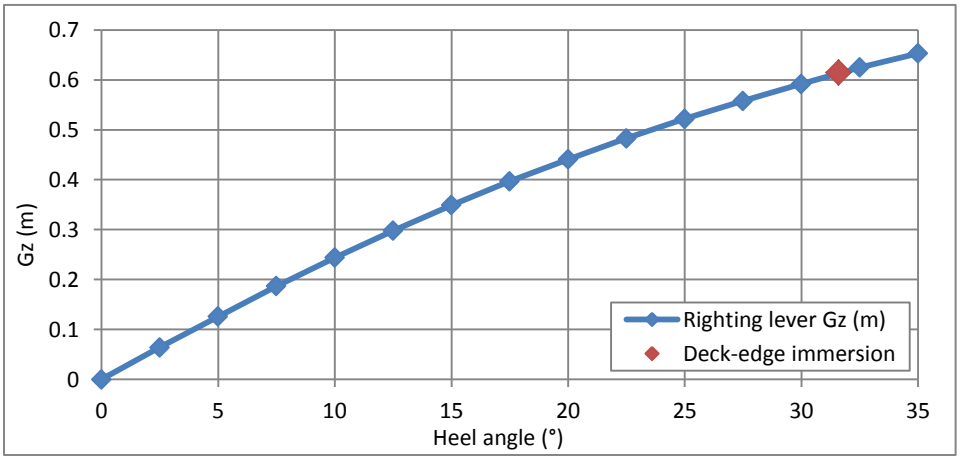

***Figure 59**: Gz curve of the Stewart 34 ascertained using Hydromax [8].*

Heel angle (°)	Gz (m)
0	0.000
2.5	0.064
5	0.126
7.5	0.187
10	0.244
12.5	0.298
15	0.349
17.5	0.397
20	0.441
22.5	0.483
25	0.522
27.5	0.558
30	0.592
32.5	0.625
35	0.653

***Table 17:** Righting lever for the Stewart 34.*

This model is however neglecting the impact of various components, such as free surface effect, the midship trough and the crew hiking, all having an impact on the stability.

I.4 Further Considerations

I.4.1 Free Surface Effect

As the yacht heels, the free surfaces on-board (fuel and water) will heel in their respective tanks, causing a shift in their respective centre of gravity, leading to a loss of stability: this is known as free surface effect (FSE). It can be accounted for in one of two ways: either a computational analysis (using Hydromax for instance), or from first principles. The later analysis attribute an artificial rise to the centre of gravity due to the free surface effect, commonly termed virtual centre of gravity and labelled $\overline{GG_V}$ [19].

The virtual centre of gravity is expressed as a function of the density of the fluid in the tank ρ_f (840 kg/m^3 for marine fuel), the tank transverse second moment of area I_t, and the mass of the vessel Δ:

$$\overline{GG_V} = \frac{\rho_f \times I_t}{\Delta} \qquad \textbf{Equation 103}$$

For small sailing yachts, free surface effect has usually a very small impact. In the case of *Pride*, the Stewart 34 on which the analysis is focussed, the vessel is sailed with an empty water tank, and the maximum capacity of the fuel tank is 40L, which renders any free surface effect to a negligible amount. As a result, the loss of stability due to free surface effect will be ignored in this instance.

However, it is to be noted that regulatory bodies will require free surface effect to be taken into account. The ISO 12217 Part 2 [39], reference standard for the stability of small crafts (less than 24 LOA) requires a careful free surface effect analysis, also taking into account area that can be flooded by green water, such as the cockpit, therefore demonstration the importance of free surface effect on the stability of yachts.

Another component that will reduce the stability is the midship trough.

I.4.2 Midship Trough

As a yacht sails faster a greater bow wave is generated, which results in a deeper midship trough, as illustrated on Figure 60. This leads to a change in volume distribution and a loss of buoyancy force where most of the yacht's volume normally lies, and where it is the furthest away from the centre line. The stability of the yacht will therefore be smaller in those conditions.

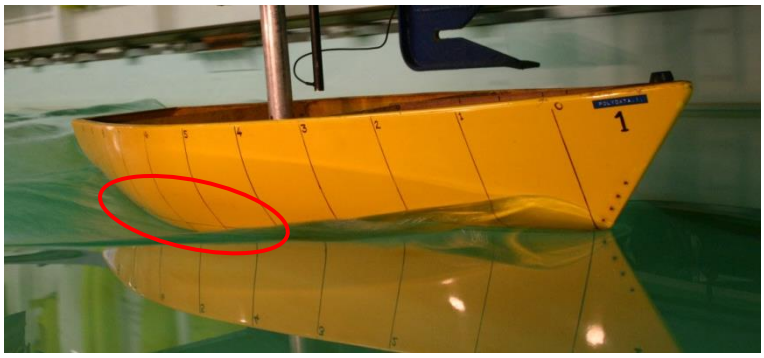

Figure 60: *Midship trough, picture from [6].*

The wave pattern can be ascertain with a CFD analysis or laser scanning [81], unfortunately the resulting loss in righting moment cannot be assessed. As a result, this parameter is not taken into account for the stability part of the VPP, which will result in discrepancies between the predicted and the actual stability and resulting performance of the boat. Some factors leading to loss in stability are neglected in this instance. Additionally, the effect of hiking will also be ignored.

I.4.3 Hiking

Under the ISAF 2013-2016 sailing rules [40] to which the Stewart 34 is subjected when racing, all movable ballast (such as non-flying sails) must be fixed, and therefore cannot be shifted across to provide additional righting moment or fore and aft trim.

Conversely, the crew is allowed to hike and move around the boat to achieve the desired trim and provide additional righting moment by sitting on windward. Alternatively, in light winds, the crew may move to leeward to increase the heeling moment, thus reducing the wetted surface area of the vessel.

There is therefore a wide range of scenarios that cause the crew to shift around the boat, therefore modifying its balance. One of the major variable being the number of crew onboard.

This is a non-negligible component of yacht racing that has a direct impact on the performances. It is however impractical and a VPP cannot be realised for each combination of crew members and crew positions. This is likely to lead to an under prediction of the speed of the boat.

I.4.4 Conclusions

Factors likely to influence the stability of the Stewart 34 and as a consequence its performance on the water have been identified, introducing some inaccuracy in the resulting velocity prediction of the vessel. Further sources of inaccuracy between the VPP and the actual behaviour of the boat have been identified and discussed in Section 5.5.4.

I.5 Conclusions

Based on small angle stability and the raw data of a previously conducted inclining experiment [79], the vertical centre of gravity of the Stewart 34 has been established. A large angle stability analysis was then conducted up to 35° of heel using Hydromax [8]. In addition to being perfectly suitable for the VPP, the restricted range of heel angles also enabled considerable time saving since modelling of the deck, coachroof and cockpit has been demonstrated not to have any impact of the stability below 35° of heel.

If the position of the centre of gravity and resulting Gz curve are relatively accurate, some sources or error have been identified. Indeed, the effect of the midship through and hiking have been neglected while they will actually have a significant impact on the performance. On the other hand, free surface effect has been considered negligible.

J Comparison of FS-Equilibrium and WinDesign

The 4 degrees of freedom VPP realised using empirical modules in FS-Equilibrium has been compared with the WinDesign analysis previously introduced for the purpose of validation and to ensure correct use of the software. The difference (Δ) in boat speed, heel and yaw angle are respectively presented in Figure 61, Figure 62 and Figure 63. Note that, despite being taken in to account in WinDesign, the rudder angle is not an available output of the program, and therefore cannot be compared to the values established by FS-Equilibrium.

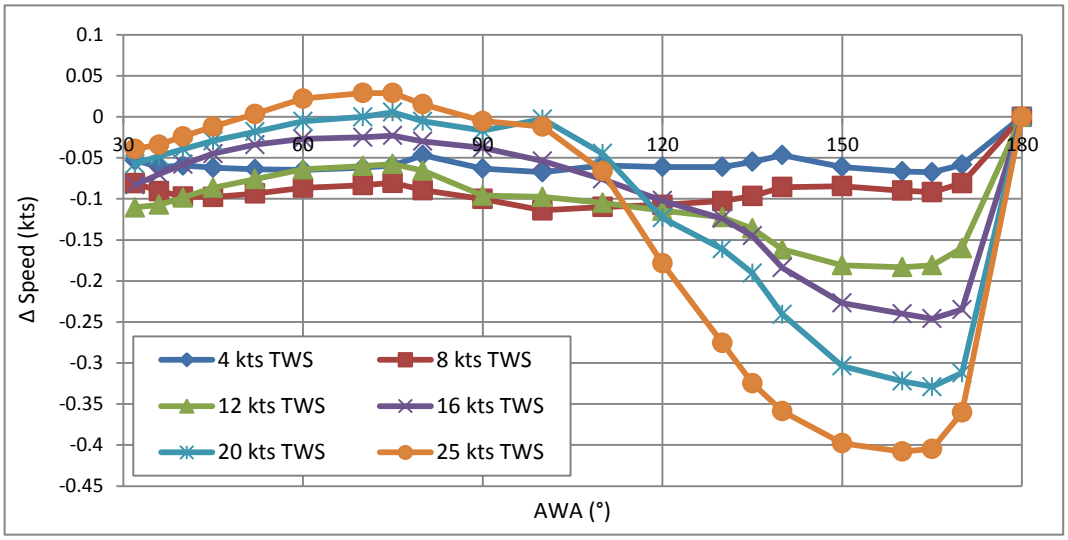

Figure 61: *Speed difference (kts) between FS-Equilibrium and WinDesign.*

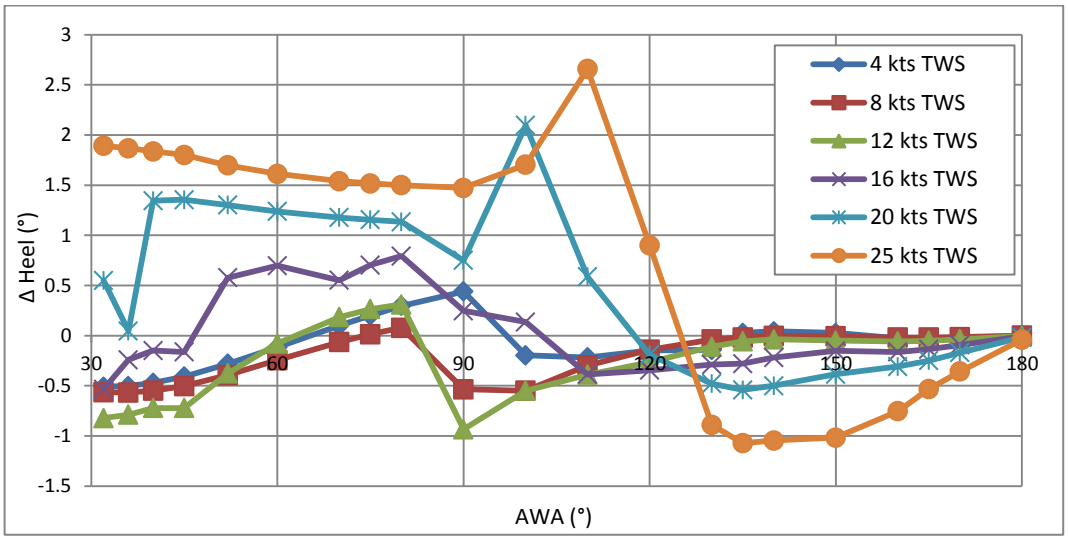

Figure 62: *Heel difference (°) between FS-Equilibrium and WinDesign.*

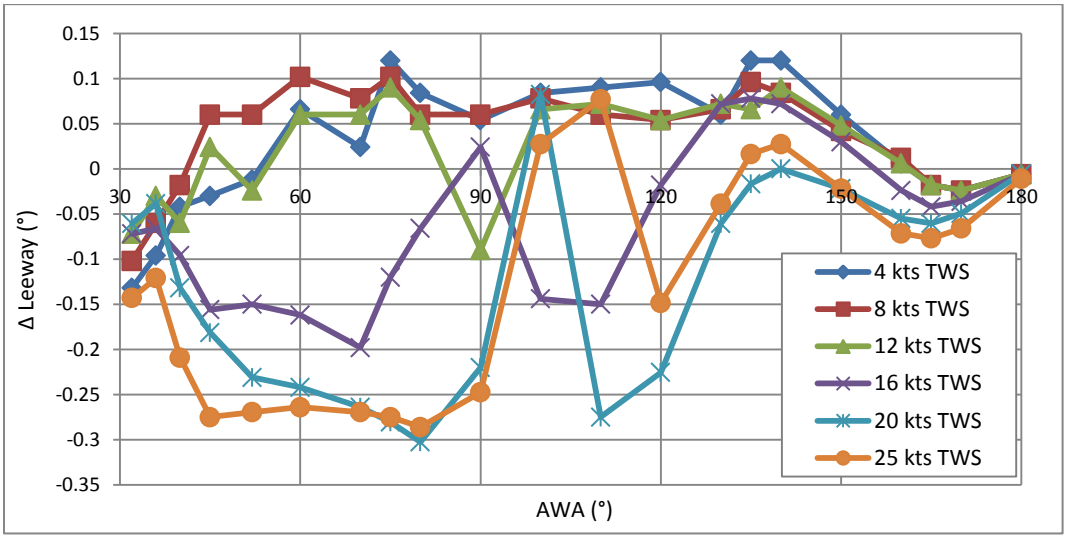

Figure 63: *Leeway difference (°) between FS-Equilibrium and WinDesign.*

In terms of boat speed, FS-Equilibrium is in the order of 0.1 knots below WinDesign upwind. The difference increases up to 0.4 knots downwind at the highest wind speeds, which constitutes a non-negligible difference. The heel angle exhibits quite a large scatter, ranging from -1° at low wind speeds to 2° at higher wind speeds. Finally, the leeway angle remains within 0.1° at low wind speeds, but drops down to -0.3° as the wind speed increases.

Both VPP programs have been set to empirical modes; there different required inputs provide an initial source of inaccuracy. In addition, the underpinning theory of both programs is not fully detailed, and intermediate calculations are not available. It therefore appears impossible to realise strict comparison of the VPPs with the exact same inputs and to check the aerodynamic and hydrodynamic models developed.

Nevertheless, the results at low wind speed (less than 16 knots TWS) are relatively close, and did not prove to impact of factors such as the angle for best VMG or the cross over between jib and spinnaker. Most of the discrepancies occur at higher wind speeds, and can be related to the use of the depowering parameters reef and flat, as illustrated in Figure 64 and Figure 65.

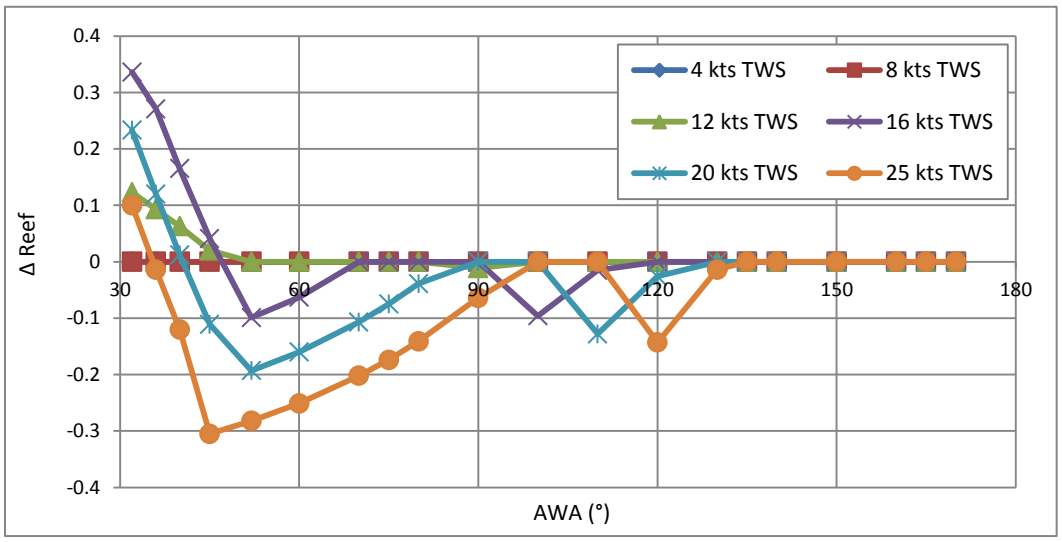

Figure 64: *Reef difference between FS-Equilibrium and WinDesign.*

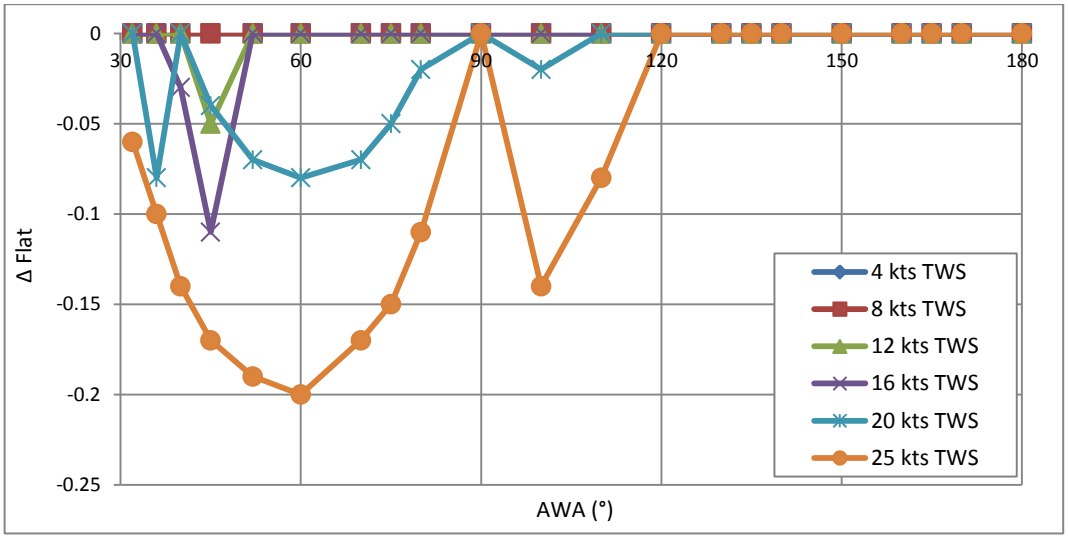

Figure 65: *Flat difference between FS-Equilibrium and WinDesign.*

WinDesign appears to introduce depowering earlier and to a high extent than FS-Equilibrium, which would explain the higher speeds and lower heel angle established by WinDesign at high wind speeds. Discrepancies in heel angle can also be linked to the assumptions made by both programs regarding the change in position of the centre of effort of the sails.

Despite the inability to realise a strict comparison of WinDesign and FS-Equilibrium to purely validate both solvers, an empirical VPP based on similar inputs has been realised. Both programs appear to provide very similar results below 16 knots of TWS. Larger differences are exhibited in stronger winds due to the different use of the depowering parameters.

K. Velocity Prediction Program Results for the Stewart 34

K.1 Boat Speed (m/s)

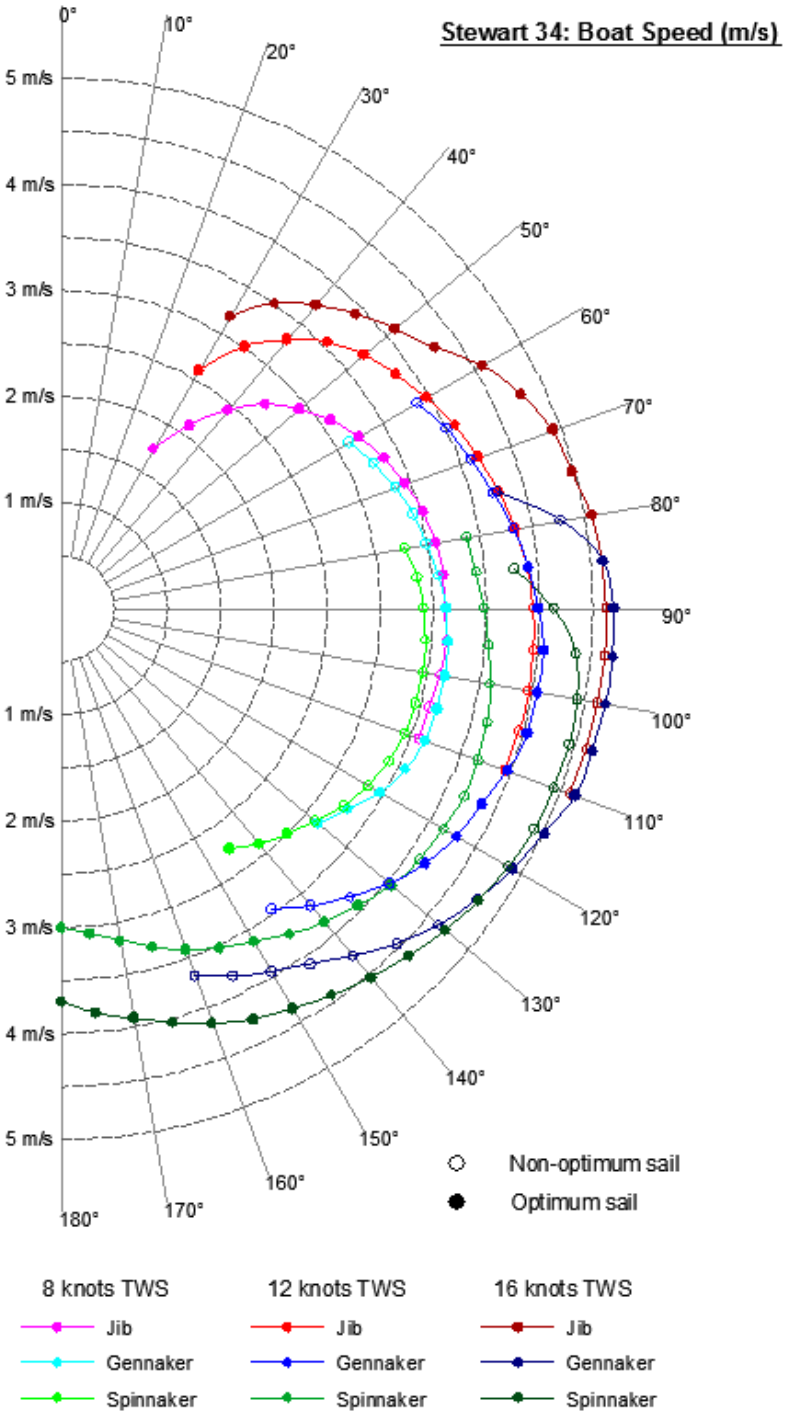

Figure 66: *Stewart 34 FS-Equilibrium VPP: boat speed (m/s).*

K.2 Boat speed (kts)

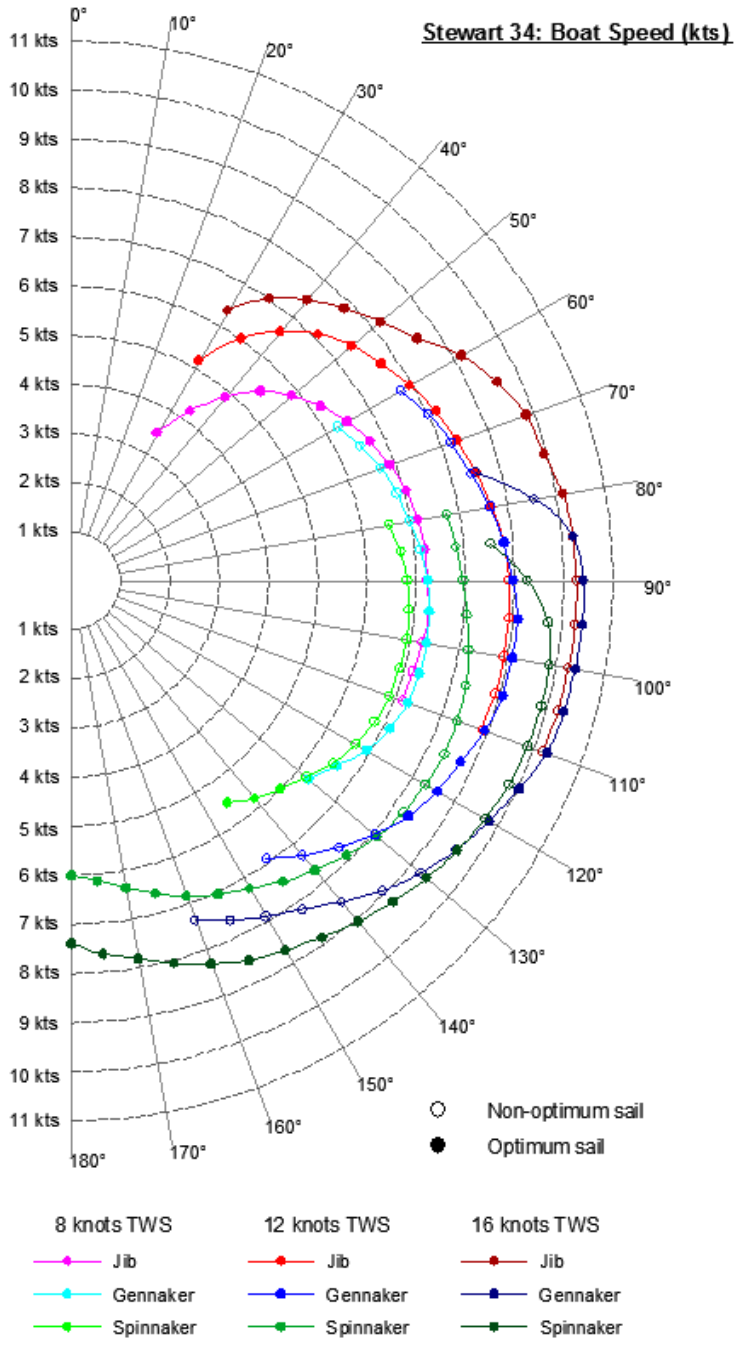

Figure 67: *Stewart 34 FS-Equilibrium VPP: boat speed (kts).*

K.3 Heel angle

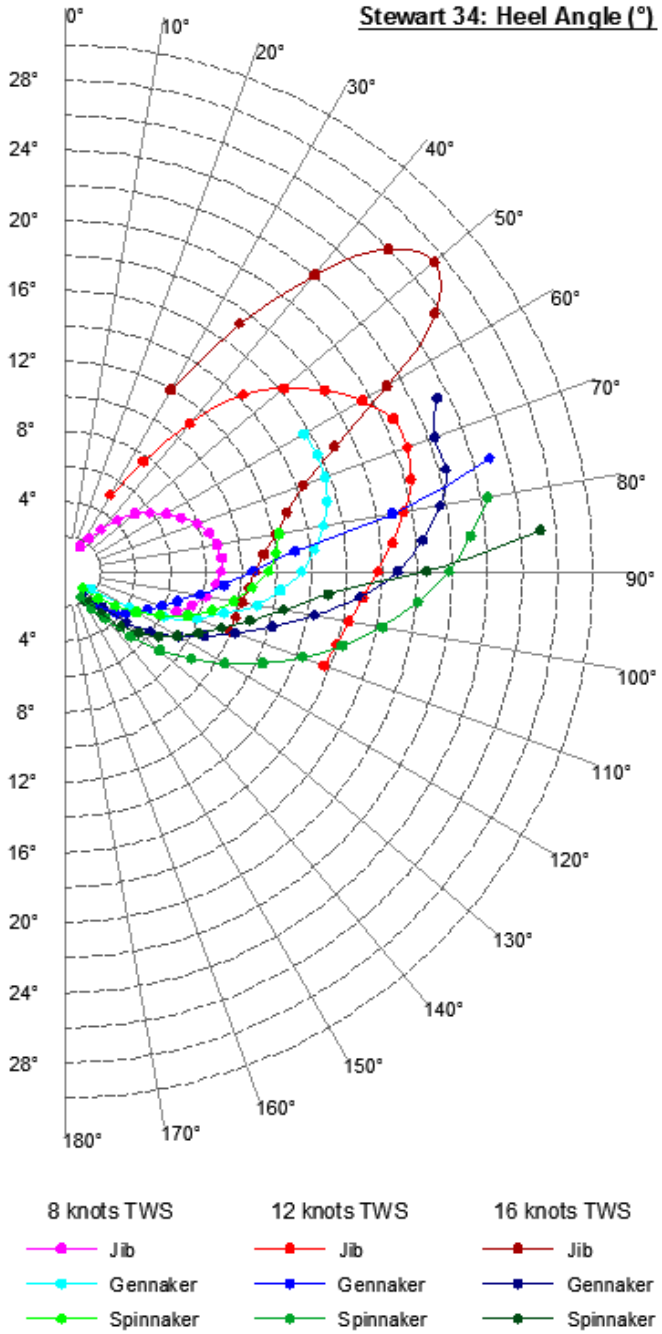

Figure 68: *Stewart 34 FS-Equilibrium VPP: heel angle(°).*

The heeling angles upwind at high wind speeds significantly decrease as the yacht bears away towards reaching. This issue was observed in previous work conducted on the upwind VPP of the Stewart 34 [99], and would suggests discrepancies in the experimental depowering data and inherent FS-Equilibrium module.

Note that despite being plotted as positive, the heel angles are actually ascertained as negatives due to the sign convention of FS-Equilibrium.

K.4 Leeway angle

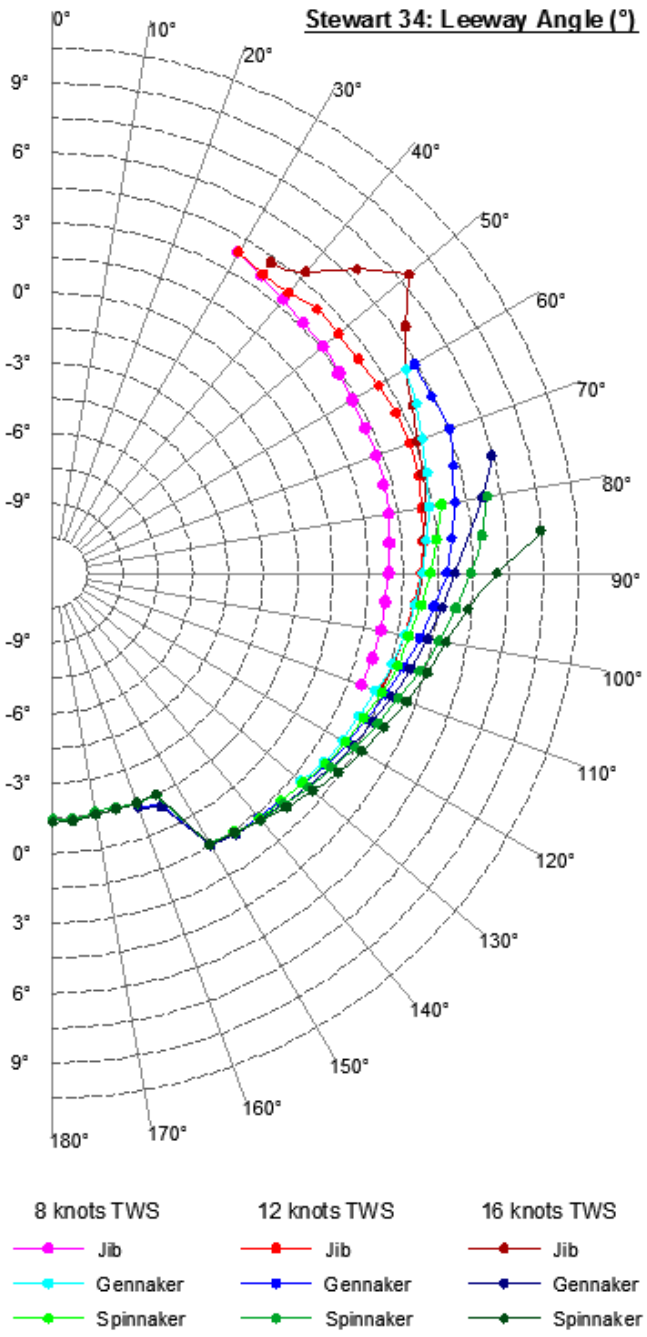

Figure 69: *Stewart 34 FS-Equilibrium VPP: leeway angle (°).*

Slight negative leeway is visible dead downwind, coherent with sailing yachts behaviour. Elsewhere, the leeway angle is positive, increasing at the yacht gets closer to the wind.

Note the drastic change in leeway for the jib at 16 knots of true wind speed due to the depowering: the heel angle reduces, and so does the leeway and the required rudder angle, as presented in Appendix K5 hereafter.

K.5 Rudder angle

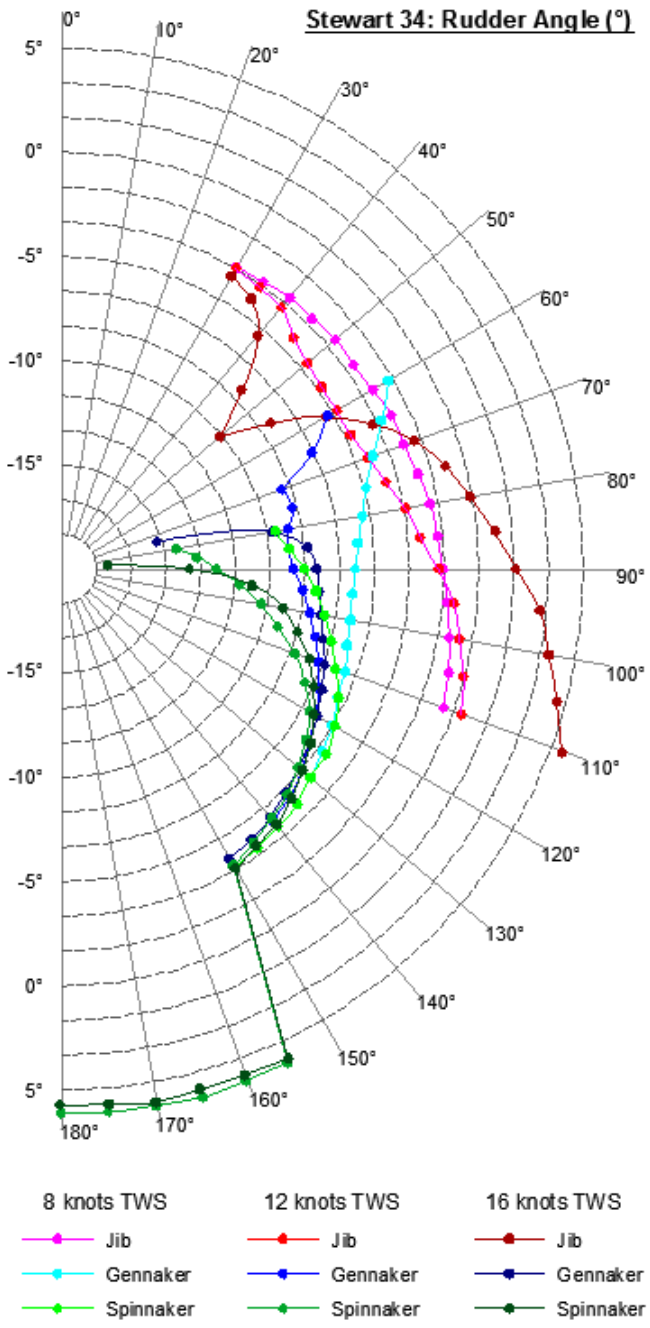

Figure 70: *Stewart 34 FS-Equilibrium VPP: rudder angle (°).*

The negative leeway dead downwind induces a lee-helm (positive rudder angle). Lee-helm is also present for the jib when reaching at high wind speeds, once again highlighting inconsistency in the depowering. The yacht experiences normal weather-helm elsewhere.

The rudder angle for the gennaker and spinnaker can be seen very close to -15° for 16 knots of TWS, revealing the rudder is close to stalling, and the absence of solution at the next TWA up indicates that the rudder has stalled and therefore the sail cannot be carried to high.

K.6 Pitch Angle

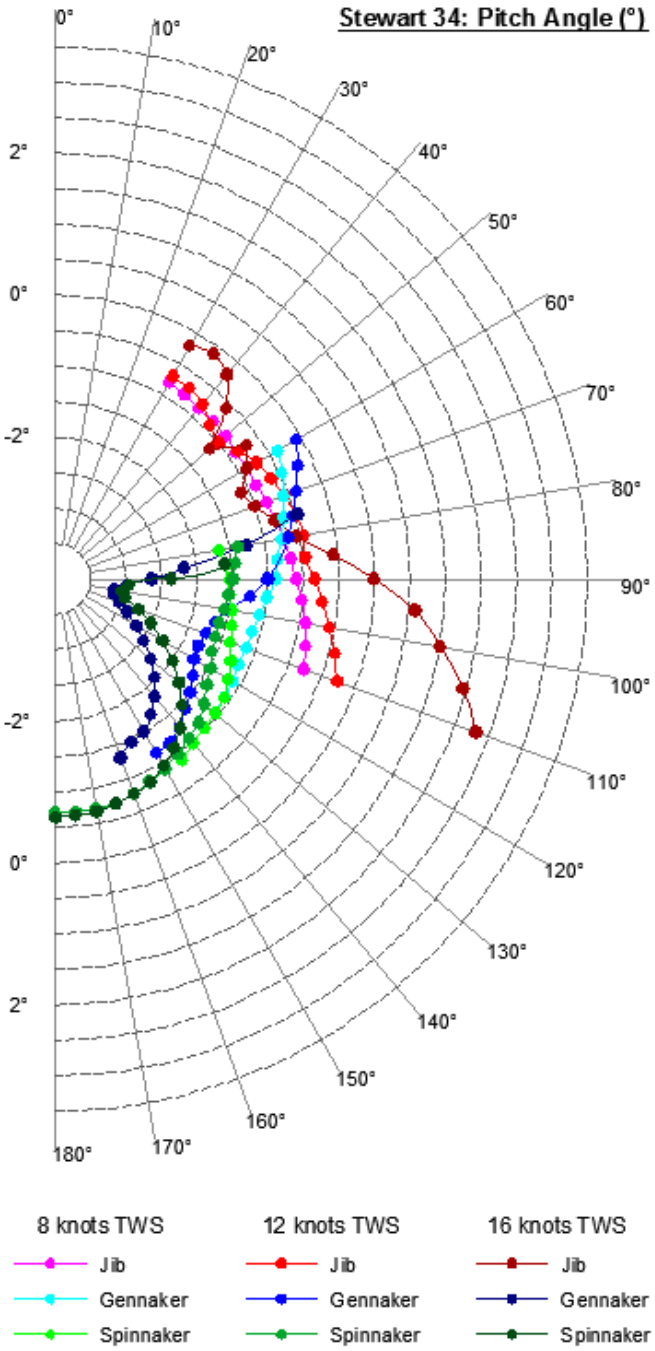

Figure 71: *Stewart 34 FS-Equilibrium VPP: pitch angle (°).*

Pitch remain very small, and has a negligible impact on the yacht behaviour, as demonstrated in Section 5.5.3. However, the values when reaching in 16 knots true wind speed further reveal some issues with the upwind depowering.

Jean-Baptiste Roger Guillaume SOUPPEZ
The University of Auckland
November 2014